Fatigue Bond Behaviour of Corroded Reinforcement and CFRP Confined Concrete

by

Ahmad Rteil

A thesis
presented to the University of Waterloo
in fulfillment of the
thesis requirement for the degree of
Doctor of Philosophy
in
Civil Engineering

Waterloo, Ontario, Canada, 2007

AUTHOR'S DECLARATION

I hereby declare that I am the sole author of this thesis. This is a true copy of the thesis, including any required final revisions, as accepted by my examiners.

I understand that my thesis may be made electronically available to the public.

Abstract

Bond in a reinforced concrete (RC) structure is the interaction force that transfers force between the steel and concrete. It influences the structural performance and serviceability of a structure under both static and cyclic loading. Corrosion of reinforcing steel in RC structures is the primary reason behind bond loss in RC elements. A loss of bond in concrete results in a decrease in the serviceability strength and eventually causes a brittle and sudden failure. Structures, such as bridges, are vulnerable to corrosion and at the same time are subjected to repeated loading rather than static loading. Nevertheless, little experimental or analytical studies that address the problem of corroded steel-concrete bond under repeated loading exist.

This study was aimed at increasing the understanding of the behaviour of bond between corroded reinforcing steel bars and concrete for structures subjected to repeated loading. In addition, the effect of fibre reinforced polymers (FRP) as a rehabilitation method was assessed. Fibre reinforced polymers is considered to be a state-of-the art rehabilitation material due to its advantages, such as high strength, light weight and ease of handling and application.

Forty-seven anchorage-beam specimens were cast and tested. The specimens' dimensions were 152 x 254 x 2000 mm reinforced with two 20M bars. The steel reinforcement in a specimen was unbonded except for 250 mm from each end. This bonded length was selected to ensure a bond failure. The corrosion was induced using an accelerated corrosion process. The parameters investigated were the corrosion level (0, 5 and 9% measured mass loss), whether the specimen was wrapped in the anchorage zone with a U-shaped carbon fibre reinforced polymer (CFRP) sheets or not, and the load range applied. The minimum load applied was 10% of the static bond capacity of the specimen. The maximum load was varied to give the desired range of fatigue lives (10^3 to 10^6 cycles). The test frequency for all repeated tests was 1.5 Hz.

Results showed that the repeated loading either pushed the bottom concrete cover away from the steel bar by wedge action for unwrapped beams or cracked and crushed the CFRP confined bottom concrete cover for wrapped beams. The concrete damage caused the bond stress to undergo a gradual redistribution, moving the peak bond stress from the loaded end towards the free end, resulting in failure of the specimens by fatigue of bond. Corrosion levels of 5% and 9% decreased the fatigue bond strength on average by 19%. The rate of slip of the steel bar increased as the corrosion level increased. CFRP sheets changed the mechanism by which the concrete resist the bond forces by engaging the bottom cover. This in turn increased the fatigue bond strength at all corrosion levels on average by 31% compared to unwrapped specimens.

Based on the test results and observations, a hypothesis of the mechanics of bond under repeated loading was postulated and a fatigue slip-growth analysis (similar to the fracture mechanics crack growth approach) was proposed to calculate the fatigue life of a specimen that fail in bond. The proposed analysis was in reasonable agreement with the experimental results.

Acknowledgements

I would like to express my sincere gratitude and appreciation to my friends and supervisors Prof. Khal Soudki and Prof. Tim Topper for their help, guidance, encouragement, support and wonderful supervision and above all friendship.

I also would also like to thank my friends: Rania and Ken. Without you guys the completion of this work would have been much more difficult. Rania was always there for help in the lab, in the break time and providing me with the food recipes. Ken was my lab mentor in conducting this research as well as other research studies I worked on during the few past years.

The help of Terry Ridgway, Doug Hirst and Stanely Ng from Civil Engineering and Andy barber of Mechanical Engineering in the lab work is appreciated and acknowledged. Thanks would also go to my colleagues in the FRP and Fatigue research groups.

I also would like to acknowledge the financial support of ISIS Canada Network, AISI fatigue bar committee and Ministry of Training, Colleges and Universities in Ontario for the Ontario Graduate Scholarship (OGS).

Finally yet importantly, I would like to thank my dad, Ali, my mom, Afaf, Youssef, Halimeh, Nour, and Farah for their support and continues encouragement.

To the ones who were

and will always be

in my mind…

in my heart…

…and in my Soul

A.R.

Table of Contents

List of Figures

List of Tables

Chapter 1
Background and Objectives

1.1 Problem Statement

Bond in a reinforced concrete (RC) structure is the interaction force that transfers force between the steel and concrete. It influences the structural performance and serviceability of a structure under both static and cyclic loading. Losing the bond interaction between the steel and concrete, interrupts the force transfer mechanism and results in an increased deflection, an increased number of cracks, an increase in crack widths and a decreased load carrying capacity of a reinforced concrete element and can cause a brittle and sudden failure (ACI 408, 2003). Therefore, it is important to predict the behaviour of RC structures not only to incorporate but also to understand correctly this mechanism (FIB 10, 2000).

Corrosion is one of the most serious problems that affect the service life of RC structures. It was estimated that the corrosion problem annually costs the US economy about $276 billion or 3.1% of the Gross Domestic Product (GDP). Approximately 30% of this cost is related to corrosion in concrete structures (Whitmore and Ball, 2004).

In reinforced concrete (RC) structures, the corrosion of the steel reinforcement results in a reduction of the reinforcing steel cross sectional area thus reducing their yield load and the ultimate capacity. Also, the volume of the rust, being several times larger than the parent steel, induces tensile forces on the concrete leading to concrete cracking and cover spalling which in turn reduces the bond between the concrete and the steel (ACI 222, 2001). Experiments have shown that cracking of the concrete cover takes place well before the loss of bar section significantly reduces the strength of the concrete member (FIB 10, 2000). Therefore, in terms of strength and serviceability the most

important effect of corrosion in RC structures is the deterioration of the bond between the concrete and the steel.

Some structures such as bridges and marine structures that are susceptible to corrosion are also subjected to repeated rather than static loading. The use of high strength materials which resulted in lighter concrete structures, thus decreased the dead load and combined with an increase of live loading (heavier trucks on bridges for example) resulted in an increased live to dead load ratio. Therefore, the effect of repeated loading has started to govern the design for the serviceability limit state (ACI 215, 1974). In extreme cases, repeated loading can cause a structure to fail by fatigue (ACI 215, 1974) however, the main effect of repeated loading is an accumulation of damage to structures under service loads that are far below the ultimate loads. This damage takes the form of an increase in the number of cracks, the crack widths and the deflection. The bond between steel and concrete directly or indirectly affects these aspects. Therefore, the residual strength of these structures can only be determined if the bond between the steel and the concrete is accurately evaluated (Oh and Kim, 2007; Mor et al., 1992; ACI 408, 1992).

Despite these problems very little work addressing this problem has been reported in the literature. Most (if not all) of the few studies reported used pullout specimens, which are known to neither correctly model true bond behaviour nor result in bond stress values that can be used to assess the bond behaviour of real RC structures. Also, the extensive studies of the effect of corrosion on bond strength conducted during the past two decades (FIB 10, 2000) were all performed under monotonic loading. Despite its negative effect on the strength and serviceability of RC structures the interaction of corrosion and repeated loading on the steel-concrete bond has not yet been investigated.

The present study was designed to fill in some of the gaps in the knowledge of the behaviour of bond under repeated loading using beam specimens. Also, the effect of corrosion on the fatigue performance of bond was examined.

The study also investigated the use of fibre reinforced polymers (FRP) as a system to repair corroded bond critical regions subjected to repeated loading. FRP has achieved acceptance as a repair material due to its many advantages over traditional strengthening materials/systems (ACI 440, 2002). Research has shown that a FRP repair system can significantly increase the strength of RC beams and decrease the corrosion activity (El Maaddawy et al., 2005a and 2006).

The remainder of this chapter will present background information relevant to the different aspects of the study namely, FRP material and its use, the corrosion and repeated loading phenomena and their effects on RC structures. Also, the bond mechanism between steel and concrete in RC structures will be explained. The effect of corrosion, repeated loading and FRP on the bond will be reviewed. Finally, the objectives of this study will be stated.

1.2 Fibre Reinforced Polymers

Fibre reinforced polymer (FRP) have emerged as an alternative to traditional methods for the strengthening (or repairing) of existing concrete structures or for new construction. Fibre reinforced polymer sheets are composites that consist of high tensile strength fibres within a polymer matrix (ACI 440, 2002).

1.2.1 Fibres

Fibres are the load-carrying elements in FRP composites. They give the FRP system its strength and stiffness (ACI 440, 2002). In general, they are characterized by very small diameters and very high length to diameter ratios. Continuous fibres of carbon, glass or aramid are used in structural

applications. The fibres, depending on the type of application they are used for, may be uni-directional, bi-directional or have some other orientation (ACI 440, 1996).

- Carbon fibre reinforced polymer (CFRP): CFRP composites exhibit many properties important to structural engineers including: a high tensile strength, an excellent corrosion resistance, a high strength to weight ratio, an excellent fatigue behaviour, a low coefficient of thermal expansion, and a high stiffness. On the other hand, they are expensive to produce.

- Glass fibre reinforced polymer (GFRP): GFRP composites have low production costs relative to carbon fibres, high tensile strength relative to steel, excellent heat resistance and low electrical conductivity. On the other hand, GFRPs have a low stiffness and a low specific strength compared to carbon fibres.

- Aramid fibre reinforced polymer (AFRP): Aramid is a generic name for aromatic polyamide. Composites made with aramid fibres are stiffer than GFRP and cheaper than CFRP. They possess a low density, a high strength and good fatigue and corrosion resistance.

1.2.2 Resin

The main function of the resin (also called the matrix) is to transfer stresses between the fibres and between the fibres and the concrete. It also supports, protects, and separates the fibres (ACI 440, 1996). Commonly used resin types include epoxies, vinyl esters and polyesters (ACI 440, 2002). A variety of resins have been formulated each aimed at optimized structural behaviour for a given range of environmental conditions. A suitable resin must be easy to apply and compatible with, and bond to the substrate (ACI 440, 1996).

Figure 1.1 compares the stress-strain behaviour of FRP systems and that of reinforcing steel bars. It is noted that FRP reinforcement exhibit a linear elastic stress- strain relationship up to failure. It is also noted that their strength is higher than reinforcing or prestressing steels.

1.2.3 Application of FRP Systems

FRP systems are either used internally mainly in new concrete construction (prestressed rods or reinforcing bars) or externally to strengthen and repair existing structures (flexible sheets, prestressed rods). FRPs are of interest to rehabilitation engineers because of their high-strength to weight ratio, high tensile strength, ease of handling and application, the elimination of the need for heavy equipment in making repairs and rapid construction and the fact that they do not corrode (ACI 440, 1996).

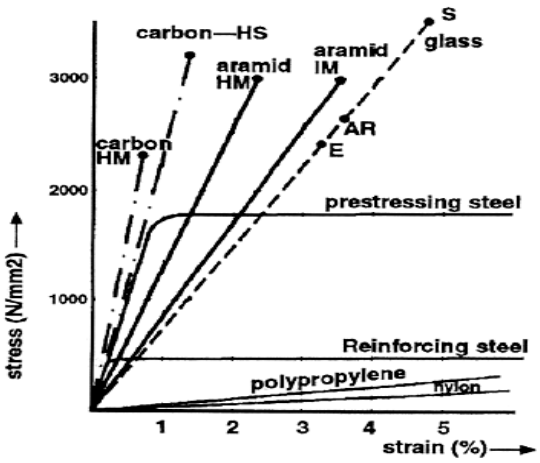

Figure 1.1 Stress-strain behaviour of steel reinforcement and FRP sheets (ACI 440, 1996)

In beams, the FRP sheets are installed on the tension side to increase the flexural strength or wrapped around the beam to confine the concrete thus increasing the shear and bond capacity. Also, they are wrapped around RC columns to repair corrosion-damage and to increase their strength and ductility (especially in seismic zones) (ACI 440, 1996).

1.3 Corrosion

Concrete has a pH level between 12 and 13. In this high alkaline environment, the steel reacts with oxygen to form a thin, dense, impenetrable layer of metal oxide on the surface. This film isolates the steel and thus protects it from corrosion (Broomfield, 1997; ACI 222, 2001).

1.3.1 Depassivation Process in Reinforcing Concrete

Corrosion occurs when there is a breakdown of the passive layer around the steel reinforcement. This may be a result of a reduction in the pH level of the concrete or of the presence of an outside chemical which attacks the passive layer (ACI 222, 2001). In some other cases, a RC structure may be exposed to an aggressive chemical which destroys the concrete matrix prior to the chemical reaching the steel, making corrosion a minor issue. However, there are two commonly occurring critical chemicals that can migrate through the concrete pore system with minimal interference and directly attack the steel (Broomfield, 1997). Carbon dioxide migrates through the concrete and reacts with it in such a way as to lower the pH to a level where the passive film on the steel is no longer sustained in a process called carbonation. The other case is known as a chloride attack, in which chloride ions diffuse through moisture in the concrete pores, and react with, and disrupt the passive layer on the reinforcing bar (ACI 222, 2001).

1.3.1.1 Carbonation Induced Corrosion

Carbonation is the result of an interaction between carbon dioxide gas (CO_2) and the alkaline hydroxides in concrete. This chemical reaction results in the formation of carbonic acid. Unlike most other acids, carbonic acid does not attack the cement paste, but just neutralizes the concrete and drops the pH level to less than 10 (Broomfield, 1997). At this pH level, the passive layer no longer adheres to the steel surface and corrosion reactions start.

The influence of carbonation on corrosion is dependent on many factors the most important are: the thickness of concrete cover, the quality of the concrete and carbon dioxide concentrations. If the concrete possess an open pore structure, the rate at which carbon dioxide penetrates the concrete increases. Concrete with closed pores or smaller pores lowers the rate of penetration of carbon dioxide, and thus lowers the rate of carbonation. Also, as the concrete cover over the reinforcing bar increases, more time is needed for the carbon dioxide to reach the steel. Finally, if the amount of carbon dioxide in the surrounding atmosphere is high, as in parking garages for example, then the rate of carbonation increases (Broomfield, 1997).

1.3.1.2 Chloride Induced Corrosion

Chlorides may be introduced into the concrete in two different ways. Cast-in chlorides may be present in the concrete matrix due to the use of set accelerators such as calcium chloride, the use of seawater, or contaminated aggregates in the concrete mix (Broomfield, 1997). Chlorides may also be introduced from external sources and diffuse into the concrete matrix. The two main external sources are sea salt for structures near seas and oceans, and de-icing salts for structures in cold regions (Broomfield, 1997). With the assistance of moisture, chloride ions migrate through the concrete until they reach the reinforcing steel. The exact nature of how the chloride ions act to accelerate corrosion is not fully understood. There are three main theories that describe how chlorides interact with the steel (ACI 222, 2001). The oxide film theory states that the chloride ions may penetrate the passive layer around the steel bar through pores or defects and attack the iron underneath. The adsorption theory describes a competition between the chloride ions and the dissolved oxygen and the hydroxyl ions for adsorption to the metals surface. The removal of the iron ions from a bar into solution is increased by an interaction of the chlorides directly with the steel. Finally, the transitory complex theory states that a soluble iron chloride is formed when chlorides replace the hydroxyl ions disrupting the passive layer. Iron chloride then migrates away from the anode and chemically breaks down, freeing the

chloride ion and allowing it to continue reacting with the steel. In this case, the chloride ion acts as a catalyst in the reaction and it is available to react with additional ferrous ions or hydrogen ions (ACI 222, 2001).

1.3.2 Corrosion Mechanism in Concrete

The occurrence of depassivation marks the initiation of the corrosion process in steel. Corrosion of reinforcing steel in concrete takes place by an electrochemical reaction (ACI 222, 2001) which is similar to the reaction that takes place in a flashlight battery. There is an anode where electrochemical oxidation takes place and a cathode where electrochemical reduction occurs. An aqueous solution (the concrete matrix) and an electrical conductor (reinforcing steel bars) must also be present (ACI 222, 2001).

The iron at the anodic section of the steel bar breaks down and releases electrons (see Figure 1.2).

$$Fe \longrightarrow Fe^{+2} + 2e^{-} \qquad \text{Equation 1.1}$$

At another location on the steel bar, a cathodic reaction takes place in which the electrons combine with water and oxygen to form dissolved hydroxide ions (see Figure 1.2).

$$2e^{-} + H_2O + \frac{1}{2}O_2 \longrightarrow 2OH^{-} \qquad \text{Equation 1.2}$$

Additional reactions occur between the iron ions and the hydroxide ions to form hydrated ferric oxide ($Fe_2O_3.H_2O$) or rust. Various other forms of corrosion product may also be obtained from similar reactions. In the anhydrate form, Fe_2O_3 occupies approximately two times the volume of the original steel. However, when it reacts with water to form hydrated ferric oxide ($Fe_2O_3 \cdot H_2O$), it may occupy up to ten times the volume of the original steel (Broomfield, 1997).

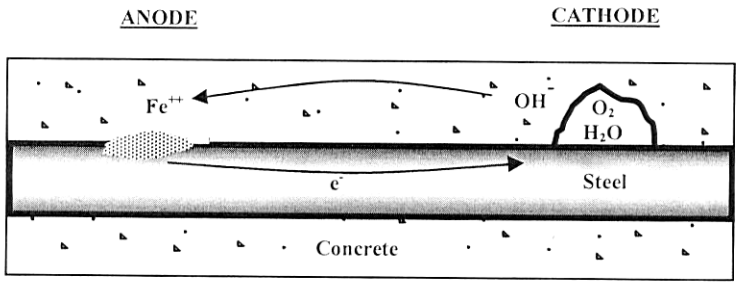

Figure 1.2: Corrosion cell in concrete

Usually carbonation-induced corrosion results in microcell reactions in which corrosion occurs locally on the steel surface, i.e. anodic and cathodic areas are in close proximity. The result is what seems to be uniform corrosion along the entire length of the bar. Macrocell reactions can occur over larger distances on a steel bar or even between two different bars in the concrete. Typically there are localized areas of corrosion (pitting corrosion) perhaps a few centimetres wide, separated by large passive areas of steel. This type of action is typical of chloride-induced corrosion (Broomfield, 1997).

To summarize the above discussion, once depassivated, the steel in concrete will corrode provided the following are present: 1) reinforcing bars that provide locations for the anodic and cathodic reactions to develop and through which the electrons are transferred from the anode terminal to the cathode terminal; 2) Pore water in the concrete matrix which acts as an electrolyte in order to carry the ionic current (OH^- ions); 3) Oxygen and; 4) Moisture (water).

Availability of oxygen near the cathode and the moisture content near the steel are the primary factors that determine the rate of corrosion (ACI 222, 2001). Oxygen can migrate from the exterior through the pore structure of the concrete. Concrete, even if it is not exposed to moisture during its service life, has a significant water content after casting that persists beyond the curing process.

1.3.3 Corrosion Damage in RC Structures

One of the direct consequences of the corrosion of reinforcing steel is a reduction of its cross-sectional area. This reduction is commonly used as a measure of the level of severity of the corrosion. In concrete the maximum rate of steel corrosion is about 50 μm/yr and hence, the main damage that takes place is not due to the loss of steel area but to the expanding volume of rust products that leads to cracking and spalling of the concrete and therefore, to a loss of bond between the concrete and the steel. This latter damage is a critical serviceability issue in RC structures (ACI 222, 2001; Broomfield, 1997).

The volume of the rust products produced is much greater than the volume of the steel that disappears during the corrosion reaction. Since most of the rust is confined within the concrete its formation generates tensile stresses that exceed the tensile capacity of the concrete. Damage is observed first as rust stains and minute cracking of the concrete surface. These cracks run parallel to the under laying reinforcement. If repairs are not undertaken at this stage, corrosion will proceed at an increasing rate since cracking allows more oxygen and water to migrate to the steel. This leads to severe damage including a complete loss of bond between the concrete and the steel due to delamination and spalling, as well as reduction of the cross sectional area of the steel to an extent that the RC structure becomes a safety hazard (Broomfield, 1997).

Research on the effect of corrosion on the flexural strength of RC beams has indicated a significant drop in the yield and ultimate load and an increase in the midspan deflection (decrease in stiffness). For beams corroded in the anchorage zone (as well as in the flexural zone), the mode of failure changed from concrete crushing (flexural) to bond splitting. In the latter studies, the decrease in the ultimate load was much more than could be accounted for due to reduced steel area. This suggests that a loss of bond between steel and concrete (especially in the anchorage zone) has a more significant effect than the reduction in steel cross sectional area (Uomoto et al., 1984; Okada et al.,

1988; Tachibana et al., 1990; Kawamura et al., 1995; Almusallam et al., 1996b; Rodrigueez et al., 1997; Mangat and Elgarf, 1999b and El Maaddawy et al., 2005a). Tests conducted on columns showed that not only was the ultimate capacity of the columns reduced, but also the columns failed with no warning signals (Lee et al., 2000).

1.3.4 Effect of FRP on Corrosion Activity and Corrosion-Damaged Beams

During the last few years, various researchers, including several at the University of Waterloo, have studied the strengthening of corroded reinforced structures by the application of FRP sheets (El Maaddawy at al., 2005a; Soudki and Sherwood, 2000; Lee et al., 2000; and Masoud et al., 2001). These studies showed that FRP sheets were able to increase the yield and ultimate load capacity of the corroded beams. In addition, corroded beams strengthened with FRP sheets exhibited a reduced deflection and an increased stiffness. Similar conclusions were drawn when FRP was used to repair corrosion damaged RC columns.

Also, research has shown that the FRP sheets can act as a low-permeability barrier that prevents a further supply of water and oxygen to the reinforcing steel. As discussed earlier, these are essential for corrosion reactions to take place. Moreover, FRP sheets impede the growth of corrosion products and thus control the corrosion reaction itself by decreasing the corrosion rate (current) and steel mass loss (El Maaddawy et al., 2006; Lee et al., 2000; Soudki and Sherwood, 2000; Debaiky et al., 2002; Suh et al., 2007; Badawi and Soudki, 2005 and Soudki and Masoud, 2006).

1.3.5 Accelerated Corrosion Process

The highest corrosion rate recorded in service is between 10 and 25 $\mu A/cm^2$ (FIB 10, 2000). At this low rate of corrosion tests in a laboratory environment would take years. Therefore, researchers have accelerated the corrosion process by a technique based on the fact that the corrosion process is activated by chloride salts and accelerated by electrical polarization of the steel reinforcement.

Salt is either added to the concrete mix or the test specimen is wholly or partially submerged in a salted solution. The high concentration level of chloride ions depassivates the steel. The steel reinforcement is connected to the positive terminal of an external power supply so that a positive electrical potential is applied to the steel. Thus, the steel is encouraged to release Fe^{+2} ions (i.e. act as anode). Researchers have used external copper or stainless steel plates or internal stainless steel bars or tubes connected to the negative terminal of the power supply to act as a cathode during the corrosion process. In addition, wet-dry cycles are applied to the specimens to facilitate the penetration of water and oxygen to the steel level where they are consumed in the corrosion process.

Power supplies can impress either a constant voltage or a constant current. When the constant impressed current technique is used, the mass loss of the steel is estimated using Faraday's law (ACI 222, 2001):

$$M = \frac{4ait}{zF\rho d_b} \qquad \text{Equation 1.3}$$

Where M is the mass loss ratio of steel, a is the atomic weight of metal (56g for Fe), i is the impressed current density (Amp/cm^2), t is the corrosion time (sec), z is the ionic charge (+2 for steel) and F= Faraday's constant =96,500 amp-sec, d_b is the bar diameter (cm) and ρ is the metal density (7.86 g/cm^3 for Fe).

Current densities as high as 10,400 μA/cm^2 have been used in experiments, however it is recommended that the maximum density applied should not exceed 200 μA/cm^2. This level ensures that the concrete strain and crack width remain the same as those observed for current density values experienced in the field (El-Maaddawy and Soudki, 2003).

1.4 Fatigue of Reinforced Concrete

Reinforced concrete structures such as bridges and offshore platforms are subjected to repeated (cyclic) loading. These structures are expected to resist up to $7*10^8$ cycles during their service life (Tilly, 1979). The effect of repeated loading on reinforced concrete structures has gained attention in the last three decades because of a widespread use of ultimate state design and high strength materials. These two factors resulted in smaller cross sections, thus decreasing the dead load and increasing the live to dead load ratio. To date there have been no reported fatigue failures in reinforced concrete structures. This may be because of the high degree of redundancy in RC structures which allows the fracture of a steel bar to go unnoticed. However, even if repeated loading does not cause fatigue failure, it still affects the serviceability behaviour of the structure by increasing the deflection and the number and width of cracks (ACI 215, 1974). ACI 215 (1974) recommended that for a satisfactory service performance reinforced concrete designers should check for the effect of repeated loading. Fatigue distress may take the form of excessive flexural, shear or bond stresses that may lead to fatigue failure. The committee recommended that the stress range in concrete should be kept to less than 40% of the concrete compressive strength. This would ensure a fatigue life of 10 million cycles. The committee also suggested that the calculated steel stress range, S, should be:

$$S \leq (161 - 0.33 f_{s_{min}}) \qquad \text{Equation 1.4}$$

Where f_{smin} is the minimum steel stress. The left hand side of Eq. 1.4 should not be less than 138 MPa.

For plain concrete subjected to repeated loading, micro-cracks initiate inside a concrete element. After a sufficient number of repeated loads, excessive cracks appear. This leads to a softer stress-strain response of the concrete (ACI 215, 1974). Fatigue fracture of concrete is accompanied by higher strains and more cracks than are found for static loading fracture.

Experiments showed that the fatigue crack in a steel bar always initiates from the base of one of the transverse lugs. The lugs found on the steel bar (introduced to increase the bond strength between steel and concrete) act as stress raisers with a concentration factor of 1.5 to 2.0 (ACI 215, 1974).

1.4.1 Fatigue of Corroded RC Structures

A recent study that examined the effect of corrosion on the fatigue flexural strength of reinforced concrete beams was reported by Al-Hammoud et al. (2007). The authors tested 14 beams subjected to different corrosion levels (0%, 8% and 12% average measured mass loss). Results showed that an 8% and 12% mass loss reduced the fatigue strength on average by 10% and 25% compared to the strength of uncorroded beams. They also reported that an 8% mass loss increased the fatigue notch factor (K_f) to 2.13 compared to a value for the uncorroded beams of 1.94, i.e. an increase of 9%. For beams corroded to a 12% mass loss K_f increased by 25% compared to the value of the uncorroded beams. This suggests that the reduction in fatigue life is proportional to the increase in the fatigue notch factor.

1.4.2 Effect of FRP on the Fatigue Strength of Beams

In recent years several studies were conducted to study the effect of FRP on the flexural fatigue performance of RC structures. The results of these studies showed that if the failure did not happen by FRP de-bonding the failure mode of the RC beam would be by steel rupture. In this case, the fatigue life will increase considerably when strengthened beams are tested at the same load level as un-strengthened beams (Aidoo et al., 2004; and Gussenhoven and Brena, 2005; Toutanji et al., 2006; Heffernan and Erki, 2004; Barnes and Mays, 1999 and Papakonstantinou et al., 2001). However, when beams were tested at the same steel stress levels, the FRP sheets had no effect on the fatigue life (Heffernan and Erki, 2004; Barnes and Mays, 1999 and Papakonstantinou et al., 2001). This is due to the fact that the fracture of the steel reinforcement controls the behaviour of the FRP strengthened

beams and that for a given steel stress the fatigue life will not change whether the beam is strengthened with FRP or not. However, when the FRP strengthened and unstrengthened beams are tested at the same load level, the steel reinforcement in the FRP strengthened beams experiences a lower stress range and therefore a longer fatigue life than the unstrengthened beams. Similar conclusions were also reported for corroded beams. The fatigue life of corroded strengthened beams increased considerably compared to the fatigue life of corroded unstrengthened beams tested at the same load range (Masoud et al., 2001 and 2005; Al-Hammoud et al., 2007).

1.5 Bond of the Steel Reinforcement in Concrete

In reinforced concrete structures, loads are always applied to the concrete and not directly to the steel. Concrete, being weak in tension, transfers at a cracked section all the tensile forces to the steel. In between the cracks, some of the force returns to the concrete. This simple yet fundamental stress transfer system dictates the behaviour of a reinforced concrete element and is the backbone of reinforced concrete theory. The stress transfer results in bond stresses at the interface between the concrete and the steel. Engineers and researchers have long known the importance of bond to reinforced concrete and studies attempting to understand the bond mechanism and its behaviour, dating back to 1877, have been reported in the literature (ACI 408, 2003). The stress transfer (bond) between the concrete and steel allows the two materials to work together and controls the structural behaviour of the RC element. Design equations for bond in codes are based on providing an adequate bond strength to transfer enough force to the steel that it will yield and provide ductility for a RC member (FIB 10, 2000).

The following sections discuss the bond mechanism and bond failure. The main factors that affect bond are also highlighted.

1.5.1 Bond Mechanism

Experiments have shown that the transfer of stresses between concrete and deformed steel bars occurs by the following mechanisms (See Figure 1.3):

- Chemical adhesion between the steel and the concrete,
- Friction between the steel and the concrete, and;
- The mechanical anchorage of the reinforcing steel ribs against the concrete.

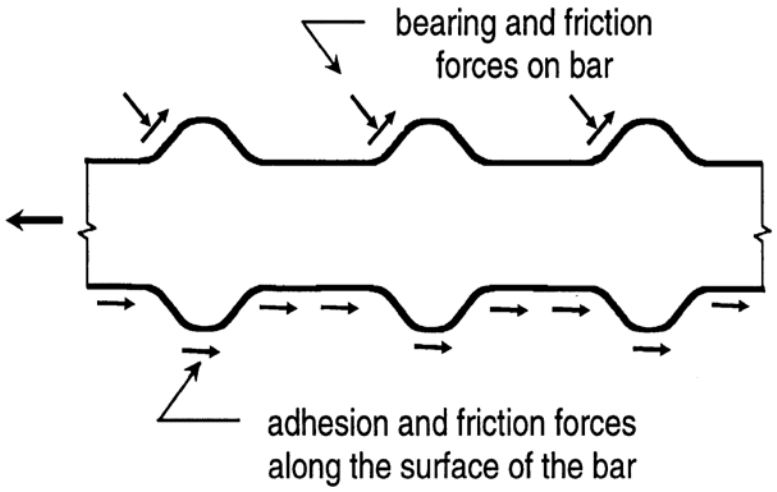

Figure 1.3: Bond transfer mechanism (ACI 408, 2003)

When a beam is loaded for the first time, adhesion initially prevents the bar from slipping (i.e. moving relative to the concrete). As the loading continues, the bond forces exceed the adhesion forces. This breaks the adhesion. Slip commences and bearing forces at the bar rib and friction forces between steel bar and concrete are mobilized. With further increases in slip the friction forces on the barrel of the reinforcing bar are reduced and the main transfer mechanisms are due to friction and bearing forces acting at the steel rib (ACI 408, 2003).

In order to preserve equilibrium, the bond forces on the bar must be resisted by compressive and shear stresses. These can be resolved into an outward component of the resultant bond force and a

shear component parallel to the bar that is the effective bond force (see Figure 1.4). The outward component of the bond force is analogous to an internal pressure exerted on a thick walled cylinder. In this case the cylinder is of concrete and has a thickness that may be modeled as being equal to the smallest concrete cover. In the concrete the outward component of the bond force generates compressive radial stresses and tensile hoop stresses (Figure 1.4). If the bar is well anchored to the concrete (i.e. the anchorage length is long enough), the bond stresses will be distributed over the anchorage length, keeping the tensile stresses on concrete below its tensile strength. This will allow for a high transfer capacity and for the stresses in the bar to become high enough to yield the bar. In this case the RC member will fail by a failure mode other than bond (shear or flexure). If the anchorage length is not long enough the bond stresses (the outward and shear stresses) (Figure 1.4) will be high enough to cause the RC member to fail in bond either by concrete splitting or by bar pullout. If the confinement (concrete cover and steel stirrups) is not adequate, the cracks initiated by the hoop tensile stresses (caused by the outward bond component) will propagate to the concrete surface causing the concrete to split along the length of the bar. When the confinement is large enough, the concrete will not split (because of the resistance provided by the confinement against concrete longitudinal cracking), but rather the shear component of the bond stresses will increase until the concrete keys between the bar lugs are sheared off causing the bar to pullout. Both splitting and pullout failures are sudden and brittle. Once the bond fails the bar slips and the RC member fails since forces will no longer be transferred to the reinforcing bar, and the RC element acts as a plain concrete element (ACI 408, 2003). In practice, given the concrete cover and stirrups provided in RC members, a splitting failure is more likely to happen than a pullout failure in most structural applications if the member is to fail by bond (ACI 408, 2003).

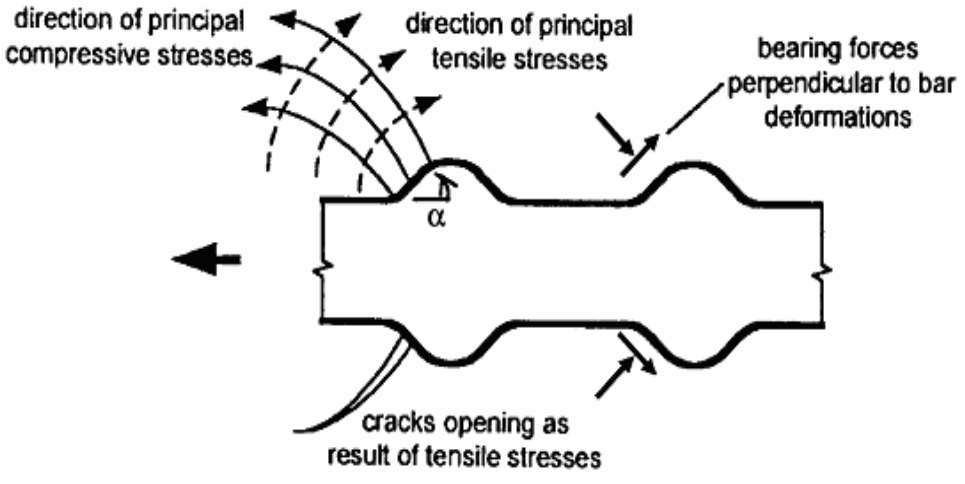

Figure 1.4: Forces and cracks in concrete (ACI 408, 2003)

1.5.2 Factors Affecting Bond Behaviour

From the above qualitative description, it is evident that the bond strength depends on the anchorage length, the concrete tensile and bearing strength, the confinement provided to the bond critical region (by the concrete cover and the internal stirrups or the presence of external FRP sheets), the surface condition of the reinforcing bar, and the geometry of the bar. The following is a discussion of some of the factors that influence the bond behaviour.

1.5.2.1 Development Length

As the bonded length increases, the crack surface at failure increases. Thus, the total bond force required (proportional to the energy required to open a crack) to fail a member increases. The increase in bond stress however is not proportional to the increase in anchorage length because more of the bond forces are concentrated near the loaded end of the bar and therefore, this end is more effective in resisting bond forces than the far free end (ACI 408, 2003).

1.5.2.2 Bar Casting Position

Experimental studies have shown that top-cast bars have lower bond strength than bars cast lower in a member. The reason is that the greater the depth of concrete below the bar, the greater will be the accumulation of bleed water underneath the bar. This water will lower the contact area between the steel bar and concrete resulting in a lower bond strength (ACI 408, 2003).

1.5.2.3 Bar Size

For the same bonded length, the larger the bar the larger the forces required to cause bond failure (since the bar area increases). However, in order to attain the same bar stress, larger bars require a larger bonded length since the surface area does not increase as rapidly as the cross sectional area (ACI 408, 2003).

1.5.2.4 Bar Geometry

It has long been recognized that deformed bars have bond properties superior to those of smooth bars. The reason is that deformed bars benefit from the mechanical anchorage provided by the concrete keys between the ribs (Figure 1.3). Several investigations were conducted to determine the effect of the rib angle and rib height on bond behaviour (Figure 1.3). Results showed that for unconfined bars, the relative rib area (defined as the projected rib area normal to the bar axis divided by the nominal bar perimeter times center to center rib spacing) has no effect on bond strength. For a confined bond critical region, however, the bond strength increases with increasing relative rib area (ACI 408, 2003).

1.5.2.5 Bar Surface Condition

Generally, the bar should be clean from mud, oil and other non-metallic materials that would decrease the surface area available for bond. Epoxy coating the steel bars increases the bar resistance to

corrosion but tends to reduce the bond strength. The main reason for the reduction in strength is the reduced friction between the steel and concrete (ACI 408, 2003).

1.5.2.6 Compressive and Tensile Concrete Strength

For the bond failure discussed in section 1.5.1, the bond strength depends on the tensile (splitting) strength of the concrete. Since the tensile strength is approximately proportional to $(f'_c)^{1/2}$, where f'_c is the compressive strength of concrete, bond strength traditionally has been expressed as $(f'_c)^{1/2}$. However, recently a statistical study on bond strength concluded that bond strength should be expressed in terms of $(f'_c)^{1/4}$ since the ¼ power better represents the effect of concrete strength on bond strength (ACI 408, 2003). This suggests that the tensile strength is not the only factor that affects bond strength. In fact, it appears that the bond strength is directly related to the fracture energy of concrete (ACI 408, 2003). However, more research is needed to validate this observation. In general, as the concrete strength increases, the bond strength increases but at a slower rate than the concrete strength and the failure mode becomes more brittle (ACI 408, 2003).

1.5.2.7 Confinement

The main factor that affects the bond strength is the confinement provided in the bond critical region. The main confinement consists of the concrete around the bar (clear bottom and side covers and one half the transverse spacing between the bars) and steel stirrups. Higher confinement levels can be achieved by providing fibres in the concrete mix (fibre reinforced concrete or FRC) (ACI 408, 2003).

As the confinement increases, the bond stiffness (the slope of the bond stress-slip curve) and the bond strength increase. If the level of confinement is high enough, the failure mode of bond changes from splitting to pullout (ACI 408, 2003).

Increasing the concrete cover and the bar spacing will increase the crack surface area. Therefore, the force required to develop a bond failure increases, thus increasing the bond strength. Transverse reinforcement confines the anchored bars by limiting the progression of a splitting crack. Heavily reinforced steel stirrup increase the confinement and prevent a splitting failure from taking place (ACI 408, 2003).

Adding fibres to the concrete mix not only increases the tensile strength of the concrete but also increases the energy required to open and propagate a crack. Research results have shown that adding fibres to the concrete mix increased the bond strength substantially (ACI 408, 2003). Results also showed that adding fibres improved the post-failure behaviour of bond (resulted in an increase in the residual bond strength), and reduced the slip at the peak bond stress.

1.5.3 The Effect of FRP on Bond

Recently, the use of FRP sheets to repair and strengthen existing structures has caught the attention of researchers working on the bond between steel and concrete. Several studies reported during the last 10 years are summarized here.

Kono et al. (1998) tested twenty-two beam-end specimens designed to fail by bond splitting. The variables examined were the bond length and the CFRP wrapping scheme (full, U-shaped along the entire bonded length and U-shape along half the bonded length) in the bond-critical zone. The tests showed that unwrapped specimens failed in concrete splitting. The use of CFRP sheets led to an average improvement in bond strength of up to 80% and changed the failure mode for fully wrapped specimens from splitting to pullout.

Another study also reported by Kono et al. (1999) investigated the effect of FRP wrapping on bond strength in beams. The study comprised of twenty cantilever type beam specimens and four bond-beam specimens. Test variables included the location of the reinforcing bar when casting (top or

bottom), the clear cover (40, 57, or 72 mm), the bar diameter (19 or 25 mm), the number of reinforcing bars (2 or 4), the type of FRP sheet (aramid or carbon) and the number of layers of FRP sheets (one, two or three). All FRP sheets were placed transversely in the bond critical region. All specimens failed by splitting of the concrete cover. Test results indicated that the confinement provided by the FRP sheets increased the load carrying capacity and lowered the load drop after failure compared to values for unconfined specimens. Bond strength was increased by 15% to 115%.

Hamad, Rteil and Soudki (Hamad et al., 2004a, 2004b, and 2004c) tested seventeen full-scale beams, each designed with reinforcing bars spliced (the splice length was 305 mm) in the constant moment region at midspan. The variables were the nominal concrete strength (28 or 70 MPa), the type of FRP sheets used (carbon or glass), the configuration of the FRP applied in the splice region (a 76 mm strip, two 76 mm strips, or a continuous sheet), and the number of FRP layers (1 layer or 2 layers). Failure of all the specimens was by face and side bond splitting. Test results indicated that FRP sheets enhanced the bond performance of the tension lap splice. The investigators observed that as the confinement due to FRP sheets increased, the post failure ductility improved and the bond strength of the lap splice increased. The increase in bond strength ranged from 8% to 34%. Based on their results they proposed an equation to calculate the additional bond strength due to the presence of FRP sheets.

$$u_{tr,f} = \frac{f_{fe} A_{tr,f}}{16.6 s_f n_b d_b} \qquad \text{Equation 1.5}$$

Where $u_{tr,f}$ is the additional bond strength due to the presence of the FRP sheets, f_{fe} is the effective stress in the FRP sheets, $A_{tr,f}$ is the total cross-sectional area of FRP sheets normal to the plane of splitting within spacing s_f, n_b and d_b are the number and diameter of the steel bars being spliced or developed, s_f is the spacing between FRP sheets, for a continues sheet s_f = width of the sheet.

Another study, which examined the effect of FRP on local bond behaviour under static loadings, used beams with a short lap splice (Harajli, Hamad and Rteil, 2004). The results were similar to those reported earlier in that the FRP was able to increase the bond strength, and provided a more ductile post-failure behaviour. The FRP sheets also were better than steel stirrups in confining the lap splice region because the external confinement is more effective in restraining the splitting crack growth. Based on the experimental results, the authors proposed a bond stress- slip law that will be discussed in section 4.1.

To sum up, research has revealed that FRP sheets confined the concrete, thus slowing down or preventing the growth of the splitting cracks. This increased the bond strength considerably, and improved the post-failure ductility.

1.6 Bond of Corroded Steel

Until recently, little or no research was reported in the literature on the effect of corrosion on bond strength. However, during the last fifteen years the awareness to this problem has increased. Studies conducted using pullout specimens, cantilever bond test specimens, RILEM bond beam and bond anchorage specimens by several researchers (Al-Sulaimani et al., 1990; Cabrera and Ghoddoussi, 1992; Clark and Saifullah 1993; Rodriguez et al., 1994; Almusallam et al., 1996a; Mangat and Elgarf, 1999a; Auyeung et al., 2000 and Fang et al., 2004; to list a few) resulted in a better understanding of the effect of corrosion on bond strength.

Despite the different specimen types, bar diameters, concrete qualities, concrete covers and accelerated corrosion techniques used in the different studies the variation of bond strength with increasing corrosion level was similar in almost all of the studies reported (FIB 10, 2000). This variation is shown schematically in Figure 1.5.

The bond strength increases during small levels of corrosion (Figure 1.5). This initial increase in bond strength was attributed to an increasing roughness of the bars with the growth of a firm layer of corrosion products that increase the frictional component of the bond force (FIB 10, 2000). With a further increase in corrosion, the bond strength starts to reduce to values that are still greater than the uncorroded value. Once longitudinal cracking due to corrosion develops, the bond strength decreases rapidly mainly due to: 1) a severe deterioration of the reinforcing bar ribs that decrease the mechanical anchorage component of the bond strength, 2) a reduced concrete confinement of the bar due to a widening of the longitudinal cracks and 3) an accumulation of a heavy layer of the flaky corrosion products around the bar that act as a lubricant and reduce the friction component of the bond strength. It was also reported that compared to the uncorroded stiffness the stiffness of the bond stress-slip curve increased with pre-cracking corrosion level and decreased with post-cracking corrosion level (FIB 10, 2000). The slip increased at a faster rate as the corrosion level increased. While some studies reported an increase in the slip at the maximum bond stress (Al-Sulaimani et al., 1990) others reported a decrease in the value of the slip (Fang et al., 2004).

In a few studies the specimens were reinforced with transverse reinforcement (stirrups) or fibres were included in the concrete mix. The general behaviour of bond with increasing corrosion levels did not differ from the one described above when these methods of confinement were added. However, a smaller reduction in the bond strength was noted and the post-cracking bond degradation was more gradual (FIB 10, 2000). This points to the fact that confinement provided by stirrups or fibres (as in the case of bond of uncorroded steel bars) increased the bond stiffness and the bond strength.

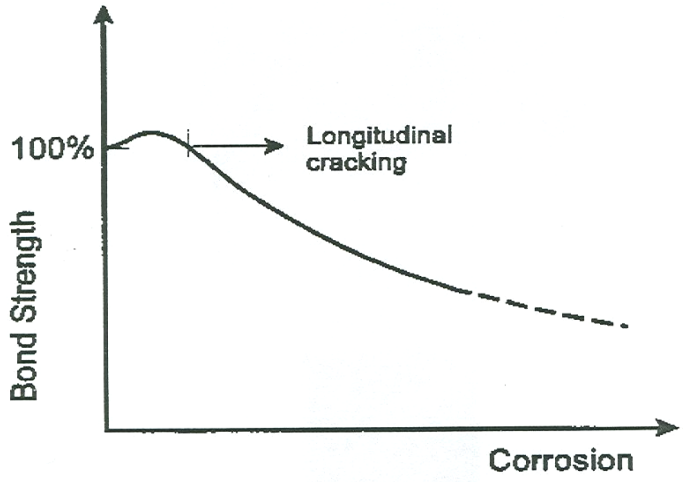

Figure 1.5 Variation of bond strength with corrosion (FIB 10, 2000)

1.6.1 Effect of FRP Confinement on the Bond Behaviour of Corroded Steel Bars

Little work has been devoted to study the effect of the confinement provided by FRP sheets on the bond strength of corroded steel bars. The only previous studies were conducted by Soudki and his co-workers (Soudki and Sherwood, 2003 and Craig and Soudki, 2005). The test specimens used were pullout and bond anchorage beams. Results showed that CFRP confined specimens had a higher bond strength than the un-wrapped specimens at all levels of corrosion. It was observed that the strengthening effect of the CFRP confinement was more evident in specimens with low c/d_b ratios since the thick concrete cover delayed the onset of corrosion. In both studies, the use of CFRP sheets to confine the corroded bond regions changed the failure mode. In the pullout specimens, the failure mode changed from splitting to pullout. While in beam specimens, the mode of failure changed from splitting to flexure failure (steel yielding).

1.7 Bond Behaviour under Repeated Loading

Repeated loading produces a progressive deterioration of bond. This in turn will affect the serviceability of reinforced concrete structures and may lead to a fatigue bond failure. Bond behaviour under repeated loading has received comparatively little attention although conclusions

from the fatigue tests pointed out that the bond between concrete and steel was an important parameter in determining the fatigue strength and the serviceability conditions of a flexural reinforced concrete member (Mor et al., 1992; ACI 215, 1974; Bresler and Bertero, 1968).

One of the first studies on the behaviour of bond under repeated loading was reported by Verna and Stelson in 1962. The authors tested beams designed to fail either in shear, concrete compression, steel rupture or bond. The yield strength of the steel bars was 300 MPa. The variables were concrete strength (19 or 32 MPa) and reinforcement ratio. Test results showed that specimens that failed in bond under static loading would also fail in bond under repeated loading; therefore, specimens that are weak in bond under static loading are susceptible to fatigue bond failure in repeated loading. It was found that bond failure was accompanied by splitting cracks and a decrease in load carrying capacity. The analysis carried out by the authors revealed that bond behaviour under repeated loading is affected by concrete strength and bonded length. They also observed that specimens failing in bond did not withstand more than 75,000 cycles at 40% of the static ultimate strength. Therefore, they recommended a fatigue bond limit of less than 40% of the static strength.

Bresler and Bertero (1968) studied bond stress distribution during repeated loading using concrete cylinders reinforced with one steel bar (28 mm in diameter) subjected to repeated tension. The steel bars were instrumented with strain gauges along the bonded length. The authors observed that during the first cycle, before the concrete cracked, the bond stress was highest at the ends of the cylinder and decreased to zero in the middle (i.e. no transfer of stresses in the middle). After the cylinder was cracked, a redistribution of stresses took place. The bond stress was highest at the ends of the cylinder where the forces are being transmitted from the steel to the concrete and in the middle of the cylinder (at the location of the crack) where the forces are being transferred from the concrete to the steel. The authors also realized that when the load increased, the bond at the ends (where the stresses are highest) of the cylinder was damaged and therefore, the peak bond stress shifted inward. Further

cycling of the same specimen at lower loads did not affect the bond stress. The load level was further increased in steps until the steel yielded. During this increase the deterioration of bond increased and the redistribution of bond stress continued. After 65 cycles, the tests were halted (without failing them in fatigue). The bond stress at cycle 65 (when the test was halted) decreased by 95% compared to the value at cycle 2 for the same applied load.

Perry and Jundi (1969) did tests on pullout specimens to study the stress distribution along reinforcing bars under repeated loading. They observed a shift of the peak bond stress from the loaded to the unloaded end as the number of cycles increased and a reduction of 65% to 90% of bond stress at the loaded end was observed because of repeated loading.

Rehm and Elingehausen (1979) studied the effect of bar diameter, concrete strength and the load amplitude using 308 pullout tests. The results showed that concrete strength and bar diameter had no apparent effect on the fatigue life of the specimens. The slip was influenced by the bond length and upper load applied, but generally, it increased linearly on a log-log scale with number of cycles. The authors realized that since the slip is related to the internal damage of the concrete, then repeated loading (which causes this damage to the concrete) has an influence on the slip and the bond strength of deformed bars that is similar to its influence on the deformation and failure behaviour of un-reinforced concrete. Therefore, they proposed a fatigue limit for bond strength of 50% of the static bond capacity (similar to the ratio of the fatigue strength to the static strength for the plain concrete). The ultimate bond capacity and slip value of the run-out specimens (specimens that sustained one million cycles without failure) loaded statically increased by 5% compared to a specimen loaded statically without prior cyclic loading. Similar to other studies a redistribution of bond stress along the bonded length was observed. The authors pointed out that similar conclusion were drawn from tests failing in bond splitting rather than bond pullout. Finally, the authors compared the slip of steel bars in specimens under repeated loading with that in specimens under sustained loading. They concluded

that the two types of loading had a similar effect on slip, and that repeated loading could be considered as time accelerator compared to sustained loading.

Balazs (1991) studied the effect of cyclic loading (repeated and seismic) on bond behaviour using pullout specimens. The results showed that bond failure can be produced as a result of an increase in slip. The variation of the slip with number of cycles (on linear scale) was as follows (Figure 1.6): first the slip increased in a decreasing rate, and then the rate stabilized until the cyclic slip reached the value of the slip corresponding to monotonic failure. Then the rate continuously increased until failure occurred. He also found that if the bonded length was long enough, the free end slip did not initiate and the loaded end slip became stable. Balazs concluded that the slip rate increased when the maximum applied load increased or the bonded length decreased.

Balazs and Koch (Balazs and Koch, 1992; Koch and Balazs, 1992 and Balazs, 1998) further studied the effect of variable amplitude loading and preloading on bond stress-slip behaviour using pull out specimens. The specimens were subjected to $2*10^6$ cycles in two blocks of 10^6 cycles each. The shape of the loading history in each block of cycles was varied in shape (parabolic, linear, constant, logarithmic or variable) and direction (increasing or decreasing). The test results indicated that with a sequence of increasing maximum loading the slip increased at increasing rate. In the second block of cycles, the slip started to increase only at load equal to 70% of the maximum load. When the loading blocks were of the decreasing type, the slip increased immediately and continued to increase at a decreasing rate as the load was decreased. The slip stopped increasing when the load applied was less than 70% of the maximum load. In the variable amplitude tests, the slip only increased if the load level approached or exceeded the previous highest level. Cycles with a load amplitude less than the previous peak load produced no slip increase and hence no bond damage. Afterwards, the specimens were tested monotonically to failure to determine the effect of the preloading on the bond stress- slip behaviour. The results showed that the bond strength (the bond

stress at failure) decreased as the slip from preloading (residual slip) increased, but for all cases the bond strength was slightly higher than of specimens without preloading. Also, as the residual slip (from preloading) increased the increase in slip to failure decreased.

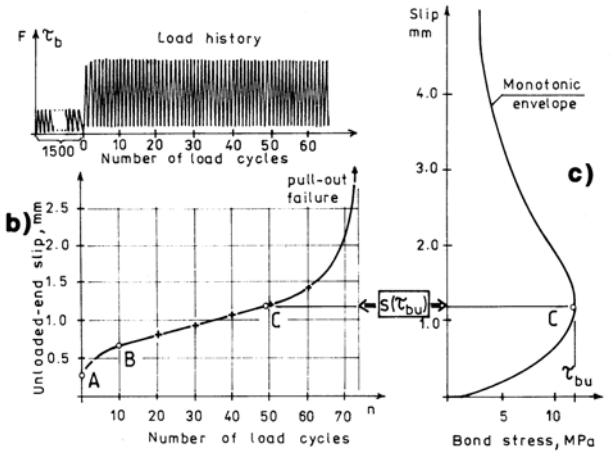

Figure 1.6 Slip-life variation for pullout tests reported by Balazs (1991)

A research reported by Plizzari, Lundgren and Balazs (2002) studied the effect of increasing the confinement on bond under repeated loading using pull out specimens. The confinement was increased either by adding more steel fibres into the concrete mix or increasing the area of the steel stirrups. The slip increasing behaviour was similar to that reported by Balazs (1991). Test results showed that increasing the confinement increased the bond fatigue strength, reduced the bar slip and splitting cracking during repeated loading.

A recently published study by Oh and Kim (2007) focused on the monotonic behaviour of pullout specimens after being subjected to repeated loading (without failing the specimen by fatigue). The variables included the ratio of the repeated stress to static strength and the number of applied cycles. Test results showed that, similar to other studies, the repeated preloading had no effect on the bond strength. Also, the slip value at the peak bond stress for the specimens tested after repeated preloading did not vary much from the slip value of specimens tested without preloading. The slip varied linearly

with cycles on log-log scale. Based on this observation and their experimental results, the authors proposed a cyclic bond stress-slip relationship together with an equation to calculate the expected number of cycles before bond failure, where the bond failure was assumed to occur when the cyclic slip reached the value of the slip corresponding to monotonic failure.

The above discussion leads to the following conclusions. Progressive deterioration of bond, measured as an increase in slip, is observed under repeated loading. The previous studies showed that the slip and therefore the bond deterioration, was significantly affected by the loading history. If the load applied was smaller than a previously applied load then no slip increase was observed. The bond deterioration resulted in a redistribution of the bond stress. If fatigue failure did not take place, then repeated loading history had little or no effect on the bond strength. Finally, it should be noted that all of the previous research on bond under repeated loading was studied using pullout specimens. This type of specimen has several drawbacks that result in a concrete stress field around the steel bar that differs from that encountered in most RC members (ACI 408, 2003).

1.7.1 Effect of FRP Confinement on Bond under Cyclic Loading

To the best of the author's knowledge, the effect of FRP sheets on the bond between steel and concrete under repeated loading has not been studied. However, some studies were reported on the effect of FRP sheets in confining a bond critical region under seismic loading. The experimental results showed that without confinement, the steel bars in the columns subjected to seismic loading slipped causing the columns to experience significant degradation. Confinement reduced the bond degradation at the column base (where a plastic hinge was formed), and thus considerably increased the column absorption and dissipation of the cyclic loading energy (Harries et al., 2006; Harajli, 2006; Harajli and Rteil, 2004).

1.8 Research Motivation

1.8.1 Research Needs

Based on the literature review presented in the previous sections, it is clear that there are several gaps in the understanding of the behaviour of the steel reinforcement-concrete bond under repeated loading especially in the case of corroded steel. These gaps will be highlighted in this section.

It is noted that despite the importance of the steel-concrete bond in determining the behaviour and life of important structures under repeated service loading (such as bridges), only a few researchers studied this aspect of the bond behaviour. Most of them used pull-out specimens which are known to give unrealistic behaviour and bond strength values. Tests conducted on specimens that give true bond performance in beams under repeated loading are missing. In addition, while studies showed that corrosion can be detrimental to bond under static loading, no one has examined the effect of corrosion on bond behaviour in cyclic fatigue loading which is more frequently encountered in bridge and off shore structures than static loading.

The use of FRP to strengthen corroded concrete structures is relatively new and while the studies conducted so far have shown the ability of FRP to confine bond and corrosion stresses and enhance the overall performance, no study has examined the capability of FRP to increase the behaviour of the steel-concrete bond under a combination of corrosion and repeated loading.

The lack of experimental data has resulted in an absence of models that are capable of predicting the performance of steel to concrete bond under repeated loading, especially with corroded steel reinforcement. Such data and models are needed to assess the performance of RC structures under repeated service load as well as in predicting the residual strength of these structures.

1.8.2 Research Objectives

This study was designed to address some of the needs discussed above and enhance our understanding of the bond-corrosion-repeated loading problem. The issues that have been focused on in this program are:

- Studying of the effect of repeated loading on the bond between concrete and uncorroded steel and the ability of the FRP sheets to enhance its performance.
- Investigating the effect of corrosion on bond under repeated loading and the capability of FRP sheets as a repair system to restore the bond strength.
- Quantifying the effect of a FRP repair on the performance of post repaired corroded bond specimens under repeated loading.
- Developing a model that is capable of predicting the capacity of the bond between steel (corroded or uncorroded) and concrete (FRP confined or unconfined) under repeated loading in RC structures.

Chapter 2
Experimental Program

2.1 General

The experimental program consisted of casting and testing forty-seven beams (152 x 254 x 2000 mm). Since the main objective of this study was to determine the fatigue bond behaviour of corroded and uncorroded reinforcing bars, the test specimens were designed to fail in the bond-critical region by concrete splitting. Thirty-five of these beams were subjected to accelerated corrosion to investigate the effect of corrosion on the fatigue bond strength. Twenty-six beams (corroded and non-corroded) were wrapped with carbon fibre reinforced polymers (CFRP) sheets in the anchorage zone to determine the effect of CFRP confinement on the fatigue bond behaviour. Two beams were tested under monotonic loading while the remaining forty-five (45) beams were tested under repeated loading until the beam failed by fatigue. This chapter describes the test program, the specimen configuration and fabrication, the accelerated corrosion process, the repair with CFRP sheets, the instrumentation, and the test setup and procedure.

2.2 Test Program

Forty-seven beams were cast and tested. Two (2) specimens (one wrapped and one unwrapped) were tested monotonically to determine the static bond capacity of the specimen, and forty-five (45) specimens were tested in repeated loading. The test variables in this study were the amount of CFRP used (none or one U shaped layer), the time of corrosion exposure when the CFRP was applied (0, 50, 100 and 150 days), the time of corrosion exposure when the beam was tested (0, 50, 100, and 150 days), and finally the load level applied.

The test matrix was divided into eight groups given in Table 2.1. Originally, the beams exposed to 100 and 150 days of corrosion were in separated in two groups. However, the mass loss analysis revealed that beams subjected to 100 and 150 days of accelerated corrosion had on average 8.3% and 9.6% mass loss (see section 3.2). The difference in steel mass loss between the two corrosion exposure times was not significant. The structural behaviour will be dictated by the actual mass loss (rather than the corrosion exposure time) since this is a measure of the rust volume that causes tensile stresses in the concrete and leads to the loss of bond between the concrete and steel. Accordingly, for analysis, the beams corroded for 100 and 150 days (theoretical mass loss of 10% and 15% respectively) were treated as a single group with an average steel mass loss of 9.0%.

Beams in group M (M for monotonic) were tested under monotonic loading to determine the static load capacity of the test specimens, two un-corroded beams, one wrapped with CFRP sheets and one without wrapping, were tested.

Table 2.1: Test matrix

Set*	**Time of corrosion when FRP applied (days)**	**Time of corrosion when tested (days)**	**Number of load ranges**	**Number of specimens**
M	No FRP	0	Static	1
	0	0		1
UW0	No FRP	0	5 to 10 load ranges	5 to 10 in each group
W0	0	0		
UW5	No FRP	50		
UW9	No FRP	100 or 150		
W5	50	50		
W9	100 or 150	100 or150		
PR	50	150		

* M for monotonic, UW for unwrapped, W for wrapped, PR for post repair and 0, 5, and 9 are the measured percentage mass loss of steel bars due to corrosion.

The other seven groups were tested under repeated loading. The difference between specimens in the same group was the load range at which the beam was tested. The difference between different groups was the measured corrosion mass loss and the presence or absence of CFRP sheets.

Group UW0 consisted of uncorroded and unwrapped beams (control beams). Group W0 contains uncorroded wrapped beams (control wrapped). Both groups acted as a benchmark to which other groups were compared. Groups UW5 and UW9 consist of unwrapped beams (UW in the group name stands for unwrapped) corroded to 5 and 9% measured corrosion levels respectively. The objective of this set of beams was to study the effect of corrosion on the fatigue of bond. Therefore, once the specified corrosion exposure time for each of these beams was achieved, they were tested. Groups W5 and W9 consist of wrapped beams (W stands for wrapped) corroded to 5 and 9% measured corrosion levels respectively. The aim of these groups was to investigate the effectiveness of CFRP sheets in confining bond critical regions under a repeated loading regime, and the effect of corrosion level on this effectiveness. After corroding the specimens in these groups to their specified corrosion times, they were wrapped with CFRP sheets and then tested. Finally, beams in group PR (post repair) were corroded for 50 days (5% mass loss), and then repaired with CFRP sheets followed by further corroding them for another 100 days before they were tested (the total corrosion exposure time for group PR was 150 days and the average measured mass loss was 10.3%). The aim in testing this group was to determine the post-repair behaviour of the fatigue bond strength.

2.3 Test Specimen

In order to get a practical bond behaviour and realistic bond stress values the test specimen selected for this research was a beam-anchorage specimen. This special type of beam has steel bars that are un-bonded in the middle span of the beam with a bonded length (anchorage length) at the ends of the beam. In this study, the beams have a rectangular cross section 152 mm x 254 mm, and are 2000 mm

in length. The beams were tested under four-point bending with a total span of 1800 mm and a constant moment region of 600 mm. Each beam was reinforced with two 20M deformed bars (d_b=20 mm) on the tension side. The bonded length (l_b) at each end of the bars was 250 mm (l_b/d_b = 12.5). This bonded length was selected to ensure a bond splitting failure. Compression reinforcement consisting of two smooth bars 8 mm in diameter was also provided. A smooth stainless steel bar in the form of a tube 9.5 mm in diameter was placed 80 mm from the bottom of the beam specimen to serve as a cathode during the accelerated corrosion process. The tensile reinforcement and the stainless steel bar were extended about 100 mm from each end of the beam to allow for electrical connections during accelerated corrosion and to allow the installation of bar slip instrumentation for testing. Stirrups consisting of smooth bars 8 mm in diameter were provided at a spacing of 125 mm along the entire length of each beam. Figure 2.1 shows the test specimen. In order to provide the required anchorage length, a low-density polyethylene (LDP) tube (Figure 2.2) was placed over the reinforcing bars in the un-bonded zones, in the middle and at 100 mm from each end of the beams (Figure 2.1). Also, two pockets (152 x 75 x 50 mm) at the end of the un-bonded length were provided to allow for easy instrumentation of the tension steel. Blocks of high-density foam (Figure 2.3) were installed around the tension reinforcement during casting to create these pockets (Figure 2.1).

2.4 Specimen Fabrication

All the reinforcing steel, the stainless steel tubes, the LDP tubes and the high-density foam blocks were cut to the desired dimensions. The stirrups were fabricated using an electric-bar bending machine. Before constructing the cages, the stirrups used in the anchorage zone (3 from each end of the beam) were cleaned with a petroleum solvent called varsol and with isopropanol, and then coated with epoxy to ensure that they would not corrode during the corrosion process. The epoxy coating used was BAR-RUST-235 manufactured by Devoe coatings. An electrical tape also covered the

stirrups to ensure that the electrical current is restricted to corroding the tensile steel reinforcement only (Figure 2.4). Then the low-density polyethylene tube (LDPT) was placed over the reinforcing bar in order to create an un-bonded length in the middle zone of the beam (Figure 2.5). Blocks of high-density foam were later installed around the tensile reinforcement at both ends of the LDPT to create the required pockets (Figure 2.5). The blocks also maintained the desired steel bar cover. The reinforcement cages were then prepared in accordance with typical construction practice. Figure 2.5 shows a fabricated steel cage.

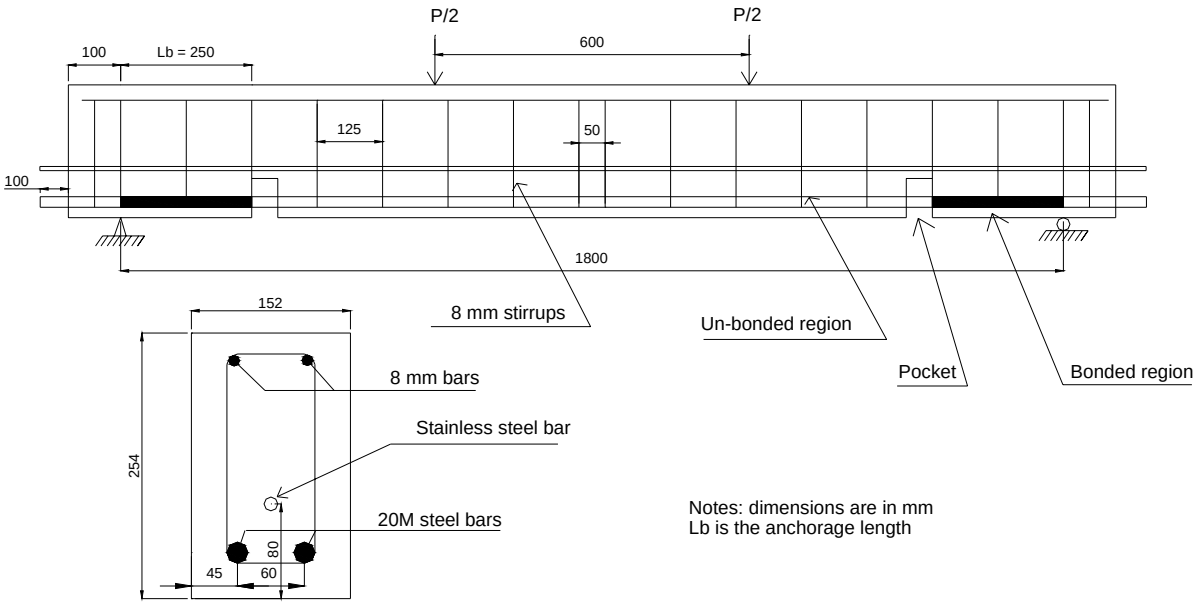

Figure 2.1: Longitudinal and cross sectional details of the test specimen

Figure 2.2 Low-density polyethylene tube used to create the un-bonded zone

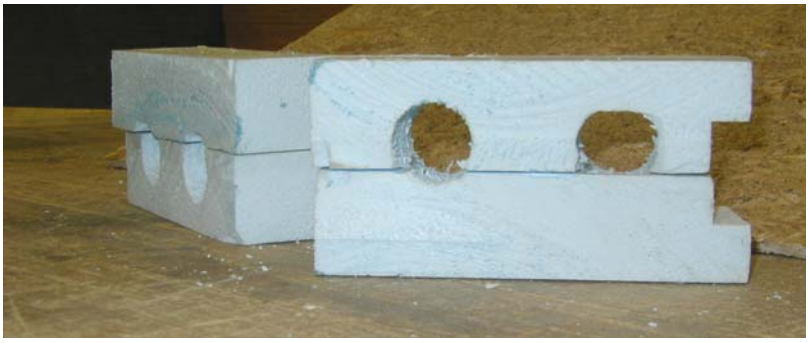

Figure 2.3: High-density foam used to create the pocket at the end of the bonded zone

Casting of the test specimens was done in two stages. Four reusable wood forms (each has a capacity of five beams) were used in addition to three steel forms. The end plates of the beams were drilled to allow for the extension of both the reinforcing bar and stainless steel. Cove moldings, 6 mm in radius, were placed along the edges of the anchorage zone. The cove molding produced a round corner to facilitate the application of the transverse CFRP sheets (Figure 2.6). Figure 2.7 shows a general view of the steel reinforcement inside the form.

Figure 2.4: Epoxy coated stirrup covered with electrical tape at the corners

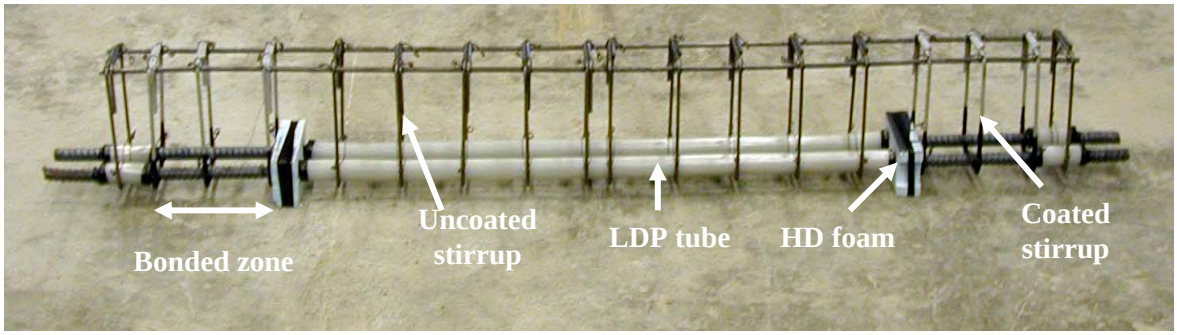

Figure 2.5: The fabricated cage

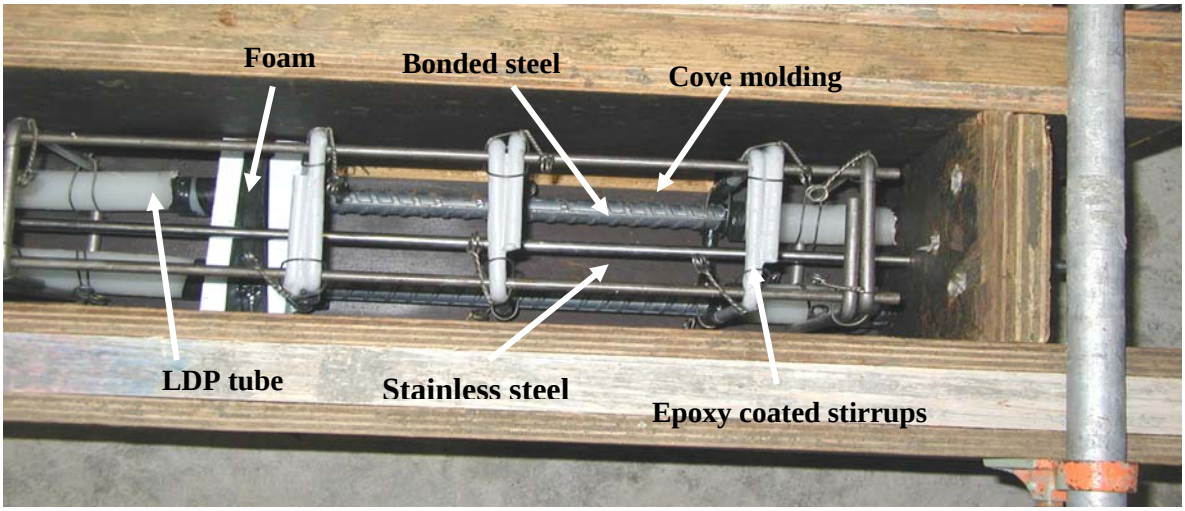

Figure 2.6: Cage inside the casting form –close up view

Figure 2.7: General view of the cages in the formwork before casting

A local ready-mix plant supplied the concrete. Salt, to help initiate the corrosion process, was added to the concrete on site. Therefore, each mix came in two trucks, one for salted and one for unsalted concrete. The concrete mix design called for a water-cement ratio of 0.60 (see section 2.7). The concrete delivered in both trucks had a water-cement ratio of 0.50. Water was added on site to both trucks to increase the water-cement ratio to 0.6 (Figure 2.8). For the salted concrete, salt was mixed in and added with the water. The water added was mixed in the truck for about 2 minutes, and then the salted concrete was poured to fill the bottom one third of the forms while the unsalted concrete was used to fill the remaining two thirds of the specimens. All specimens were cast in a horizontal position. The concrete was compacted using hand held vibrators and trowel finished after the completion of the cast (Figure 2.9a). Several concrete cylinders 100 mm x 200 mm were cast with the beams for later use in measuring the compression strength of both the salted and unsalted concrete.

A few hours after the casting, the forms were covered by wet burlap for curing. After three days, the beams were stripped, stacked and covered with wet burlap and plastic sheets to moisture cure them for about 14 days (Figure 2.9b).

Figure 2.8: Salted and unsalted water added to the ready-mix concrete

a) Concrete vibration

b) Beams Curing

Figure 2.9: Vibrating and curing of the beams

2.5 Accelerated Corrosion Technique

In order to achieve significant levels of corrosion in a reasonable amount of time, an accelerated corrosion technique is used in the laboratories worldwide. As discussed in section 1.3.5, in this procedure corrosion is initiated by either adding chlorides to fresh concrete or immersing the concrete specimen in salted water. The corrosion is accelerated by electrical polarization of the reinforcing steel bars that act as anodes while stainless steel, either cast in the concrete specimen or attached externally to it, acts as a cathode. The specimen is subjected to wet and dry cycles during this process.

In this study, salt was added to fresh concrete during casting (see section 2.4). Salted concrete was poured and consolidated in the bottom third of the beam. Unsalted concrete was used for the remainder of the beam. The polyethylene tube, used to un-bond the reinforcement in the middle and end zones of the beams, acted as a barrier to protect the bars in this region so that they would not corrode. Consequently, the reinforcing steel bars were corroded only in the bonded zone (see Figure 2.1 and Figure 2.5). The amount of salt added to the concrete mix corresponded to a weight of chloride (Cl^-) equivalent approximately to 2.3% of the weight of the cement. This amount of chloride is well above the corrosion initiation threshold required to ensure that corrosion does start (ACI 222, 2001).

In order to accelerate the corrosion process, the beams were connected to external power supplies (Figure 2.10a). The power supplies have a capacity of 500 mA and allow the application of a constant current with an accuracy of 1.0 %. The beams were connected in series to ensure an equal current in all the beams. The direction of the current was adjusted so that the tension steel served as the anode and the stainless steel served as the cathode (Figure 2.10b). Each group of beams with a target corrosion level was connected to one power supply. The power supplies were adjusted to give a constant current density of 150 $\mu A/cm^2$. This level was suggested by El Maaddawy and Soudki (2003) based on their experimental results. To achieve the required current density for a surface area of 612 cm^2 of corroding steel per beam, the current applied through the power supplies was 92 mA. Using Faraday's law (Eq. 1.3), the theoretical mass loss was calculated for each exposure time. Therefore, the theoretical mass loss for 50, 100 and 150 days were 5%, 10% and 15% respectively. The corrosion started at least 28 days after casting.

In order to provide wet/dry cycles the beams were corroded in a special chamber. A fogging compressed air mist nozzle was used to spray mist over the test specimens. The nozzle combines air and water to provide an ultra-fine spray during the wet cycle.

2.6 CFRP Repair

2.6.1 Repair Scheme

A single repair scheme was implemented in this study. One layer of U-shaped CFRP flexible sheet (250 x 650 mm) covered both bonded areas of the beam. For the CFRP sheets to be able to confine the concrete against corrosion and bond stresses, the fibres were oriented transversely to the longitudinal steel reinforcement in the bonded region (Figure 2.11).

a) Power supplies

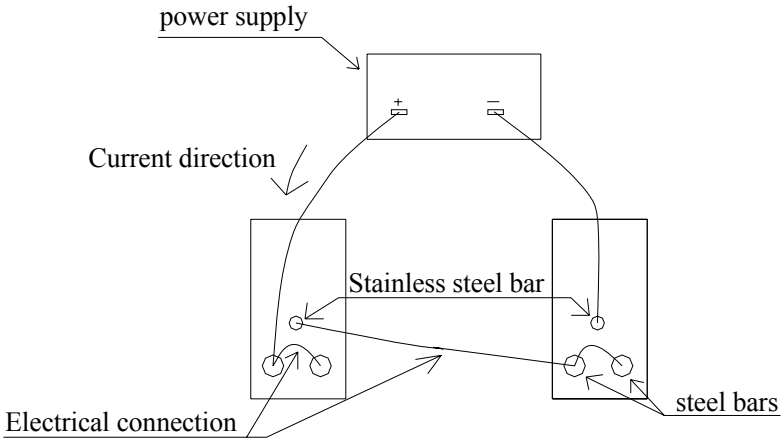

b) A schematic of the accelerated corrosion setup

Figure 2.10: Electrical connections for accelerated corrosion

2.6.2 CFRP Application

Prior to the application of the CFRP sheets the longitudinal corrosion cracks in the corroded beams were sealed using an epoxy paste adhesive, SIKADUR 31 Hi-Mod Gel, manufactured by SIKA Canada (SIKA, 2007). The epoxy adhesive was applied manually using a trowel. After the epoxy had cured for about 24 hours, the concrete surface was ground to remove the weak concrete surface layer and to round the specimen corners for the CFRP application. A high-pressure air-jet was used to clean the surface of all dust and foreign particles after grinding (Figure 2.12a).

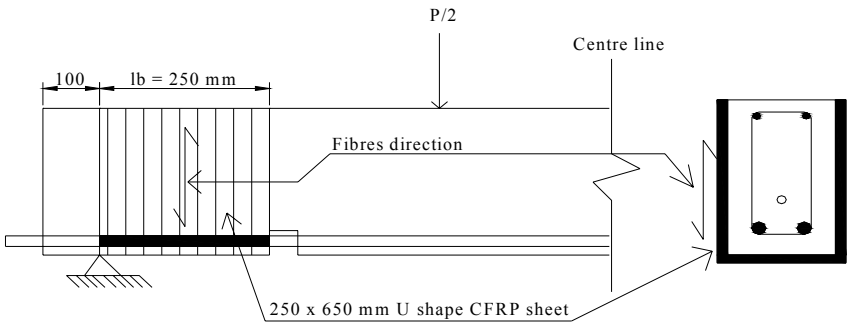

Figure 2.11: Repair scheme

The CFRP sheets were cut to the appropriate dimensions (250 mm x 650 mm). Then the epoxy was prepared by mixing its two components for about 5 minutes using a low speed drill (400-600 rpm) (Figure 2.12b). The epoxy was then applied to the beams at the appropriate location. The CFRP sheets were then bonded to the beams (Figure 2.12c). Finally, in order to achieve a better bonding between the concrete and CFRP sheets, the sheets were subjected to pressure using a threaded roller that forced the epoxy to squeeze out between the fibres and expelled air pockets between the CFRP sheets, the epoxy and the beam. The beams were wrapped 28 days after casting or for corroded beams after the end of the corrosion process. The wrapped beams were left for at least 14 days for the CFRP system to cure (Figure 2.12d) before they were either tested or subjected to further corrosion.

a) Ground beams

b) Epoxy mixing

c) CFRP sheet application

d) CFRP system curing

Figure 2.12: CFRP application procedure

2.7 Material Properties

The concrete was made with an ordinary Portland cement (Type 10) and a maximum aggregate size of 20 mm. The concrete mix proportions are provided in Table 2.2. The average of the measured compressive strength of the first concrete mix at the time of testing was 40 MPa and 41 MPa for the salted and unsalted mixes respectively, while that of the second mix was 42 MPa for both salted and unsalted mixes.

The 20M deformed tension steel bars and the 8 mm smooth compression and stirrup steel bars used in this study were Grade 400 with a nominal yield strength of 420 MPa (as provided by the steel supplier). The stainless steel used was in the form of seamless tubes with outer and inner diameters of 9.5 mm and 8.6 mm respectively. The tubes were Type 304L ASTM A213.

The CFRP sheets used were SIKAWRAP 230C and the epoxy was SIKADUR 330 (Sika, 2007). Both the sheets and epoxy were supplied by SIKA Canada. The mechanical properties of the fibres, epoxy and the cured system are provided in Table 2.3.

Table 2.2: Concrete mix proportions

	Un salted concrete	**Salted concrete**
Coarse aggregate (kg/m^3)	1130.0	1130.0
Sand (kg/m^3)	875.0	875.0
Cement (kg/m^3)	290.0	290.0
Water (kg/m^3)	174.0	174.0
Salt (kg/m^3)	0.0	11.1
Water cement (w/c) ratio	0.6	0.60

Table 2.3: Mechanical properties of the CFRP 230C system

	Fibres	**Epoxy**	**CFRP system**
Tensile strength (MPa)	3450	30	715
Tensile modulus (MPa)	230000	--	61012
Elongation (%)	1.5	1.5	1.09
Thickness (mm)	--	--	0.381

* Supplied by the manufacturer data sheet (SIKA, 2007)

2.8 Instrumentation

2.8.1 Strain Measurements

All wrapped beams were instrumented with eight electrical strain gauges (2 gauges x 2 sides x 2 ends) that measured the stress in the CFRP sheets during testing. The locations of the strain gauges on one side of the CFRP sheet are shown in Figure 2.13. The orientation of the strain gauges on the CFRP sheets was along the fibre direction. They were placed at the level of the centroid of the steel reinforcing bars.

Prior to the attachment of the strain gauges to the CFRP sheets, a small amount of SIKADUR 300 (SIKA, 2007) was poured on the surface of the CFRP at the location of the strain gauges to form a thin film. This epoxy film provided a smooth surface to mount the gauges. After it cured, the surface was then cleaned using isopropanol. A special adhesive was applied to the gauge-bonding surface, which was immediately bonded to the epoxy film on the CFRP surface. An adequate pressure was imposed manually on the gauge surface to expel entrained air and to ensure full bonding between the strain gauge and the CFRP laminates. Subsequently, the strain gauges were connected by shielded wires to a data acquisition system.

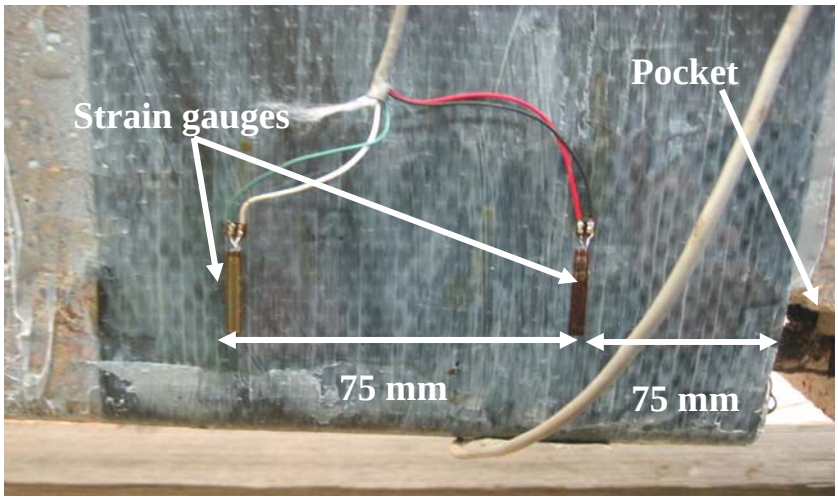

Figure 2.13: Location of the strain gauges on the CFRP sheets

The steel strain was also measured during testing by means of electrical resistance strain gauges. The steel strain gauges were mounted on the tension steel bars in the pocket. Two strain gauges were used; one in each pocket at both ends of the beam (Figure 2.14). The steel bars were filed to smooth their surface, and then cleaned with acidic chemicals. Finally, the strain gauges were bonded to the steel bars.

In addition, for the uncorroded beams (Groups UW0 and W0) six strain gauges (3 on each end) were mounted along the anchorage length and another six on the stirrups (3 at each end) to measure the variation of the steel stress along the bonded length and the contribution of the steel stirrups in confining bond critical regions. Figure 2.15 shows the location of the internal strain gauges on the steel bars. To protect the strain gauges and their connection from moisture during casting, they were coated with a protective wax.

All the strain gauges used had a resistance of 120 Ω and were manufactured by KYOWA Japan. The strain gauges mounted on the CFRP had a 30 mm gauge length while those mounted on the steel in the pocket had a 5 mm gauge length and those used in the anchorage zone on the steel bar and on steel stirrups were 2 mm in length.

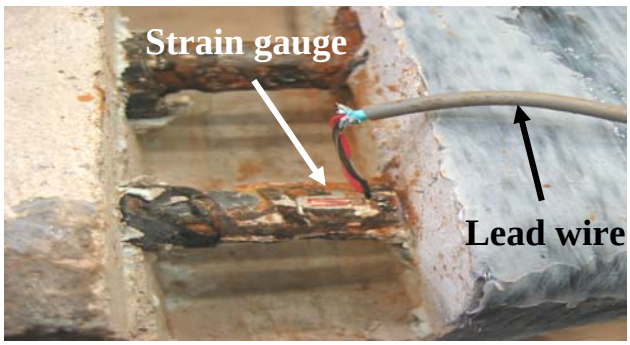

Figure 2.14: Steel strain gauge mounted in the pocket

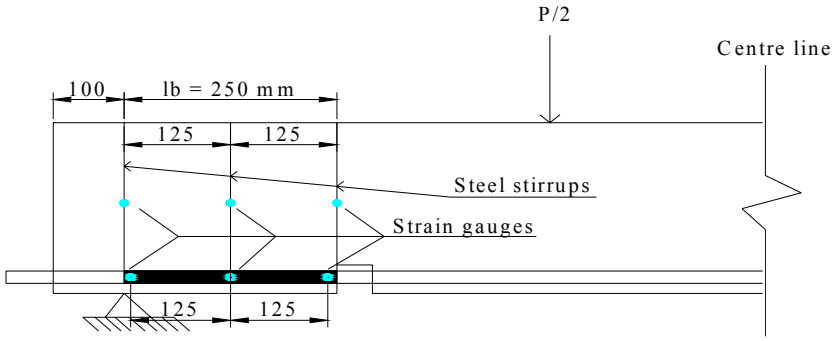

Figure 2.15: Internal steel strain gauge locations

2.8.2 Load, Slip and Deflection Measurements during Testing

During testing (static and repeated loading regimes), load was measured using a 330 kN load cell mounted on the actuator. Midspan deflection was monitored using a linear variable differential transducer (LVDT) with a 100 mm range placed at the beam midspan. Eight (8) LVDTs (4 on each side, 2 for loaded end slip measurement and 2 for free end slip measurement), with a 12 mm displacement range, were fastened to the extended end of the tension bars and in the pocket using specially designed mounts in order to monitor both the free and loaded end slip of the steel reinforcing bar (Figure 2.16). In this study, slip refers to the movement of the reinforcing bar relative to the concrete.

Figure 2.16: Free and loaded end slip measurements

2.8.3 The Data Acquisition System

A SCXI system from National Instruments (NI) was used as a data acquisition system. This system is capable of handling 32 strain gauge channels as well as 32 analog channels (LVDT and load cells). The system was connected to a computer that runs a LabView program that was specially developed for long-term repeated loading. The program was structured such that the user can specify the interval of time at which data is sampled and saved. The software was set to a sampling rate during testing of 30 KHz and it saved the data at a rate of 30 Hz. Figure 2.17 shows the hardware components of the data acquisition system used to capture the data.

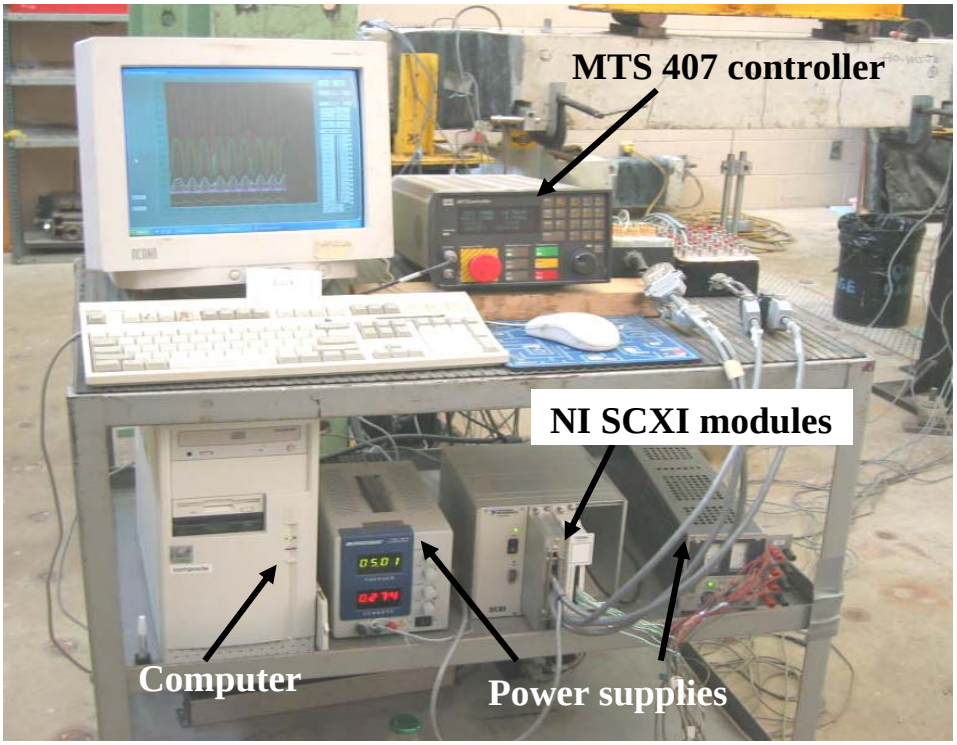

Figure 2.17: Data acquisition system

2.9 Test Setup and Procedure

The specimens were tested in four point bending (Figure 2.18) using a servo-hydraulic actuator controlled by a Material Testing System (MTS) 407 controller (Figure 2.17). The monotonic tests

were performed in stroke control. All the fatigue tests were performed in load control. Initially load was applied manually until the desired maximum load was reached. The load was then decreased until the mean load was reached. Then the controller was used to automatically apply a repeated loading-unloading sequence about the mean load in a sine wave path with a frequency of 1.5 Hz (Figure 2.19). The minimum load was kept constant for all tests at 10% of the specimen's static load carrying capacity while the maximum loads, which were different for each specimen, was varied to give the desired range of fatigue lives (between 1,000 and 1,000,000 cycles). Tests were stopped either when the specimen failed or at 10^6 cycles (categorized here as a run out). Failure was defined as the point at which the maximum load was no longer achieved, because the specimen had lost its ability to carry the test load. Specimens that ran out were tested again at a higher load range.

Figure 2.18: Test setup

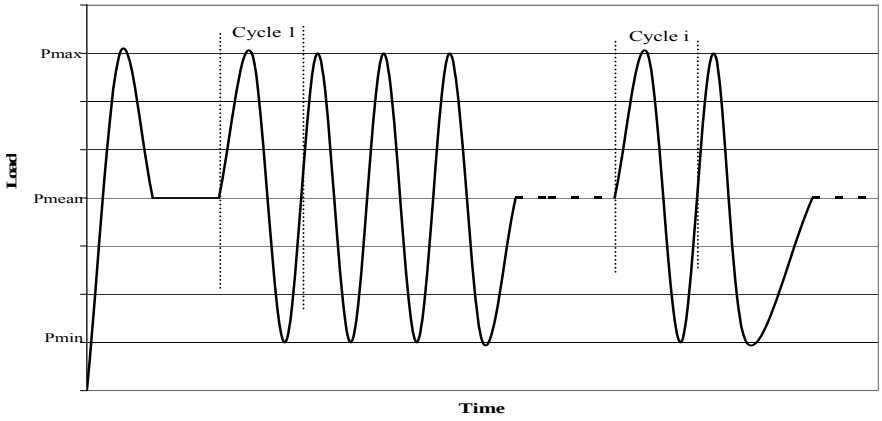

Figure 2.19: Load history

2.10 Gravimetric Steel Mass Loss Measurements

Faraday's law was used to calculate the theoretical mass loss due to corrosion given the exposure time and current density. However, laboratory experiments have shown that the actual mass loss deviates from the predictions of this law (Fang et al., 2004; and Badawi and Soudki, 2005). Therefore, in order to determine the actual steel mass loss, a mass loss analysis was conducted according to the ASTM standard (ASTM G1, 2003). The ASTM standard recommends six different chemical solutions to clean corroded steel bars; procedure C.3.5 in the ASTM standard was used in this study because it works at room temperature, requires inexpensive chemical products and has shorter cleaning times than the other procedures. The chemical solution was made with 500 ml of concentrated hydrochloric acid (HCl), 3.5 gm of hexamethylenetetramine and 500 ml of reagent water (Figure 2.20a). At the end of each corrosion phase and after testing the beam to failure, four coupons of the corroded bars, each 250 mm long, were extracted from the bonded (corroded) zone of each beam (Figure 2.1 and Figure 2.5). These coupons were cleaned of rust using the chemical solution described above. The cleaning process included submerging the steel coupons in the chemical solution for at least 2 hours (Figure 2.20b), and then brushing each one with water, followed by drying and weighing them. The procedure was repeated until the weight change of each coupon between successive applications of the procedure was negligible.

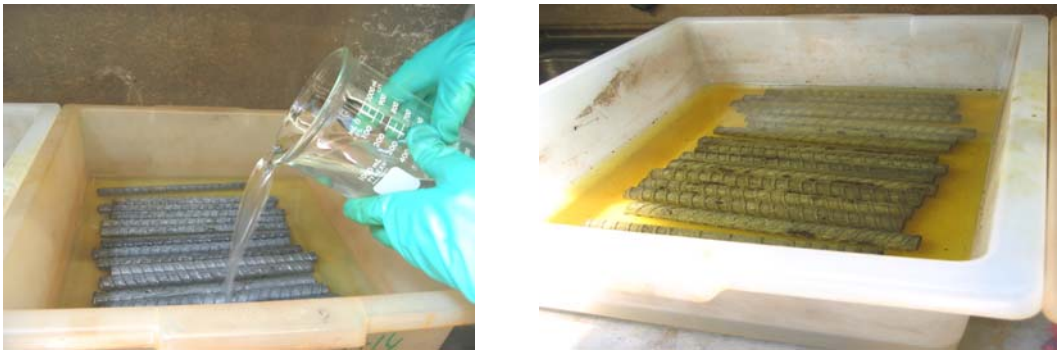

a) Adding HCl solution to steel bars b) Chemical cleaning process

Figure 2.20: Corrosion products cleaning process

Chapter 3
Experimental Results and Discussion

3.1 General

This chapter presents results pertaining to the performance of the fatigue of bond between corroded and uncorroded reinforcing bars and concrete in unconfined and CFRP confined beams. Forty-five beam-anchorage specimens were cast and tested under repeated loading. Thirty-five of these specimens were corroded to different values of mass loss. Twenty-five of the specimens were repaired using CFRP sheets. In addition, two specimens (one wrapped and one unwrapped) were tested monotonically to determine the static bond capacity of the specimens. After the specimens were tested, coupons of the steel reinforcement were extracted and the corrosion mass loss was measured. The results of the static tests and the fatigue performance of the beams are presented and discussed. The discussion will focus on the behaviour of the tested specimens, the variation of their life with the applied load range, and the variation of the slip of the steel bars with the number of load cycles.

3.2 Steel Mass Loss Results

In order to determine the actual steel mass loss due to the accelerated corrosion, steel mass measurements for all corroded beams were performed according to ASTM standards (see section 2.10). The mass loss per beam was taken to be the average of the four (4) bonded steel coupons each 250 mm in length (i.e. the total corroded length of the steel bars in each beam).

A visual inspection of the bars was first conducted. For steel bars corroded for 50 days (a theoretical mass loss of 5% according to Faraday's law), the corrosion was almost uniform with a shallow cross-sectional area loss (Figure 3.1). Small pits were also observed in this group. The steel

bars corroded for 100 and 150 days (theoretical mass losses of 10% and 15% respectively) had more pits. Often, the pits were deep and large enough to form one long pit especially in the steel that was exposed for 150 days of corrosion (Figure 3.2).

For beams corroded for 50 days, the measured mass loss per coupon ranged from 3.5% to 8.0%. The average mass loss per beam (4 coupons) ranged from 4.4% to 6.5%. The overall average for all the beams was 5.6%, close to the 5% predicted using Faraday's law.

Figure 3.1: Uniform corrosion for steel bars corroded for 50 days

a) Exposure time 100 days b) Exposure time 150 days

Figure 3.2: Pits shown on a steel bar corroded for 100 and 150 days

In the beams corroded for 100 days, the measured steel mass loss ranged from 7.0% to 10.1%. However, the average per beam (4 coupons) ranged from 7.4% to 9.2% with an overall average of

8.3%. Beams corroded for 150 days experienced a similar scatter. The measured mass loss of the coupons varied between 7.2% and 12.3%. The average steel mass loss per beam varied between 8.0% and 11.5% with an overall average steel mass loss of 9.6%. The beams repaired after 50 days corrosion exposure and then further subjected to 100 days of corrosion showed similar results (an average mass loss 9.8%) to the beams subjected to continuous corrosion for 150 days. Faraday's law overestimated the steel mass loss for beams exposed to 100 and 150 days of corrosion. This kind of deviation was also reported by other researchers (Badawi and Soudki, 2005 and Soudki and Masoud, 2006). This is believed to be due to the penetration of the corrosion products building up around the reinforcing bar surface through the surrounding concrete pores, thus forming a physical barrier to the ingress of water and oxygen and slowing their movement toward the bar (Badawi and Soudki, 2005). Figure 3.3 presents the actual mass loss versus the exposure time for all the corroded beams. The complete data for the mass loss measurements are presented in Appendix A.

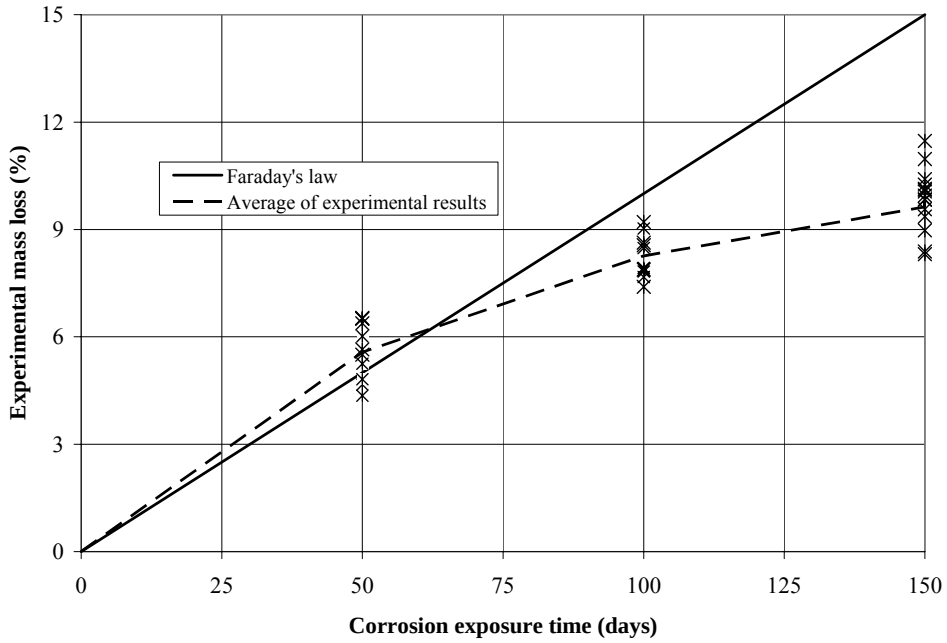

Figure 3.3: Variation of the experimental steel mass loss with corrosion time

For the specimens that were corroded to 5% (50 days corrosion exposure), repaired then subjected to further corrosion, the corrosion level did not differ from that of specimens that were subjected to the same continuous corrosion time. This is because, although the CFRP wraps prevented the oxygen and moisture from penetrating the concrete in the bonded zone, the oxygen and moisture were still able to get to the corroding bar from the unwrapped area (in the middle) of the beam. Therefore, the corrosion reaction was not greatly affected by the presence of the FRP sheets. It is recommended that if FRP sheets are to be used to control the corrosion activity, they should be used along the entire beam, either as a continuous sheet or as intermittent sheets with epoxy covering the areas between the sheets.

3.3 Load Ranges and Test Results

The beam notation used was in the form of: Ax-Wy-Tz. The first two letters give the loading regime (F for fatigue and M for monotonic) and the load range x (as a percentage of the static load capacity) applied. The second two letters indicate whether the beams were wrapped (W for wrapped and N for unwrapped) and the measured steel mass loss y when the beam was wrapped, and the third part of the notation, Tz, indicates that the beam was tested when it had a measured steel mass loss of z. The letters a, b or c that appear after the last part of the notation are to differentiate between beams in the same group tested at the same load range.

As mentioned previously, the minimum load applied in the repeated load tests was equivalent to 10% of the beam's static capacity. The unwrapped beams had a static capacity of 100 kN, therefore, the corresponding minimum load was 10 kN (Table 3.1, groups UW0, UW5 and UW9). The wrapped beams were able to sustain 139 kN in the static test. The minimum load applied on those beams was 14 kN (Table 3.1, groups W0, W5, W9 and PR).

The maximum load applied to the unwrapped beams varied between 40 kN and 65 kN. This corresponds to load ranges between 30% and 55% of the static capacity of the unwrapped beam (M-N-T0) respectively (Table 3.1, groups UW0, UW5, and UW9). For the wrapped beams, the maximum load applied ranged from 76 kN to 111 kN. This corresponds to load ranges between 45% and 70% of the static capacity of the wrapped beam, M-W0-T0 (Table 3.1, groups W0, W5, W9 and PR).

Table 3.1: Test results

Group	Beam notation	Time of corrosion when FRP applied (Days)	Time of corrosion at test (Days)	Load			Life to failure (N)	Failure mode**
				Min (kN)	Max (kN)	Range (%)*		
M	M-N-T0	No FRP	0	0	100.3	100	Static	S
	M-0-T0	0	0	0	138.7	100	Static	S
UW0	F45-N-T0	No FRP	0	10	55	45	442,134	S
	F47-N-T0				57	47	31,423	S
	F50-N-T0				60	50	2,041	S
	F53-N-T0				63	53	25,052	S
	F55-N-T0				65	55	1,714	S
UW5	F37-N-T5	No FRP	50	10	47	37	2,912	S
	F40-N-T5				50	40	222,263	S
	F45-N-T5				55	45	245,318	S
	F50-N-T5				60	50	0.5	S
	F55-N-T5				65	55	340	S
UW9	F30-N-T9a	No FRP	100	10	40	30	999,263	S
	F35-N-T9a				45	35	1,116,795	S
	F37-N-T9a				47	37	82,690	S
	F40-N-T9a				50	40	342	S
	F45-N-T9a				55	45	66	S
	F30-N-T9b	No FRP	150	10	40	30	1,000,000	N
	F35-N-T9b				45	35	89,887	S
	F37-N-T9b				47	37	59,568	S
	F40-N-T9b				50	40	360,156	S
	F42-N-T9				52	42	0.5	S
	F45-N-T9b				55	45	923	S

Table 3.1: Test results (Continued)

Group	Beam notation	Time of corrosion when FRP applied (Days)	Time of corrosion at test (Days)	Load			Life to failure (N)	Failure mode**
				Min (kN)	Max (kN)	Range (%)*		
W0	F55-W0-T0	0	0	14	90	55	901,418	R
	F60-W0-T0				97	60	413,418	R
	F62-W0-T0				100	62	131,046	S
	F65-W0-T0				104	65	22,487	S
	F70-W0-T0				111	70	1,030	S
W5	F48-W5-T5	50	50	14	80	48	1,000,000	N
	F50-W5-T5				83	50	142,208	S
	F52-W5-T5a				85.5	52	523,270	S
	F52-W5-T5b				85.5	52	1,950	R
	F55-W5-T5				90	55	17,731	S
	F65-W5-T5				104	65	113	S
W9	F45-W9-T9	100	100	14	76	45	510,313	R
	F48-W9-T9				80	48	9,027	S
	F50-W9-T9a				83	50	51,319	S
	F52-W9-T9a				85.5	52	2,529	S
	F55-W9-T9a				90	55	1,523	S
	F47-W9-T9	150	150	14	80	48	452,836	R
	F50-W9-T9b				83	50	14,145	S
	F50-W9-T9c				83	50	293,023	S
	F52-W9-T9b				86	52	8,742	S
	F55-W9-T9b				90	55	127,973	R
PR	F50-W5-T9	50	150	14	83	50	237,891	R
	F55-W5-T9				90	55	441,586	R
	F58-W5-T9a				94	58	351,582	R
	F58-W5-T9b				94	58	238,532	R
	F60-W5-T9				97	60	8,956	S

* Percentage of static capacity

** S = bond splitting; R = steel bar rupture; N = No failure after 10^6 cycles

3.4 Static Test: Discussion

3.4.1 Behaviour and Mode of Failure

Two beam-anchorage specimens were tested under monotonic loading (Group M, Table 3.1) to determine the static capacity of the specimens used in this study. Specimen M-N-T0 was unwrapped while specimen M-W0-T0 was wrapped with CFRP sheets.

Since both beams were unbonded in the middle, only one or two flexural cracks initiated and propagated to about 75% of the specimens' depth in the constant moment zone.

In specimen M-N-T0, longitudinal cracks started to appear at the loaded end of the bonded zones at about 85 to 90 kN (85% to 90% of the static capacity) and the bar started to slip. Shortly thereafter, the longitudinal cracks increased in width and number. At this time, the beam was no longer able to resist the load applied, and it failed. The side-and-bottom splitting cracks indicated that the final mode of failure was bond splitting (Figure 3.4a).

In the wrapped specimen, M-W0-T0, it was difficult to see the initiation and propagation of the longitudinal cracks because of the presence of the CFRP sheets. However, the specimen kept resisting the increasing applied load until a CFRP sheet at one end ruptured. After the test was halted, the CFRP sheets were removed and the concrete cracks were inspected. The cracks in the bond-critical region, at the end where the CFRP sheet ruptured, were at the level of the reinforcing steel bars and ran parallel to the bars. This indicated that the concrete had split and that the final mode of failure for the wrapped specimen was by a side-and-bottom split failure (Figure 3.4b). This suggests that when the concrete cracked longitudinally, the CFRP sheets were able to sufficiently confine the bond critical zone that it resisted the additional load until the CFRP sheet ruptured and the beam failed.

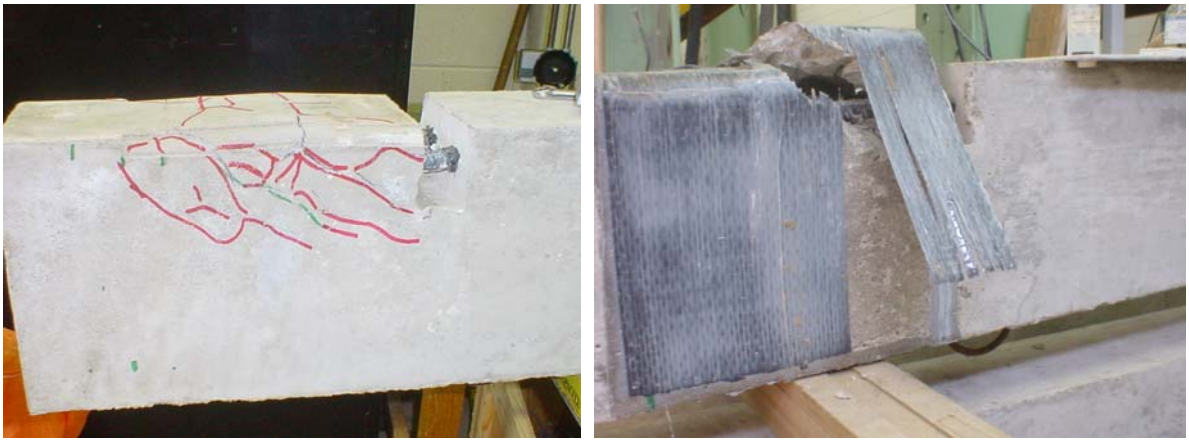

a) Unwrapped beam b) Wrapped beam

Figure 3.4: Failure cracks for static beams (beams shown upside down)

3.4.2 Load- Deflection Behaviour

The load-deflection behaviour of the two specimens tested monotonically is shown in Figure 3.5. The cracking load of the beams was 10 kN and 19 kN for the unwrapped and wrapped specimens respectively, while the stiffness of the two beams was almost the same. The addition of the CFRP sheets increased the maximum load capacity of the specimen from 100 kN for the unwrapped beam (Beam M-N-T0), to 139 kN for the wrapped beam (Beam M-W0-T0), i.e. an increase of 39%. After failure, the load dropped in the unwrapped beam while it was maintained in the wrapped beam for a while before it dropped. However, after the CFRP sheet ruptured, both beams were almost identical and therefore had the same residual strength.

3.4.3 Bond Strength

Since the mode of failure in both beams was splitting of the concrete in the bond critical zone, this indicates that the anchorage length reached its maximum bond capacity and the bond stress was almost uniform along the anchorage length. Therefore, the bond strength was calculated as the maximum steel force developed in the bonded zone divided by the surface area of the anchorage length as given in Eq. 3.1.

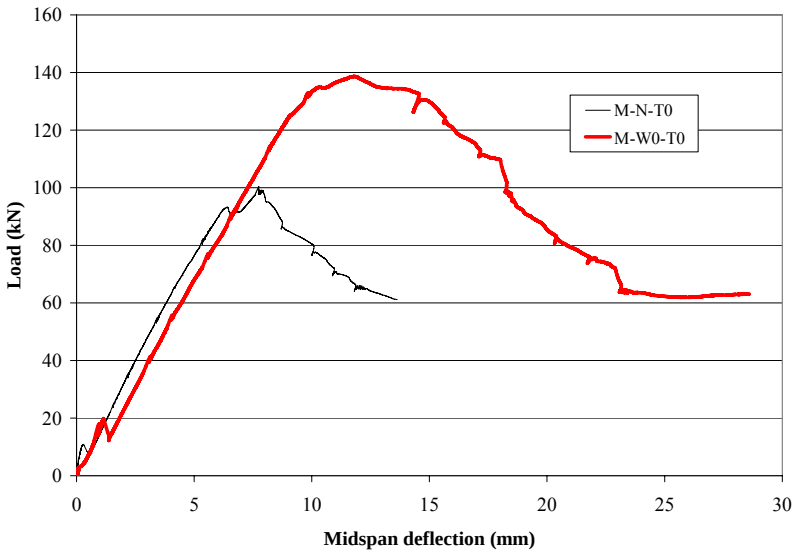

Figure 3.5: Load deflection behaviour for beams in group M

$$u = \frac{A_b f_s}{\pi d_b l_b} = \frac{f_s d_b}{4 l_b}$$ Equation 3.1

Where: u is the bond strength in MPa, A_b is the steel bar cross-section area (mm^2), f_s is the steel stress (MPa), d_b is the bar diameter (mm) and l_b is the anchorage length (mm). The steel stress at the maximum load was determined from readings of the strain gauges installed in the pockets created in the beam. The average bond strength for specimen M-N-T0 was 5.7 MPa, while that for the wrapped beam, M-W0-T0, was 8.4 MPa. Therefore, the CFRP sheets increased the bond strength by 47%.

3.4.4 Steel Strain Behaviour

The steel strain-load variation for both beams is shown in Figure 3.6. The steel strain was measured in the pocket at the edge of the bonded region in the beam. The steel strain increased as the load increased. However, as the beam failed, the steel bars slipped and the steel strain decreased (Figure 3.6). This is due to longitudinal cracks throughout the bonded zone that led to a loss of the bond

between the concrete and the steel. When the bond was lost, the force could not be transferred from the concrete to the steel and the steel stress dropped.

3.4.5 Steel Slip Behaviour

Longitudinal cracks in the concrete initiated at the steel bar ribs. The initiation and propagation of the longitudinal cracking weakened the resistance of the concrete keys (concrete between the steel bar lugs). As the concrete resistance decreased, the steel bar started to slip at the free end in the wrapped and unwrapped beams (at about 90% of the maximum load for both beams). The CFRP sheets provided enough confinement to the concrete to prevent the initiation of free end slip until a load 36% above that in the unconfined beam was reached (Figure 3.7). Also the bond stiffness for the wrapped specimen, M-W0-T0, increased by about 25% in comparison to that of specimen M-N-T0 which was unwrapped (Figure 3.8). After failure, the load dropped in the unwrapped beam as the slip increased. However, in the CFRP wrapped beam, the load was maintained as the free end slip increased from 0.5 mm to 2.5 mm (Figure 3.7) providing a more ductile post-failure behaviour for the wrapped beam than that of the unwrapped beam. This is similar to the behaviour reported by other researchers (Hamad et al., 2004a, 2004b, 2004c and Harajli et al., 2004).

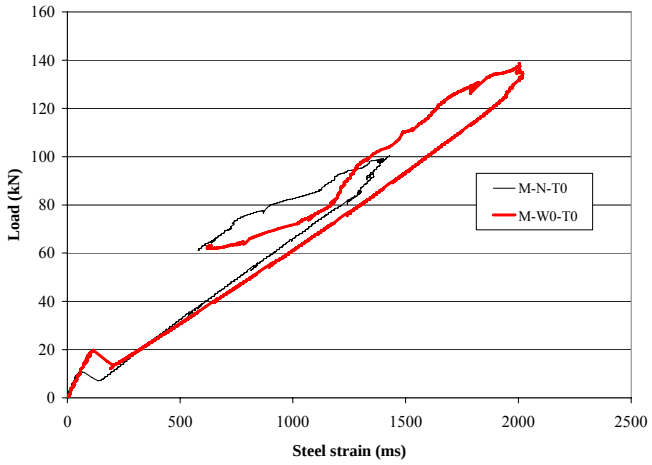

Figure 3.6: Variation of steel strain (measured in the pocket) with load for the 2 static beams

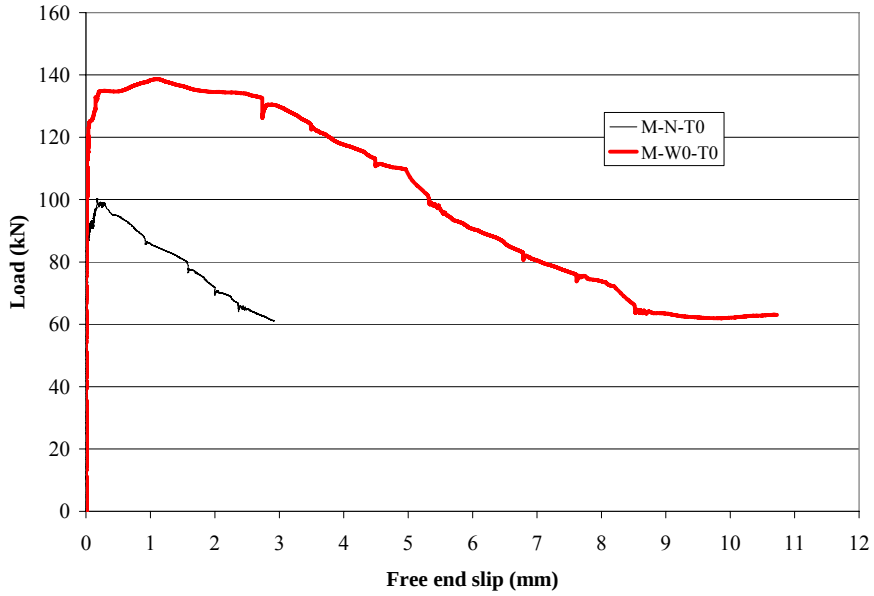

Figure 3.7: Behaviour of the free end slip for the wrapped and unwrapped static beams

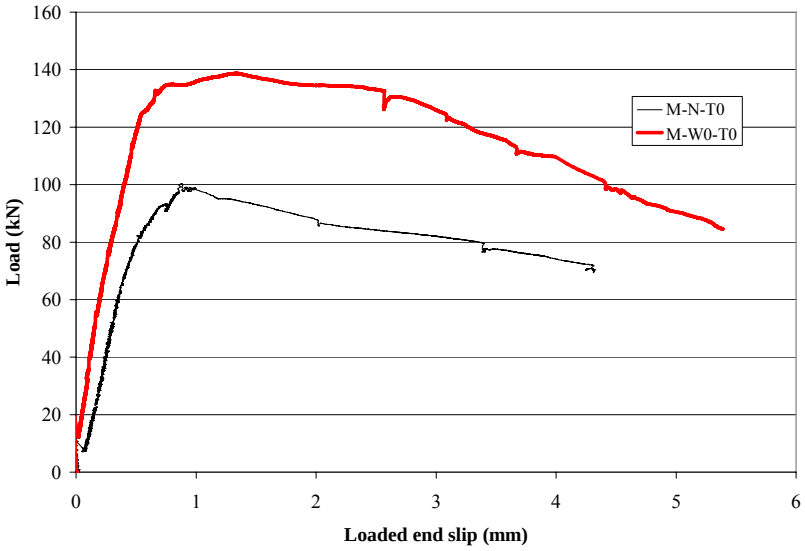

Figure 3.8: Variation of loaded end slip vs. load for static beams

In summary, while the application of CFRP sheets did not change the failure mode the CFRP sheets confined the cracked concrete and prevented the steel bar from slipping until the sheets ruptured. This increased the load carrying capacity of the specimen by 39% and the bond strength by

47%. It also increased the bond stiffness by 25% and the load at which the free slip initiated by 36%. Post-failure performance was also improved since the CFRP sheets made the wrapped beam more ductile (Figure 3.7).

3.5 Fatigue Test Discussion: Behaviour and Mode of Failure

In all the beams tested under repeated loading, a flexural crack opened in the constant moment region during initial loading. As the load increased, the crack propagated to about 75% of the beam's depth. The cracking load ranged from 20 kN to 25 kN. Usually another flexural crack also opened in the constant moment region close to the loading point. The second crack either opened during the first manual loading cycle or during the first few cycles. Upon further cyclic loading, the cracks did not propagate but their width increased. The following sub sections will go over the observed behaviour for the unwrapped and wrapped beams.

3.5.1 Unwrapped Beams

For unwrapped uncorroded beams (group UW0), hairline longitudinal cracks initiated from the pocket and ran along the reinforcing bars during the first few hundred cycles. The longitudinal cracks continued to grow in width and length until failure. The corroded unwrapped beams (groups UW5 and UW9) had longitudinal side and bottom corrosion cracks along the steel bar in the anchored zones before fatigue load testing. During testing, new longitudinal cracks initiated and started to propagate in the anchorage zone and the corrosion cracks widened. For both uncorroded and corroded beams, the rate of growth of the longitudinal cracks increased with increasing applied load range. Nevertheless, a single pattern of crack growth was observed for all unwrapped beams. For approximately the first 20 to 25% of the beams' fatigue life longitudinal cracks propagated at a continually decreasing rate. Then the propagation and widening of the cracks either stopped or took place at a slow rate. At about 80% to 90% of a beam's life, the longitudinal cracks started propagating

again at a continually increasing rate at only one end of a beam. The bottom and side concrete covers started to bulge out. The bulging continued until failure occurred. Failure of all unwrapped beams occurred by bond splitting in the side and bottom concrete cover along the steel bar (Figure 3.9a). In some of the corroded beams, the failure was associated with spalling of the concrete cover (Figure 3.9b). The failure was brittle and accompanied by a loud bang.

It should be mentioned that specimens F50-N-T5 and F42-N-T9 both failed by bond splitting while they were being loaded for the first time. The loads achieved were 58 kN and 47.5 kN for specimen F50-N-T5 and F42-N-T9, respectively. Failure occurred just before reaching their intended maximum loads of 60 kN and 52 kN, respectively.

After each test was halted, the failure surface was inspected. It was observed that for the unwrapped uncorroded beams, the lower concrete cover was cracked into two or three pieces (Figure 3.9a). The concrete above the steel bar in the vicinity of the bar lugs was cracked and crushed (Figure 3.10a) while the concrete in the bottom cover was intact (Figure 3.10b). This suggests that the concrete above the steel bars resisted the bond forces, and therefore was cracked and crushed while the bottom cover was pushing away and did not participate in bond resistance. For the unwrapped corroded beams, a similar observation was noted; except that the bottom concrete cover had more cracks and the depth of the concrete keys (concrete between the steel and bar lugs) was less than for the ones in the uncorroded beams (Figure 3.11). This was noted for both sides of the beam (failed and sound sides), which suggests that the increase in the number of cracks and decrease in concrete key depth is due to the corrosion.

a) Concrete splitting for uncorroded beams b) Concrete cover spalled for corroded beams

Figure 3.9 Typical failure cracks for unwrapped beams

a) Concrete above the steel bar b) Concrete below steel bar (bottom cover)

Figure 3.10 Failure plane for unwrapped uncorroded beams

Figure 3.11 Failure plane for unwrapped corroded beams

3.5.2 Wrapped Beams

The presence of the CFRP sheets prevented visual monitoring of crack initiation and propagation in the wrapped beams. However, for specimens which failed by bond splitting (see Table 3.1), it was noted that at about 40 to 50% of the beams' life the matrix of the CFRP sheets started to exhibit cracks parallel to the fibres. Failure of these specimens took place when the fibres ruptured at the level of the steel bars at one end of a beam (Figure 3.12a). After the failure of the specimens, the CFRP sheets were removed and an inspection of the cracks under the CFRP sheets was conducted. The end of the beam where the CFRP sheet did not rupture had only a few or no cracks (except for the corrosion cracks in the corroded wrapped beams). However, at the end where the CFRP sheet ruptured longitudinal cracks along the steel bars were observed. In general these cracks were finer and less numerous than those in the unwrapped beams (Figure 3.12b). When the bottom cover was removed for a more detailed inspection of the crack surface, it was noted that the concrete around the steel bar (in the neighbourhood of the lugs) was crushed into a powder and that the concrete keys were totally lost (Figure 3.13 and Figure 3.14). The remainder of the bottom concrete cover was heavily cracked (Figure 3.13 and Figure 3.14).

a) Rupture of CFRP sheets b) Concrete splitting cracks

Figure 3.12 Typical bond failure for wrapped beams

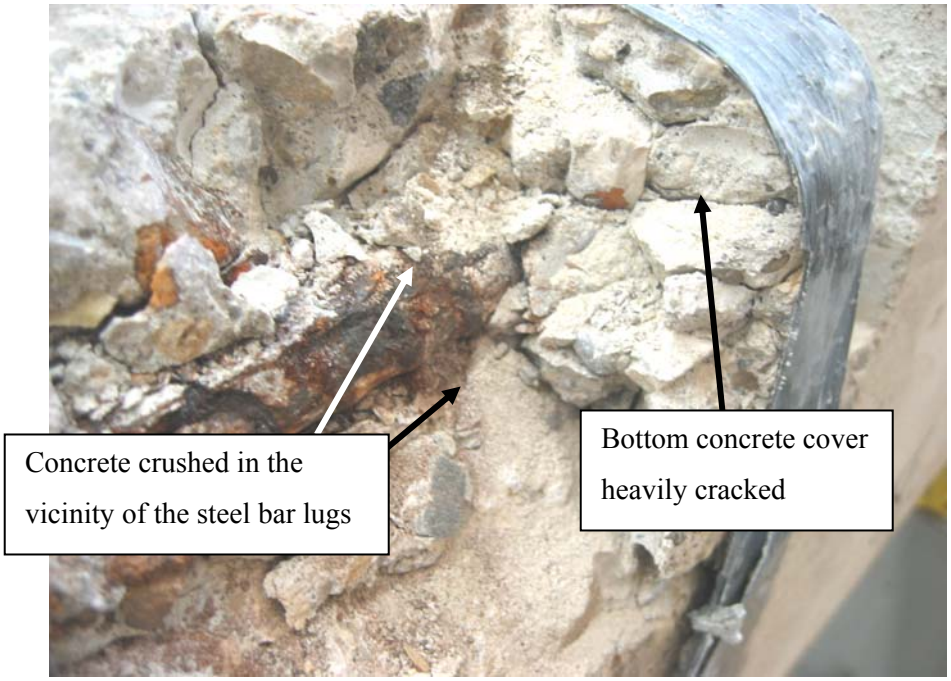

Figure 3.13 Failure plane for wrapped beams

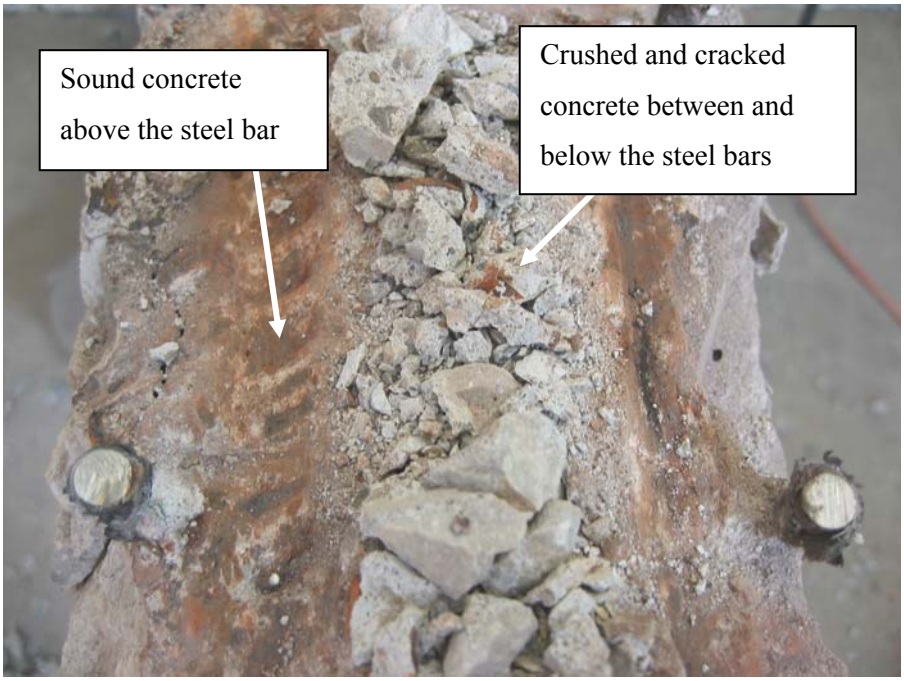

Figure 3.14 Close up view of the concrete in the wrapped beams

On the other hand, for the ten (10) specimens (2 with 0% corrosion, 1 with 5% corrosion, 3 with 9% corrosion and 4 post repaired after 9% corrosion) that failed by steel rupture (Table 3.1), it was noted that the concrete in the middle of the beam was crushed. In addition, it was realized that the un-fractured steel bar had slipped much more than the other fractured bar. Also, the CFRP sheets ruptured only from one side at both ends of the beam where the steel bar had slipped (rather than rupturing from both sides at one end of the beam as in the case for the specimens that failed by bond splitting). After the tests were halted, the sheets were removed and the cracks and the failure plane were inspected. There were splitting cracks at both ends for one side of the beam (where the CFRP sheets ruptured and bar slipped), while the other side was almost intact (where the steel bar ruptured). Further investigation revealed that these beams failed by flexural fatigue (indicated by one of the steel bars rupturing either in the middle of the beam or in the pocket) (Figure 3.15). In specimens F55-W0-T0 and F60-W0-T0 (uncorroded), the steel ruptured in the middle region of the beam where the stress was highest. For the other corroded specimens, one with 5% corrosion, three with 9% corrosion and four post-repaired with 9% corrosion, the steel ruptured in the pocket. The rupture of one steel bar resulted in a sudden increase of the stress in the other bar in the beam. This increased stress in the un-ruptured bar resulted in higher bond stresses and a large increase in bar slip and rupture of the CFRP sheet. The increase in the slip in the un-fractured bar started immediately after the other bar ruptured.

Figure 3.15 Flexural fatigue failure by steel rupture

It is worth noting that the specimens that failed by rupture of the steel bar in groups W0, W5 and W9 were all wrapped and in general were tested at lower load ranges than the specimens which failed by concrete splitting (see Table 3.1). This suggests that because of the wrapping the bond fatigue capacity was increased. This increase in bond strength coupled with the existence of corrosion pits (especially in the pocket, where the un-bonded steel was least protected) that lowered the flexural fatigue strength, resulted in these specimens failing in flexural fatigue rather than in bond fatigue. Since specimens failed by steel rupture at different corrosion levels (0%, 5% and 9%), it seems that the average corrosion level was not the factor that determined the failure mode but rather the size and location of the largest pit.

Since these beams failed by a flexural failure mode that was different from the bond failure which is the scope of this study, specimens that failed by steel rupture will be excluded from further discussion.

3.6 Fatigue Tests Discussion: Fatigue (Load) Strength

The fatigue lives of the specimens varied linearly with the load range applied (given here as a percentage of the static capacity of the specimen) on logarithmic scales (the lives of the specimens increased as the load range decreased) for all the repeated loading tests (Figure 3.16). The data points shown in Figure 3.16 include only the specimens that failed in bond. Specimens that failed during first loading (F50-N-T5 and F42-N-T9) or that failed in flexural fatigue (see Table 3.1) were excluded from the analysis and are not included in Figure 3.16. However, a complete set of applied load range versus fatigue life data for all the specimens tested in repeated loading is presented in Appendix B and given in Table 3.1.

Examining Figure 3.16 it is noted that the unwrapped corroded beams (groups UW5 and UW9) had more scatter than the wrapped corroded beams (groups W5 and W9). In the case of unwrapped

corroded beams, the width of the corrosion-induced crack and the decrease in the relative rib area of the steel lugs varied for beams with the same corrosion level. This affected the fatigue capacity of the bonded length and the results showed a considerable scatter. On the other hand, CFRP confinement preserved the integrity of the wrapped corroded beams, offset the negative effect of the corrosion crack and the decreased steel bar rib size on the capacity of the bonded area, and tended to make the fatigue capacity uniform thus reducing the scatter of the results for the corroded wrapped beams (Figure 3.16).

The fatigue strength (measured as the load range applied) of the unwrapped beams corroded to a 5% and a 9% mass loss decreased on average by 12% and 23% respectively at all fatigue lives compared to the fatigue strength of the unwrapped uncorroded beams (Figure 3.17). In the CFRP wrapped beams, the percentage decrease of the fatigue strength due to the 5% and 9% corrosion levels was on average 16% and 21% respectively compared to the fatigue strength of the wrapped uncorroded beams (Figure 3.17).

The addition of CFRP sheets increased the fatigue strength (as measured by the load range applied) compared to that of the unwrapped beams at all corrosion levels and all fatigue lives (Figure 3.18). The average fatigue strength increased by 32%, 26% and 35% compared to the fatigue strength of unwrapped beams for corrosion levels of 0%, 5% and 9% respectively. The overall average increase was 31%, which was close to the increase of 39% achieved in static loading.

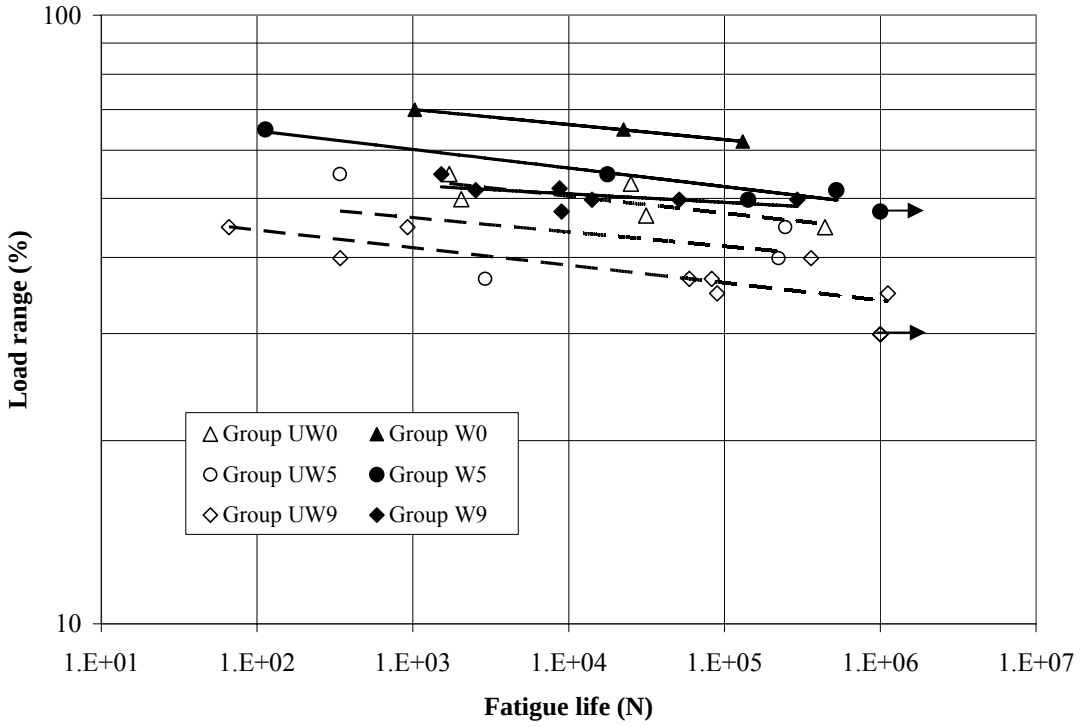

Figure 3.16 Variation of load range with life for all beams failing in fatigue of bond

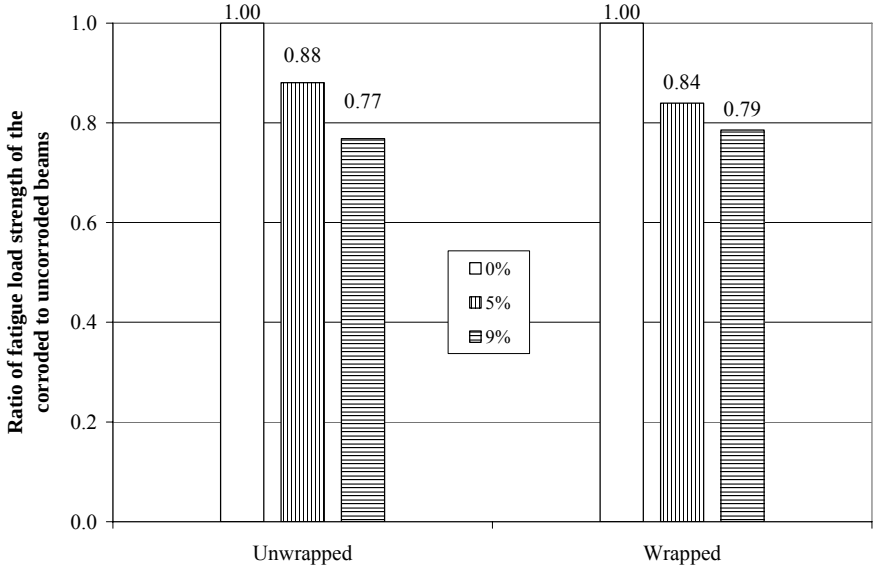

Figure 3.17 Effect of corrosion on the fatigue load strength

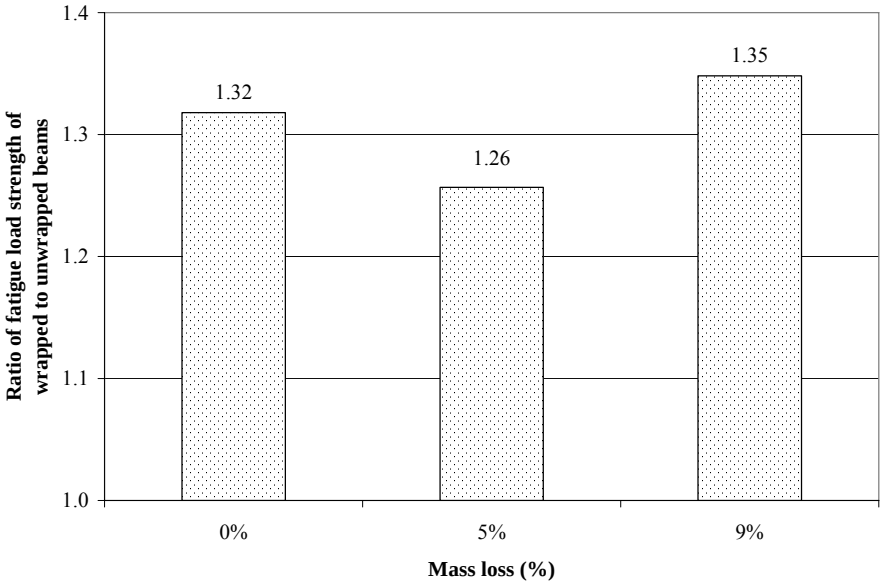

Figure 3.18 Effect of CFRP sheets on the fatigue load strength

3.7 Fatigue Tests Discussion: CFRP Confinement

For the beams that were wrapped with CFRP sheets (corroded and uncorroded), four strain gauges were installed at each end of the beam. Two strain gauges were close to the loaded end of the anchorage length and the other two were close to the free end of the anchorage length (see Fig. 2.13).

The strain in the CFRP sheets increased sharply in the first 4 to 8% of a beam's fatigue life (i.e. the first 1,000 to 10,000 cycles). After that, the strain reading levelled off until failure (Figure 3.19). This behaviour was the same for all the beams irrespective of the corrosion level (see Figure 3.19). For the wrapped beams, the maximum load applied varied from 90% to 110% of the unwrapped uncorroded beam's static bond capacity. Therefore, the bond hoop stresses generated were high enough to push the concrete cover away from the steel bar by wedge action, as was the case for the unwrapped beams (see section 3.5.1). This subjected the CFRP sheets to a tensile force and the bottom concrete cover to a compressive force that held the concrete cover in place. As a result, the concrete cover, both above and below the steel bars, was crushed around the steel lugs and cracked away from the steel lugs by

the bond forces (see Figure 3.13). The crushed concrete powder in front of the steel lugs was compressed and moved with the steel bar (see Figure 3.20). Thus, the effective face angle of the steel lugs with the concrete was decreased and the wedge action force increased (Lutz and Gergely, 1967). This in turn, increased the stress in the CFRP sheet. This phenomenon continued until the crushed concrete powder in front of the lugs, that was found to extend in front of the lug for a length of 6 to 7 times the height of the lug (Lutz and Gergely, 1967), stopped changing the effective face angle of the bar lugs. This stabilized the wedge action of the steel bar and hence the increase of the stress in the CFRP sheet. This trend is consistent with the post-failure observations described in section 3.5.2 for wrapped beams (concrete crushed in front of the steel bar lugs and cracked away from them).

It is of interest to note that the CFRP stress was less for the corroded beams than for the uncorroded beams (Figure 3.19). This is because the corrosion cracked the concrete cover and lowered the height of the steel lugs, thus decreasing the wedging action of the steel bar. A similar observation was reported by Fang et al. (2004), except that they used only steel stirrups to confine the bond region. For the uncorroded beams (group W0), the CFRP strain reading at 5% of the life ranged between 2400 and 4200 micro-strain. The corresponding range for groups W5 and W9 were between 700 and 3800 micro-strain and 1200 and 2000 micro-strain respectively (see Appendix C). It is noted that the difference in CFRP strain readings between the two corrosion levels (5% and 9%) is less than the difference between corroded (5% and 9%) and uncorroded beams. This is because after a certain crack width, any increase in the corrosion level, although it increases the corrosion crack width, has only a small effect on the bond stress since the contribution of the concrete forces to the confinement was lost. Almusallam et al. (1996a) found that for increases in the crack width above 1 mm, the reduction of the bond strength was negligible. Appendix C gives the CFRP strain results for all wrapped beams.

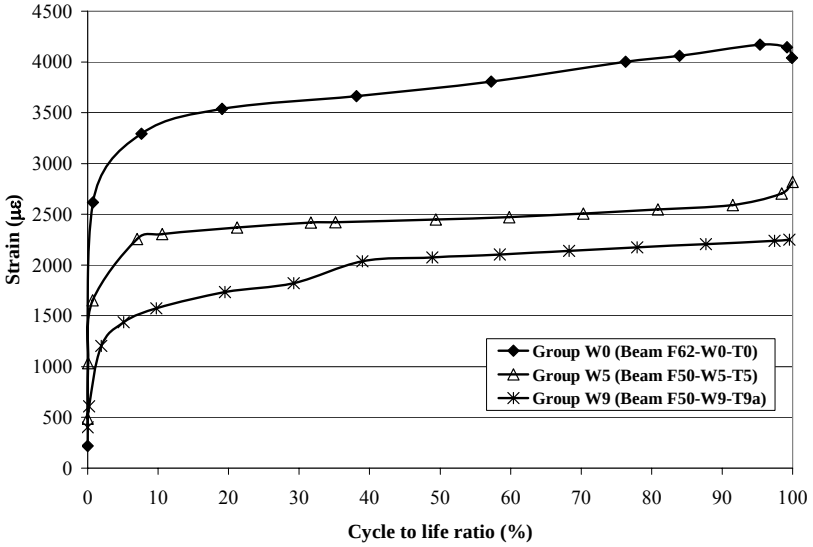

Figure 3.19 Typical CFRP strain versus cycles behaviour

Figure 3.20 Traces of the condensed concrete in front of the steel bar lugs

3.8 Fatigue Test Discussion: Fatigue Bond Stress

For the uncorroded beams (groups UW0 and W0), strain gauges were mounted on the steel bars along the bonded length in order to monitor the variation of the bond stress distribution (see Fig. 2.15).

The peak bond stress for each cycle was calculated using Eq. 3.1. The steel stress used in that equation was taken to be the difference of two consecutive strain readings multiplied by the steel modulus of elasticity (200,000 MPa). The term l_b in Eq. 3.1 was taken as the distance between strain gauges, 125 mm. The behaviour of the distribution of the bond stress for wrapped and unwrapped uncorroded beams was similar. As the number of cycles increased the bond stress close to the loaded end decreased, while the bond stress close to the free end increased (Figure 3.21). This behaviour is explained in the following. Since the beam was unbonded in the middle, the concrete transferred tensile forces to the steel bar when they first made contact, i.e. close to the pocket. The unbonding of the steel bar in the middle of the beam created a bond stress raiser at the end of the pocket. This generated a high bond stress in that area. Away from this bond stress raiser, the bond stress decreased to a level equal to that of a fully bonded beam. As the number of cycles increased, the bottom cover in the unwrapped beams was pushed away due to wedge action. In the wrapped beams, the bond stress decreased as the concrete around the steel lugs was crushed, thus decreasing the face angle of the lug. Therefore, the bonded length close to the pocket area, that had the highest initial bond stress and damage, became less effective in transferring force from the concrete to the steel. However, in order to maintain the applied load on the beam, the tensile forces in the concrete had to be transferred to the steel. Therefore, the bond stress raiser moved along the bonded length. This decreased the bond stress close to the pocket area and increased the bond stress closer to the free end (Figure 3.21). The bond stress redistribution continued until the bonded length could not transfer the force required to maintain the peak load and the beam failed. A similar behaviour was reported by other researchers (Bresler and Bertero, 1968 and Perry and Jundi, 1969).

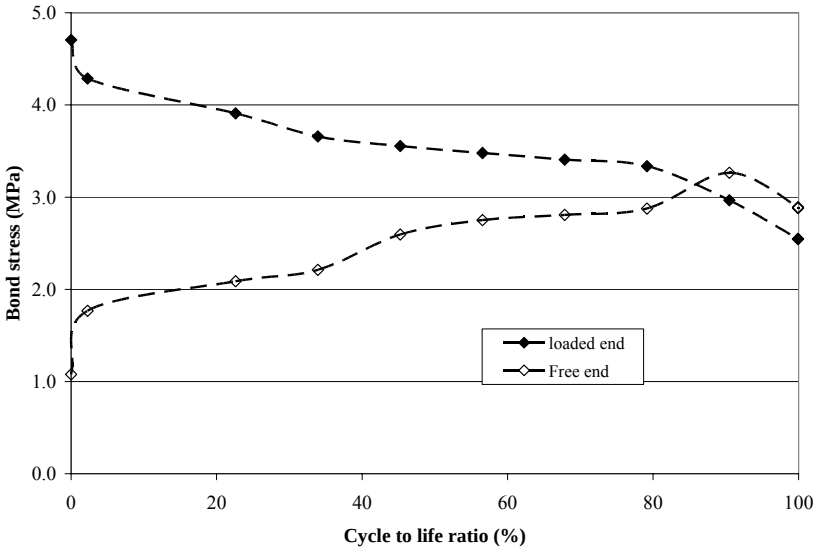

Figure 3.21 Typical variation of the bond stress (Beam F53-N-T0)

For the corroded beams, it was decided not to install strain gauges along the bonded length since it was difficult to protect them from corrosion damage (Appendix D shows the variation of the steel strain in the pocket with fatigue cycles). In order to determine the effect of corrosion and CFRP sheets on bond stress, the bond strength at a fatigue life of 100,000 cycles was calculated. In order to do that, the load range corresponding to a fatigue life of 10^5 cycles was determined from Figure 3.16. The steel stress was then calculated using an elastic cracked section analysis. The bond strength was calculated assuming a uniform bond stress distribution along the bonded length (l_b = 250 mm) using Eq. 3.1. The results are shown in Figure 3.22.

The decrease in the fatigue bond strength at a fatigue life of 10^5 cycles for unwrapped beams was 12% and 23% for the 5% and 9% corrosion levels compared to unwrapped uncorroded beams (Figure 3.22). For wrapped beams, the two corrosion levels (5% and 9% mass loss) decreased the fatigue bond strength by 15% and 31% respectively compared to wrapped uncorroded beams.

The bond strength of the CFRP wrapped corroded beams increased on average by 29% compared to unwrapped corroded beams (Figure 3.22).

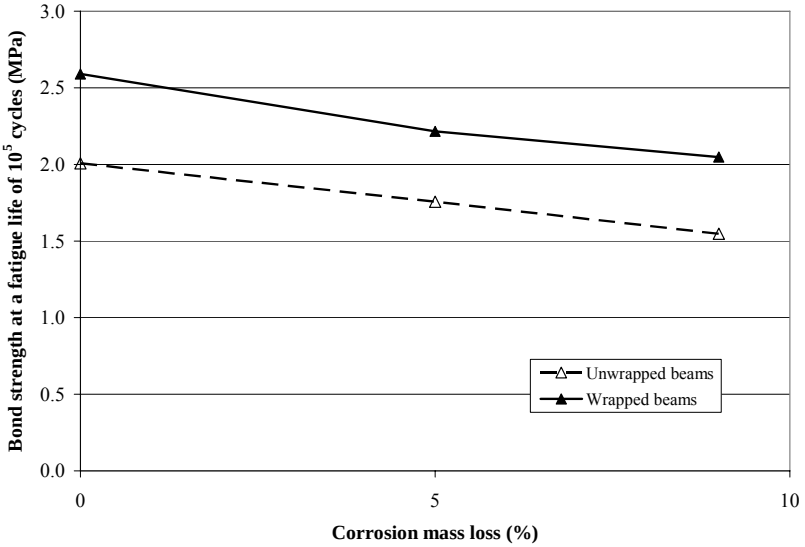

Figure 3.22 Fatigue bond strength at 10^5 cycles

3.9 Fatigue Test Discussion: Steel Slip Behaviour

The slip of a reinforcing bar relative to the concrete is a measure of the bond behaviour since the weaker the bond; the greater will be the slip (ACI 408, 2003). An accumulation of bond damage under repeated loading is caused by progressive cracking and crushing of concrete in front of the steel bar lugs. The effect of the bond damage is observed as an increase in slip (FIB 10, 2000). In this study, in order to monitor the degradation of the bond stress, the slip was measured at the loaded and free ends of the bonded region by mounting LVDTs to measure the motion between the concrete and the steel bar (section 2.8.2).

3.9.1 Slip Behaviour for Unwrapped Beams

For the unwrapped uncorroded beams (group UW0), the slip behaviour of the steel bar is divided into two stages. In stage 1, the slip did not change much. For beams tested at a low load range this behaviour lasted until about 90% of the beams' life but decreased to about 30% of a beam's life for beams tested at a high load range. This stage was followed by a stage of exponentially increasing slip

until failure (see Figure 3.23). In the first stage, the concrete (located above the steel bar) between the steel bar lugs resisted the movement of the bar, therefore, as the load range increased the tensile bond stresses increased and the rate of degradation of the concrete resistance increased. Therefore, for beams tested at high loads, stage one was shorter than for beams tested at low loads. This was accompanied by shorter fatigue lives for the beams tested at high loads than for the ones tested at lower loads.

The slip behaviour for unwrapped corroded beams (groups UW5 and UW9) can also be divided into two stages (Figure 3.23). Slip of the reinforcing bar was resisted by the concrete cover, however, because the concrete in the corroded beams was already cracked and the steel bar lugs were reduced in size because of the corrosion, the concrete resistance to slip was decreased compared to that of the uncorroded beams. Therefore, the slip in corroded unwrapped beams increased throughout the first 90% of the beams life (see Figure 3.23). The rate of slip increase for group UW5 and UW9 was 0.017 and 0.020 mm per 1% of the number of cycles to failure, i.e. an increase of corrosion level from a 5% to a 9% mass loss increased the slip rate by 17.5%. It is also noteworthy that the transition between the first and second stage for the corroded beams was at around 85% to 90% of the beams' life irrespective of the load range applied. In Group UW0 (unwrapped, uncorroded), the higher the load the more rapid the damage of the concrete, and therefore, the shorter was stage one. In corroded beams (groups UW5 and UW9), the concrete was already damaged due to corrosion. Therefore, increasing the load applied did not affect the cracked concrete cover. As a result, the shift from stage 1 to stage 2 in the slip behaviour for corroded unwrapped beams was not affected by the load level. The second stage of the slip behaviour for corroded unwrapped beams was characterized by an exponential slip increase until failure (similar to the behaviour of the uncorroded unwrapped beams).

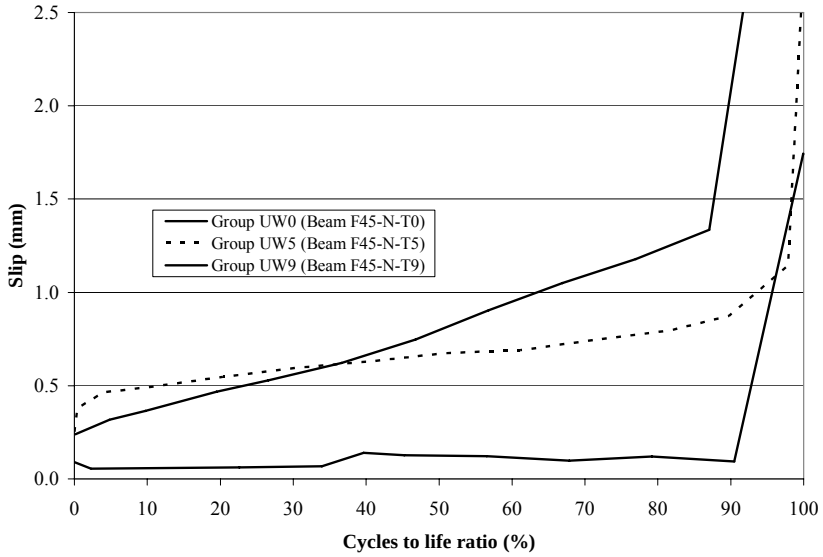

Figure 3.23 Typical slip variation for unwrapped beams (Loaded end slip)

3.9.2 Slip Behaviour for Wrapped Beams

For the wrapped beams, the presence of the CFRP sheets changed the behaviour of the slip from a two-stage to a three-stage process. In the first stage, the slip of all wrapped beams (corroded and uncorroded) increased dramatically for the first 5 to 10% of the beams' life (Figure 3.24). As was explained in section 3.7 the CFRP sheets at the beginning of the beams' cyclic loading (first 5 to 10% of the beams' life) were not fully mobilized (Figure 3.19), and the wrapped beams were loaded to higher levels than the unwrapped beams. Therefore, only the concrete initially resisted the tensile bond forces and was subject to a high bond stress (relative to its capacity) in the first stage. As such, the concrete rapidly cracked resulting in a rapid increase in slip. The slip reached values between 1.25 mm and 2.0 mm, which correspond to failure for the unwrapped beams.

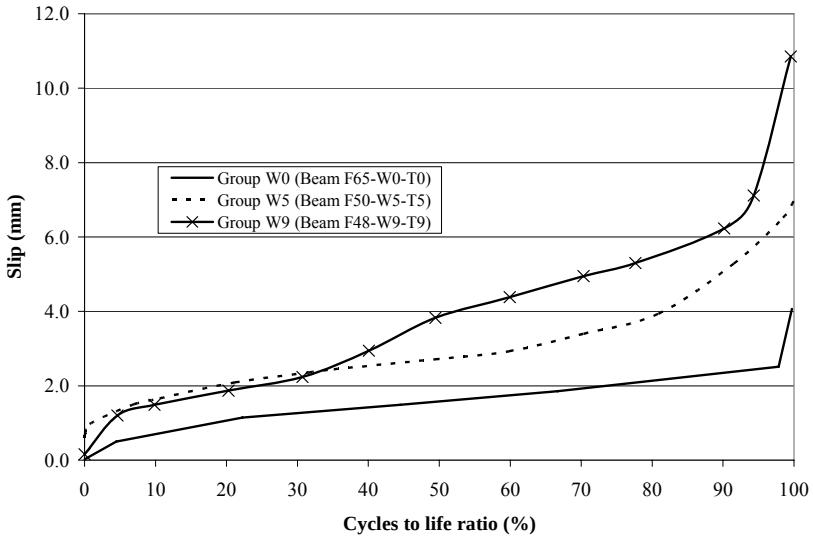

Figure 3.24 Typical slip variation for wrapped beams (loaded end)

This slip forced the concrete cover outward and generated forces in the confining CFRP sheets (as was explained in section 3.7) and stage two began. In this stage, slip continues to increase but at a much slower rate. For the wrapped uncorroded beams (group W0), the slip increased on average by 0.0117 mm per 1% of the cycles to failure ratio. For the corroded beams (groups W5 and W9), the slip had an average rate of 0.033 mm per 1% of the cycles to failure ratio, therefore corrosion almost tripled the slip rate of the wrapped corroded beams compared to the wrapped uncorroded beams. During the first stage of the slip behaviour for the wrapped beams, the concrete cover was cracked and crushed due to the relatively high bond forces. Therefore, the forces resisting the increase in slip in stage two were due primarily to the confinement provided by the CFRP sheets. The CFRP sheets provided similar confining forces for groups W5 and W9 (the strain readings of the CFRP sheets for groups W5 and W9 were close to each other, see section 3.7); and therefore, the rate of increase of the slip for groups W5 and W9 was similar. The second stage ended for all wrapped beams (corroded and uncorroded) at about 80 to 90% of the beams' fatigue life. Stage 3 that followed was characterized by an exponential increase in the slip rate until failure (see Figure 3.24). A similar slip behaviour was

reported by Balazs (1991), however, in his study, Balazs used a pullout specimen that failed by pullout of the steel bar, therefore, the steel bar was confined by a large concrete cover. In this study, the confinement was provided by CFRP sheets. Nevertheless, the behaviour of the slip of the steel bar was similar in both studies.

3.9.3 Loaded and Free End Slip

The above-described behaviour for unwrapped and wrapped beams was the same for both the loaded and free end slip, but the loaded end slip was initially greater than the free end slip (Figure 3.25). The measured slip of the loaded end consists of a rigid body motion and the elongation (elastic and plastic) of the steel bar. Slip in a strict sense is only the former part of the measurement (FIB 10, 2000). However, when the slip started to increase exponentially (stage two in unwrapped beams or stage three in wrapped beams) the concrete cover either was pushed away by wedge action for unwrapped beams or was heavily cracked for wrapped beams. In both cases, the bond stress along the bonded length became nearly uniform. Consequently, in this stage, the steel bar experienced a rigid body motion and both the free and loaded end slip were equal in value (Figure 3.25).

3.9.4 Initial Slip

The initial slip (defined as the loaded end slip recorded at the maximum load during the first cycle) increased approximately linearly with the maximum applied load (Figure 3.26). For unwrapped beams, the slope of the initial slip-maximum load curve decreased as the corrosion level increased (Figure 3.26). This is expected since the corrosion-induced crack width, thus the damage to the concrete increased with corrosion level. For the wrapped beams, the CFRP sheets maintained the concrete in contact with the lugs irrespective of the corrosion level thus the slope of the initial slip-maximum load curve did not change with increasing corrosion level (Figure 3.26).

For a maximum load equivalent to 70% of the static bond capacity of the specimen, the initial slip increased by 15 and 21 times for wrapped corroded (to 5% and 9% respectively) beams compared to uncorroded wrapped beams. The corresponding increase in the unwrapped corroded (to 5% and 9%) beams was 2 and 63 times compared to unwrapped uncorroded beams.

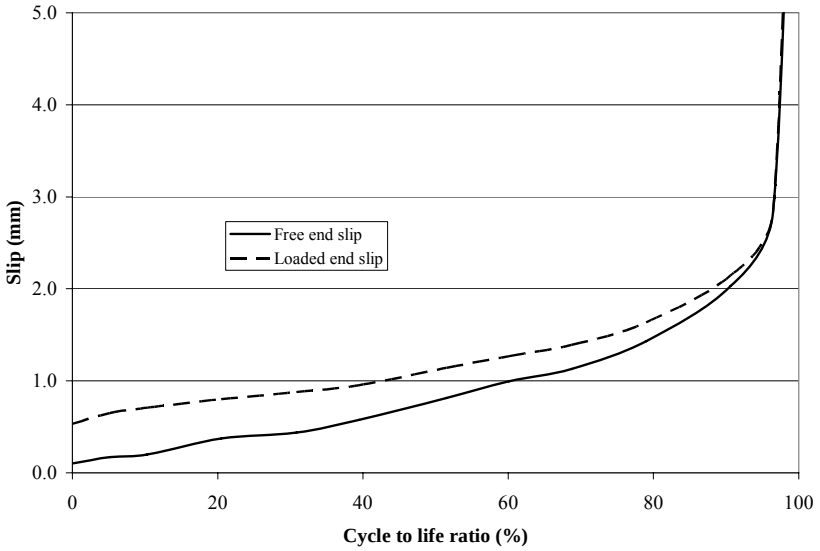

Figure 3.25 Typical variation of the loaded and free end slip (Beam F37-N-T5)

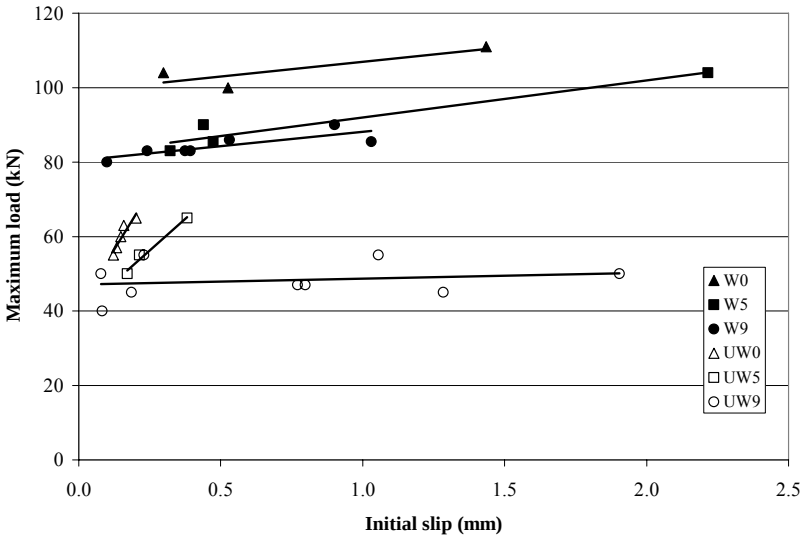

Figure 3.26 Variation of the initial loaded end slip with the applied maximum load

3.9.5 Variation of the Failure Slip with Corrosion Levels

The values of the free and loaded end slip were compiled and averaged to examine the effects of corrosion and confinement by CFRP sheets (Figure 3.27). Corrosion to 5% and 9% corrosion mass losses increased the slip at failure on average by 94% and 131% respectively for unwrapped corroded beams compared to unwrapped uncorroded beams (UW0) and by 39% and 54% respectively for wrapped corroded beams compared to wrapped uncorroded beams (W0) (Figure 3.27). Mangat and Elgarf (1999a) reported similar behaviour for monotonically tested specimens. However, an increase in corrosion from 5% to 9% increased the failure slip by 19% and 10% for unwrapped and wrapped beams respectively.

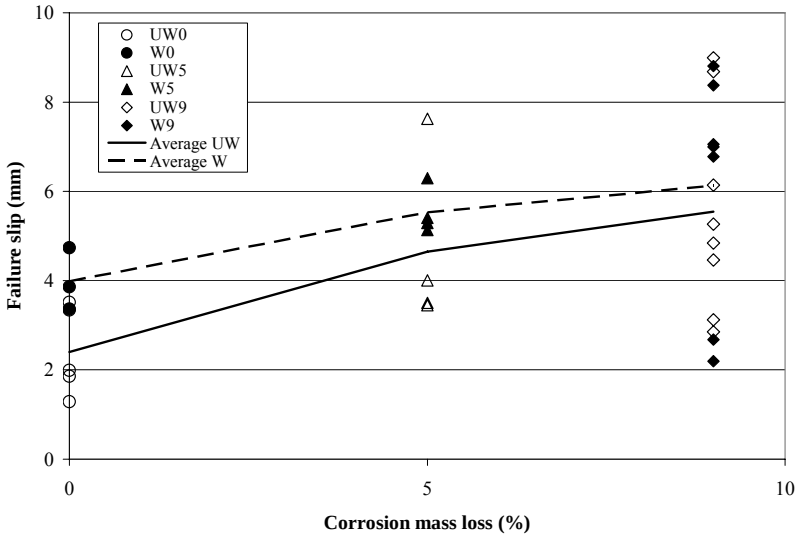

Figure 3.27 Failure slip variation with corrosion mass loss

It is worth noting that the failure slip values for the wrapped beams are much higher than for the unwrapped beams. As explained before (section 3.7), the wrapped beams were tested at loads that correspond to 80 to 105% of the static capacity of the unwrapped beams and the CFRP sheets were not mobilized until some slip had taken place. Meanwhile, the concrete provided the resistance to the tensile bond forces. This resulted in rapid damage of the concrete around the steel bar (in the form of

crushing in front of the steel bar lugs, and cracking in the rest of the concrete cover). The final slip values of the wrapped beams were much higher than those of the unwrapped beams. Had the wrapped beams been tested at a lower load range (equal to that of the unwrapped beams) their initial slip would probably be similar to that of the unwrapped beams. However, in that case, the wrapped beams would not fail in fatigue since the confinement of the CFRP sheets would prevent further slip from occurring.

Chapter 4
Analysis of Bond under Monotonic and Repeated Loading

4.1 Monotonic Bond Stress-Slip Model

In order to predict the performance of any reinforced concrete (RC) element, whether under static or cyclic loading, the bond between steel and concrete should be taken into consideration. The magnitude and distribution of bond stress along the steel bar is complex, which makes it difficult to properly include the bond effect into RC flexure and shear models. The relationship between bond stress, u, and the relative slip, s, between concrete and steel bar is of fundamental importance to better understand the bond behaviour. Bond stress-slip relationships had been used to solve the bond problem analytically and numerically (FIB 10, 2000). They were also incorporated in models used to predict the flexure and shear performance of RC members under cyclic and static loading (El-Maaddawy et al., 2005b; and Kwak and Kim, 2006).

In this study, the bond stress- slip behaviour of the two beams in group M (one wrapped and one unwrapped, both tested under monotonic loading) will be modeled using a bond stress- slip law that was recently proposed by Harajli, Hamad and Rteil (2004).

4.1.1 Model Background

For bond splitting failure, Harajli, Hamad and Rteil (2004) proposed a bond-slip law that takes into consideration the effect of confinement. In this study, this model will be used in order to predict the bond stress-slip behaviour for beams tested under monotonic loading (Group M).

The bond stress-slip behaviour for splitting failure is divided into four stages (Harajli et al., 2004). In the initial stage, the stiffness of the bond stress-slip response is identical to that of the pullout failure (Figure 4.1). As tensile cracks start to develop due to the radial stress component of the bond

forces, a second stage starts (corresponds to ($s_{\alpha,}$, αu_{max}) in Figure 4.1). This stage is characterized by a softer response compared to the pullout behaviour. The second stage continues until the cracks have propagated to the surface thus splitting the concrete. The splitting of the concrete indicates a bond failure mode ((s_{max}, u_{max}) in Figure 4.1). A sudden drop in the bond stress will follow the bond failure (stage three), which ends when the bond forces are in equilibrium with the post-splitting concrete tensile strength ((s_{ps}, u_{ps}) in Figure 4.1). The fourth stage then starts and continues until the bond drops to zero due to the widening of the concrete splitting cracks (Figure 4.1). When confinement is provided (in the form of steel stirrups or FRP sheets) the splitting cracks are finer in width, and the resistance of the concrete matrix after splitting is increased. This increases the bond stress at failure and enhances the post-splitting behaviour. The equations describing the parameters that define the bond stress-slip law are presented below (Harajli et al., 2004).

$$u = \begin{cases} u_1 \left(\frac{s}{s_1}\right)^{0.3} & for \quad s < s_\alpha \\ u_{max}\left[\left(\frac{s - s_\alpha}{s_{max} - s_\alpha}\right)(1-\alpha) + \alpha\right] & for \quad s_\alpha < s < s_{max} \\ u_{max}\left[1 + \left(\frac{s_{max} - s}{s_1 - s_{max}}\right)\right] & for \quad s_{max} < s < s_{ps} \\ u_{ps}\left[1 - \left(\frac{s - s_{ps}}{s_3 - s_{ps}}\right)\right] & for \quad s_{ps} < s < s_3 \end{cases} \qquad \text{Equation 4.1}$$

Where u is the bond stress in MPa and s is the slip in mm. u_1 is the maximum bond stress corresponding to pullout failure and s_1 is its corresponding slip given as:

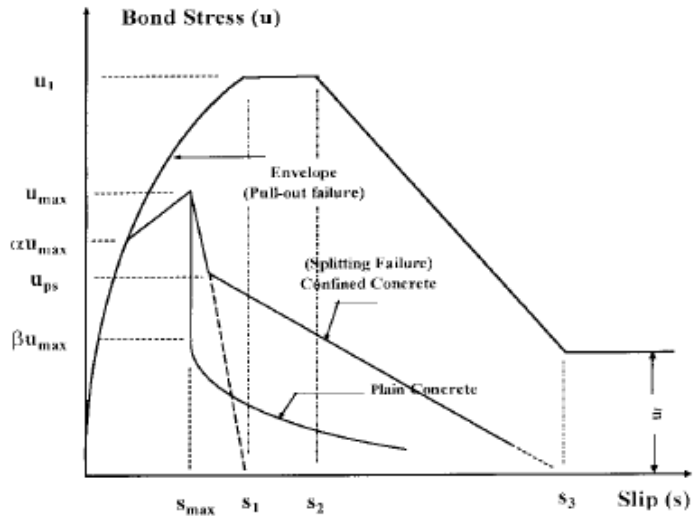

Figure 4.1: General bond stress-slip law (Harajli, Hamad and Rteil, 2004)

$$u_1 = 2.57\sqrt{f_c^{'}}$$ Equation 4.2

$$s_1 = 0.15c_o$$ Equation 4.3

$$s_\alpha = s_1\left(\frac{\alpha u_{\max}}{u_1}\right)^{1/0.3}$$ Equation 4.4

$$u_{\max} = A\sqrt{f_c^{'}}\left(\frac{c+K_c}{d_b}\right)^{2/3} \le u_1$$ Equation 4.5

$$s_{\max} = s_1 e^{(1/0.3)\ln\left(\frac{u_{\max}}{u_1}\right)} + s_0 \ln\left(\frac{u_1}{u_{\max}}\right)$$ Equation 4.6

$$u_{ps} = u_{\max}(B + K_{cs}) \le u_{\max}$$ Equation 4.7

$$s_{ps} = \left[\left(\frac{u_{\max} - u_{ps}}{u_{\max}}\right)(s_1 - s_{\max}) + s_{\max}\right]\left(\frac{K_c}{2}\right) \le s_1$$ Equation 4.8

Where: c_o is the clear distance between the ribs of the reinforcing bar normally equal to 9 to 10 mm (s_3 is equal to c_o), f'c is the concrete compressive strength, c is the minimum clear cover to the steel bar, d_b is the bar diameter, s_0 is a constant either 0.4 mm for concrete confined with stirrups or 0.2 mm for concrete confined with externally applied FRP sheets. The factors α, A and B are constants determined from experimental results. Harajli et al. (2004) suggested the 0.7, 0.78 and 0.5 for α, A and B respectively. It should be noted that Eq. 4.8 was derived based on the experimental results of the present study.

K_c and K_{cs} are factors that take into consideration the confinement effect of FRP and stirrups. They are calculated from the following equations (Harajli et al., 2004):

$$K_c = \frac{7.0A_{tr}}{sn} + \frac{28.0r_eA_{frp}}{sn} \qquad \text{Equation 4.9}$$

$$K_{cs} = \frac{7.5A_{tr}}{snc} + \frac{22.0r_eA_{frp}}{snc} \qquad \text{Equation 4.10}$$

where, s is the spacing between stirrups or FRP sheets (for continuous sheet, s = w = width of the sheet), n is the number of reinforcing bars being confined and A_{tr} and A_{frp} are the areas of steel stirrups and FRP sheets respectively within the spacing s, and crossing the potential plane of splitting. The factor r_e is the modular ratio of elasticity of FRP sheets relative to ordinary steel ($r_e = E_{frp}/E_s$).

4.1.2 Model Implementation

The local bond stress-slip (u vs. s) relation described above was used to model the bond stress-slip for beams M-N-T0 and M-W0-T0. In this study, the factors α and B were determined from test results to be 0.9 and 0.8 respectively. The factor A was 0.57 for unwrapped beams and 0.78 for wrapped beams.

Figure 4.2 and Figure 4.3 compare the experimental and the predicted bond stress-free end slip relation for unwrapped and CFRP wrapped beams respectively. The model gave good predictions of the experimental behaviour.

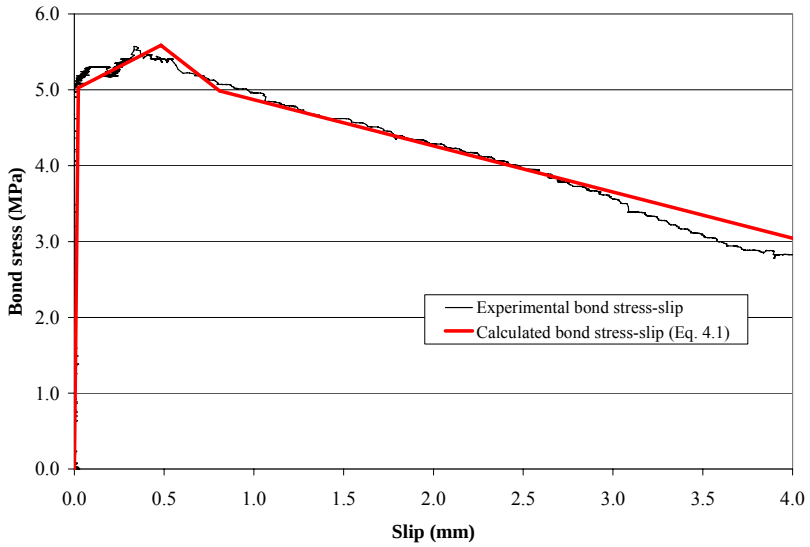

Figure 4.2 Bond stress- slip behaviour for M-N-T0

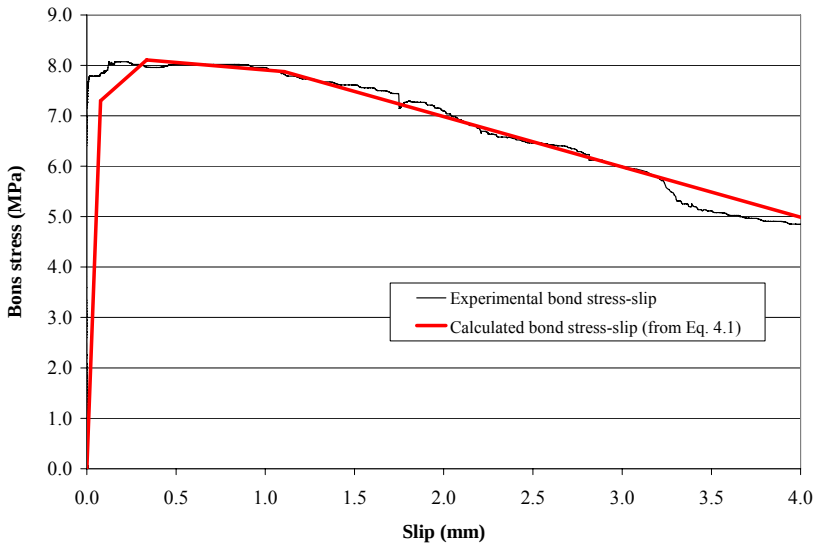

Figure 4.3 Bond stress- slip behaviour for M-W0-T0

4.2 Mechanics of Bond under Repeated Loading

4.2.1 Bond Stress Distribution

As the beam was subjected to an increasing load, the moment in the constant moment zone increased. The tensile stress in the concrete also increased, and eventually the concrete cracked. Since the specimen was unbonded in the middle, the first transfer of force between concrete and steel took place beyond the pocket, where the two materials first came into contact. Since the central region of the beam was unbonded, therefore, all the forces that would otherwise have been transferred from the concrete to the steel by bond in the central region were transferred close to the pocket resulting in a high local bond stress (the discontinuity acts as a stress raiser). The bond stress then decreases toward the value that would occur for a fully bonded beam with increasing distance from the stress raiser (Figure 4.4).

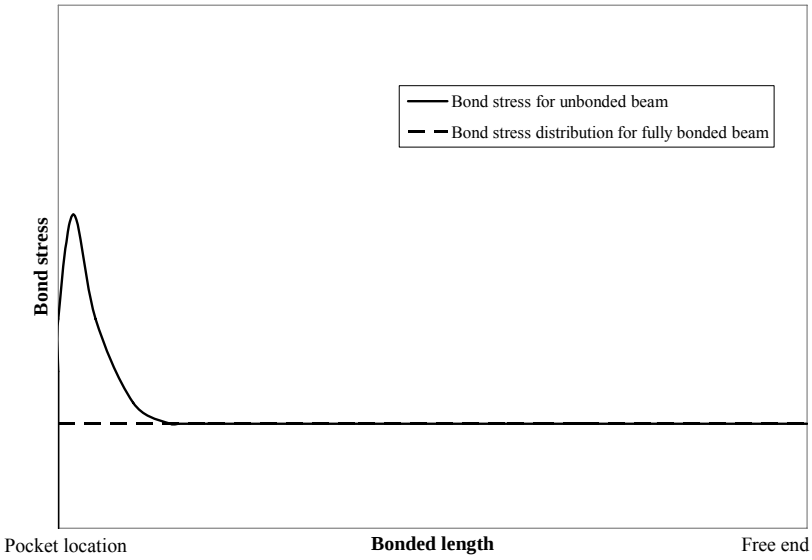

Figure 4.4 Schematic of the bond stress distribution in the shear zone at cycle 1

4.2.2 Unwrapped Uncorroded Beams

For rib angles less than 40-45^{o}, Lutz and Gergely (1967) suggested that the slip of the reinforcing bar relative to concrete takes place by wedge action. The measured rib angle for the steel bars used in this study was 37^{o}. Therefore, the high bond stress close to the pocket pushed the concrete bottom cover away by wedge action. The concrete cover cracked and a surface longitudinal crack appeared. This allowed the bar to slip without damaging the bottom cover thus leaving the concrete keys in front of the steel lugs uncrushed (Figure 4.5). However, the concrete above the bar was held in place by stirrups and resisted the movement. In front of the lugs, the concrete above the bar crushed and the concrete powder condensed and moved with the steel bar, therefore, decreasing the angle the ribs made with the axis of the steel bar. As a result, the bond stress decreased.

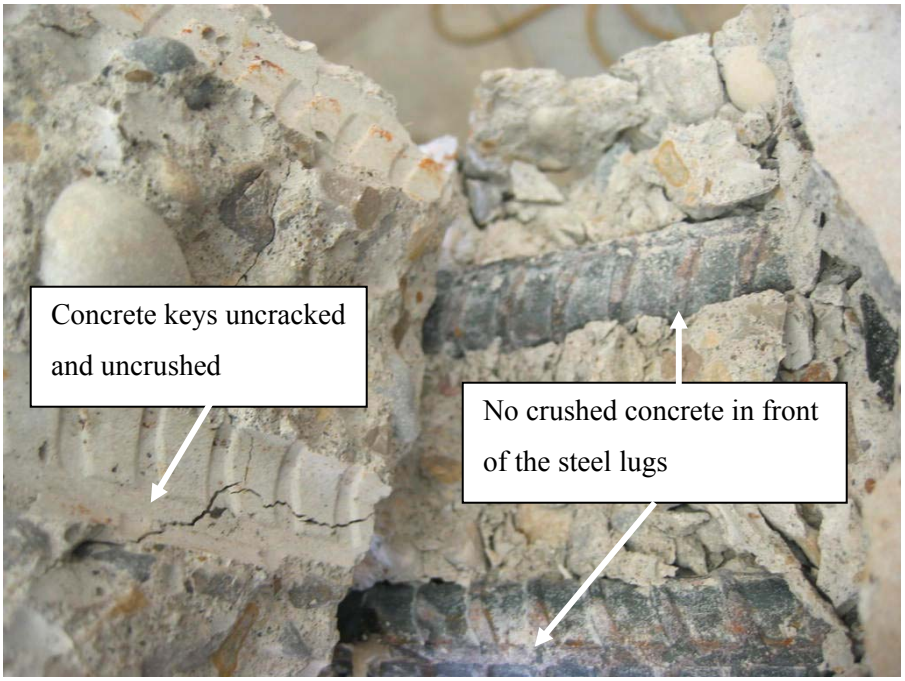

Figure 4.5 Bottom concrete cover and steel bar condition for the unwrapped uncorroded beams

In order to preserve the beam in equilibrium, the forces between the steel and concrete increased further along the bonded length where the concrete was still sound. Hence, the peak bond stress moved further inside the bonded length as the bond stress close to the pocket area decreased and the

bond stress close to the free end of the beam increased (Figure 4.6 and 3.21). This in turn increased the free end slip rate and stabilized the loaded end slip rate. The concrete close to the new position of the peak bond stress then cracked and crushed in the same way as the concrete near the pocket, and a further redistribution of the bond stress took place. This redistribution of bond stress continued for most of the beam's life (Figure 3.21). Near the end of the beam's life, all the concrete along the bonded length was damaged, the bond stress was almost uniform along the bonded length (Figure 4.6 and 3.21) and the slip in the free and loaded ends were equal (rigid body motion of the steel bar) and increased exponentially (see Figure 3.25). In addition, the surface cracks increased in width and number due to the hoop stresses along the entire bonded length. Eventually, the beam could not hold the applied load since the concrete could no longer transfer the tensile forces to the steel bars, and the beam failed.

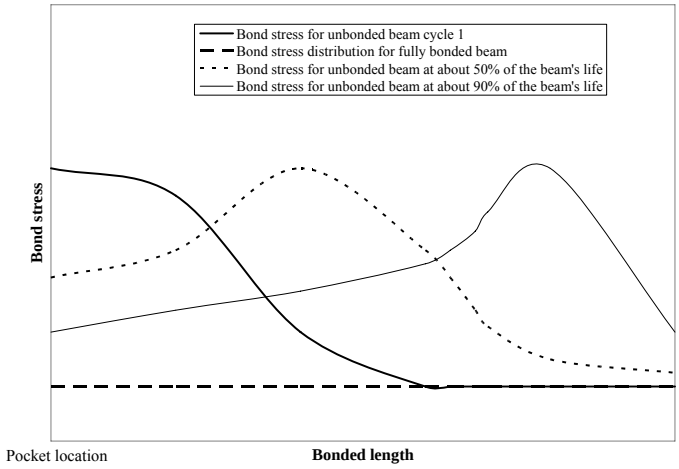

Figure 4.6 Schematic of the bond stress redistribution during fatigue cycling

The duration of bond redistribution was observed to be dependent on the load range applied. This was consistent with the observations reported by Balazs (1991) for pullout failure. As the applied load range increased, the moment increased, therefore, all the bond stresses increased. It took fewer cycles for the redistribution of the bond stresses to take place for beams tested at a high load range than for

beams tested at a low load range, also the onset of failure decreased from 90% to 70% of the beams life (see section 3.9.1).

4.2.3 Wrapped Uncorroded Beams

A major difference between the wrapped and unwrapped beams was that the wrapped beams were tested at higher load ranges (expressed in kN) than the unwrapped beams. This induced a high bond stress in the wrapped beams that cracked the concrete cover during the first few load cycles. As in the case of the unwrapped beams, the concrete was pushed away from the steel bar by wedge action. However, the presence of the CFRP sheets resisted the motion of the concrete cover, forcing it to stay in contact with the lugs of the steel bar. At the same time, the crushing of concrete in front of the lugs changed the effective angle of the face of the rib with the concrete (Figure 4.7). This in turn reduced the bond stress. In order to maintain the applied load, the peak bond stress moved toward the free end. The change of the rib angle also increased the hoop stress, which resulted in more cracks in the concrete cover and increased the loaded end slip as well as the stress in the CFRP sheets during the first 5 to 10% of a beams' life. After that, the whole bonded length was engaged in resisting the bond force resulting in an almost uniform bond stress. This condition would signify a beam failure for unwrapped beams (all the bonded length was highly stressed and slip reached about 2.0 mm). However, because the CFRP maintained the concrete cover in contact with the lugs of the steel bar, the beam did not fail; instead, it continued to resist the repeated loading. The face angle of the lugs ceased to increase (Figure 4.7); since the crushing in front of the lugs did not greatly affect the face angle, once it reached a distance 6 to 7 times the rib height (Lutz and Gergely, 1967). The increase in the hoop stresses then ceased, which in turn stabilized the CFRP stress and led to a slow increase of the slip of the steel bar (see Figures 3.19 and 3.24). With continued cycling the concrete cover continued to crack, the CFRP stress increased slowly and the steel bar slipped at a slow rate until the

CFRP sheets ruptured and removed the forces that were holding the concrete cover in place. This resulted in a complete slip of the steel bar and the beam failed.

Figure 4.7 Condensed crushed concrete in front of the steel bar lugs for wrapped beams

4.2.4 Corroded Beams

The corrosion of the steel bars did not alter the behaviour for the unwrapped and wrapped beams. The unwrapped corroded beams behaved similarly to the unwrapped uncorroded beams and the wrapped corroded beams performed similarly to wrapped uncorroded beams. However, in the corroded beams the initial loaded end slip increased at a faster rate than for their uncorroded counterparts. Several factors were changed due to corrosion and played a role in this increase 1) a reduced concrete confinement due to cracking of the concrete cover; 2) a lower friction between the concrete and the steel due to flaky corrosion products and; 3) a lower rib height that decreased the friction and interlock components of the bond force. Therefore, the redistribution of bond stress over the entire bonded length in corroded beams took fewer cycles than for the uncorroded beams. This resulted in shorter fatigue lives for the corroded beams than for the uncorroded ones.

Balazs (1991) and ACI 408 (1992) reported that an increase in slip indicates the progress of micro crushing and micro cracking in front of the lugs. This is true for highly confined bond critical regions as is the case for the CFRP wrapped beams (tested in this study) or the pullout specimens tested by various researchers (which ACI committee 408 relied on to draw this conclusion). However, it is not true for the beams with an unconfined concrete cover since the concrete was pushed away by wedge action without contributing much resistance to the bond forces. A similar observation was reported by Verna and Stelson (1962) who tested beams (rather than pullout specimens); where they noticed that the bottom concrete cover full off during testing.

4.3 Fatigue Slip Growth Analysis

4.3.1 Background

In fracture mechanics, it is always assumed that some initial crack exists in a component or structure. During repeated loading, the primary variable that affects the fatigue growth of the crack is the range of the stress intensity factor (SIF) ΔK (Dowling, 1999), where ΔK is given in Eq. 4.11.

$$\Delta K = (S_{\max} - S_{\min}) F \sqrt{\pi a} \qquad \text{Equation 4.11}$$

Where S_{min} and S_{max} are the nominal stress at maximum and minimum load applied (S is usually defined using the gross area of the uncracked section), a is the crack length, and F is a dimensionless factor that is a function of the geometry.

The fatigue crack growth analysis is based on the assumption that during crack growth, the increment in crack length per cycle (da/dN), varies linearly with ΔK on a log-log plot. Therefore, calculating the fatigue life of a component is a matter of integrating the da/dN- ΔK relationship between the initial and final crack lengths (Dowling, 1999).

4.3.2 Formulation of a Fatigue Slip Growth Model

In this study, a damage model similar to the fracture mechanics fatigue crack-growth analysis was adopted. However, in a bond failure in concrete, several cracks initiate and propagate in various directions in the reinforced concrete specimen (rather than a single crack as in the case of metals). Also, the damage in the concrete in front of the steel bar lugs, due to bond forces, may take other forms such as wedge action and crushing. Slip of the steel bar relative to concrete, s, which takes place only if the concrete around the steel bar is damaged (i.e. cracked, crushed and/or pushed away from the steel bar) is chosen as a damage criterion in this study.

A bond stress intensity factor (B-SIF), K_{bond}, similar to the stress intensity factor used in fracture mechanics, was used in the form given in Eq. 4.12.

$$K_{bond} = (u_{\max} P)\sqrt{s} \qquad \text{Equation 4.12}$$

Where u_{max} is the maximum static bond stress calculated from Eq. 4.5, P is expressed as the ratio of the maximum load applied to the static capacity of the specimen and s is the slip of the steel bar.

Similar to the crack growth rate in fracture mechanics, the relationship between the cyclic slip growth rate (ds/dN) and the bond SIF, K_{bond}, take the form given in Eq. 4.13.

$$\frac{ds}{dN} = C(K_{bond})^m = C\left[(u_{\max} P)\sqrt{s}\right]^m \qquad \text{Equation 4.13}$$

Where C and m are constants that depend on the corrosion level and whether the specimen was confined or not.

In order to determine the fatigue life of a given specimen, Eq. 4.13 is integrated over the interval $[s_i, s_f]$ (see Eq. 4.14) where s_i and s_f are the slip of the steel bar at the first and final fatigue cycles (N_i and N_f) respectively.

$$N_f = \int_{N_i}^{N_f} dN = \int_{s_i}^{s_f} \frac{ds}{C(K_{bond})^m} = \frac{s_f^{1-m/2} - s_i^{1-m/2}}{C(u_{\max} P)^m (1-m/2)} \qquad for\ m \neq 2 \qquad \text{Equation 4.14}$$

4.3.3 Determining the Initial and Final Slip

The values of the final slip used in Eq. 4.14 were set equal to the average of the values of the slip readings at failure for each group. These are shown in Table 4.1. The values of the initial slip for each group of beams were plotted against the maximum load applied (Figure 4.8). The equations from a best fit of the data are presented in Table 4.1.

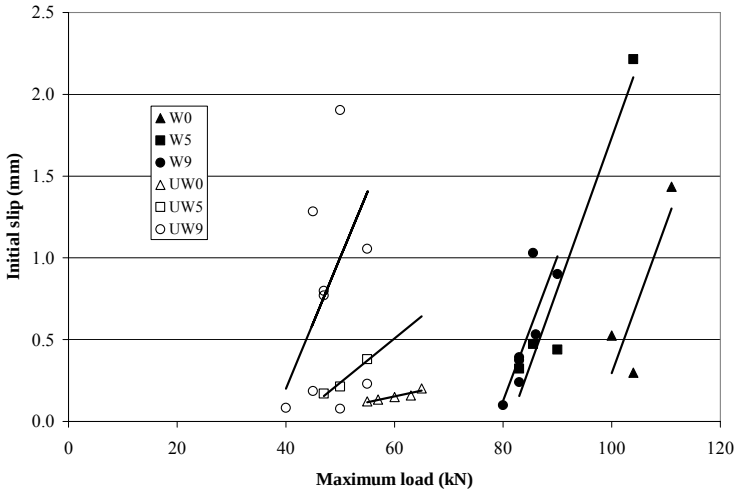

Figure 4.8 Variation of the initial slip with the applied maximum load

Table 4.1 Proposed values for the initial and final slip

Group	s_i (mm)	s_f (mm)
UW0	$0.007P_{max}$-0.2684	2.4
UW5	$0.0144P_{max}$-0.5613	4.7
UW9	$0.08P_{max}$-3	5.5
W0	$0.0916P_{max}$-8.868	4
W5	$0.0928P_{max}$-7.5479	5.5
W9	$0.0883P_{max}$-6.9419	6

P_{max} is the maximum applied load

4.3.4 Determining the Constants C and m

The constants C and m were determined from the experimental load range-life data and the initial slip. Ideally, these constants would have been determined from the measured experimental ds/dN vs. K_{bond}, but theses data had considerable scatter, which made it difficult to use such curves.

It was noted that the slope of the best-fit curves of the experimental load range-life data (Figure 3.16) are almost parallel. This was expected since the failure mechanism presented in section 4.2 was almost the same for all beams tested under repeated loading that failed by fatigue of bond. Therefore, the value of m was taken to be constant for all the tested beam groups. To determine the value of m, Eq. 4.14 was plotted against the experimental load range-life data. A value of m = 9 was found to fit the data accurately. The value of C was determined from an iterative solution that aimed at reproducing the slip-life curve from the experimentally known initial and final slip values for each beam using Eq. 4.13. The value of C was changed until the fatigue cycle at the final slip was close to or equal to the fatigue life of the given beam. The procedure to calculate C is shown in the flowchart presented in Figure 4.9 and the values for different groups tested in this study are given in Table 4.2.

Calculated slip-life curves together with the experimental data to which they were fit are shown in Figure 4.10 for two different beams (the complete set of curves is presented in Appendix D). It should be noted that while the shape of the slip-life data was similar to the calculated curve as shown in Figure 4.10a for most of the beams (see Appendix D) in a few cases the slip-life data had a significantly different shape as shown in Figure 4.10b.

In order to determine the adequacy of the values of C and m determined from the above method, the experimental and the predicted values of ds/dN are plotted versus K_{bond} values in Figure 4.11 for Group W9 (a complete set of curves are given in Appendix E). Most of the predicted ds/dN curves fall within the scatter of the experimental results.

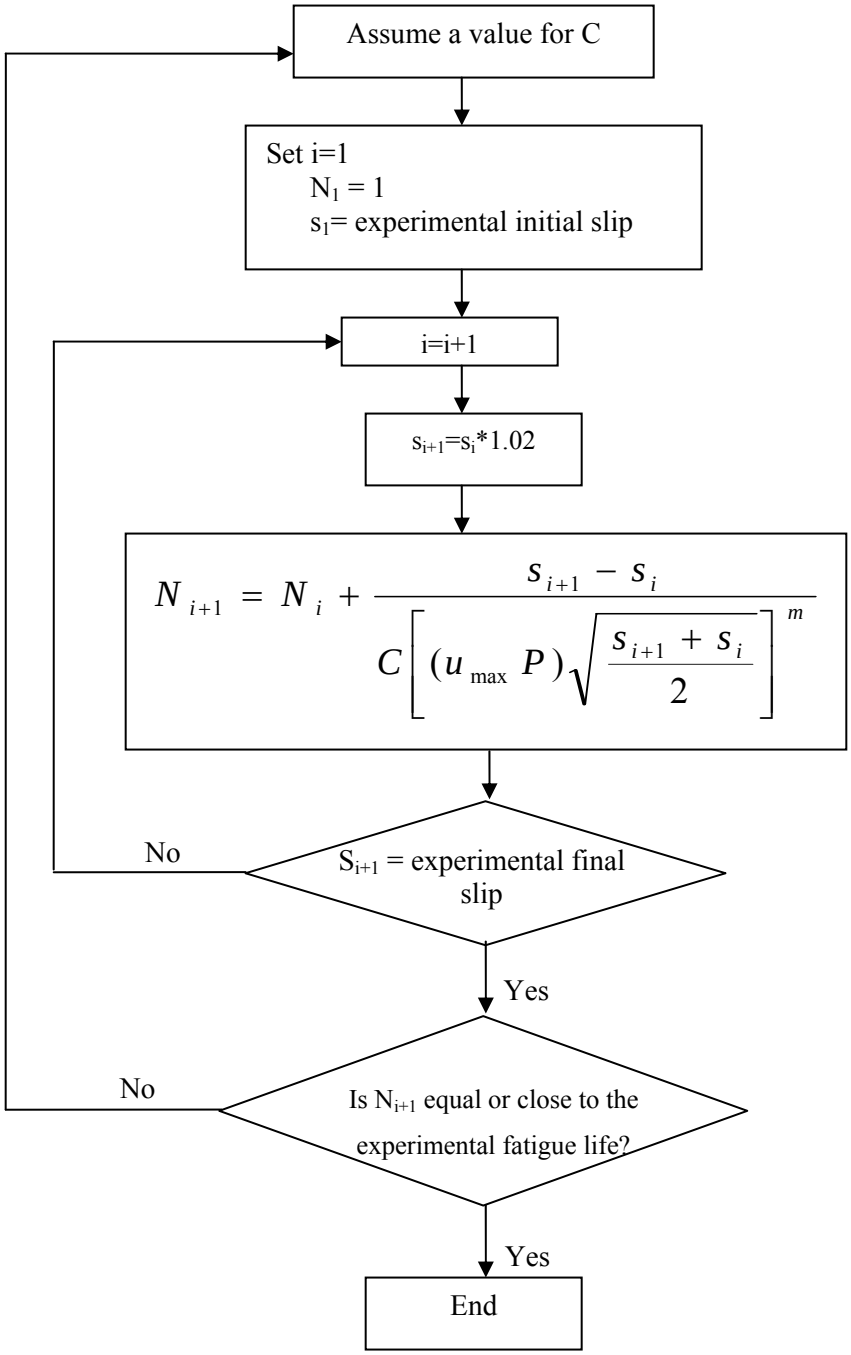

Figure 4.9 Flow chart of the procedure to determine the constant C

Table 4.2 Constants of the fatigue slip growth model

Group	C	m
UW0	$1.3*10^{-6}$	9
UW5	$9.4*10^{-8}$	
UW9	$4.2*10^{-7}$	
W0	$7.5*10^{-12}$	
W5	$7.0*10^{-12}$	
W9	$1.1*10^{-11}$	

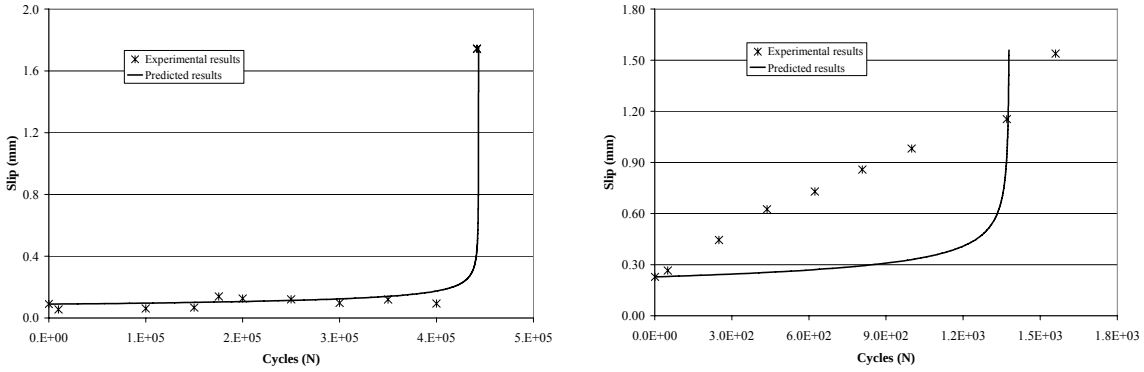

a) Beam F45-N-T0 b) Beam F55-N-T0

Figure 4.10 Predicted and experimental slip-life curves

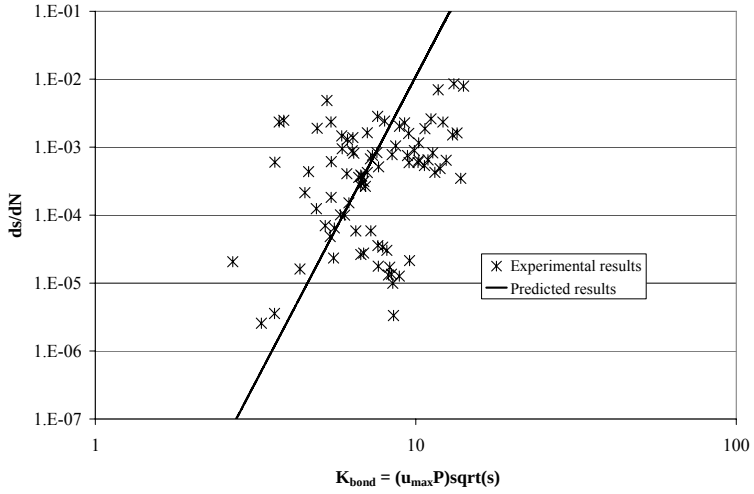

Figure 4.11 Variation of the experimental and predicted ds/dN values with K_{bond}

4.3.5 Model Implementation

Equation 4.14 was used to calculate the fatigue lives of all the beams tested in this study. The values of the initial slip were determined from the proposed equations in Table 4.1 and the final slip value used in implementing the model in each group was taken from Table 4.1. The values of the constants C and m in Eq. 4.14 were determined from Table 4.2. Figure 4.12 compares the predicted fatigue lives using Eq. 4.14 to the experimental results (Appendix F shows the predicted and experimental results for each test group separately). The fatigue slip-growth approach was in good agreement with the experimental results.

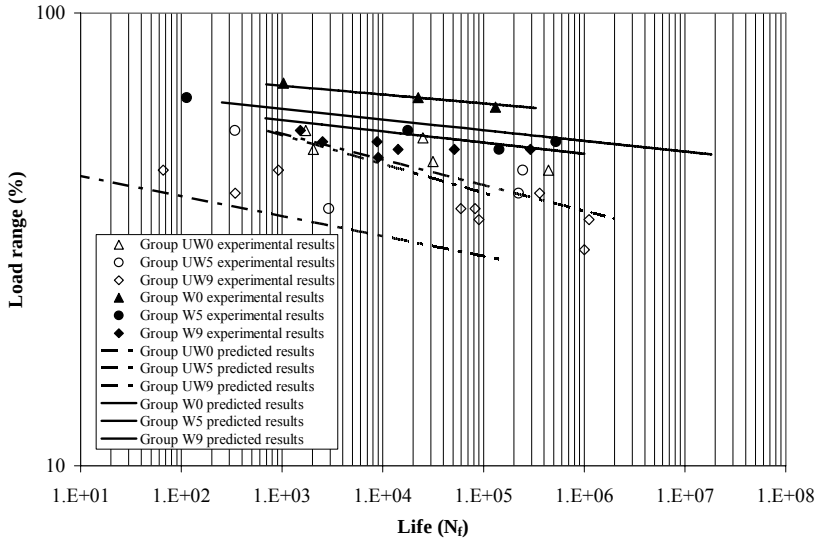

Figure 4.12 Predicted and experimental fatigue lives using proposed initial slip

4.3.6 Limitations of the Proposed Approach

The fatigue slip-growth approach uses the initial slip and the constants of the slip-life curve, all of which showed a considerable scatter. In addition, very few variables were studied in this research (corrosion level, applied load range and whether the specimen was wrapped with CFRP sheets or not).

Chapter 5
Closure

5.1 Conclusions

The study presented herein was aimed at investigating the performance of the bond between corroded steel reinforcement and CFRP confined concrete under repeated loading. Forty-seven anchorage-beam specimens were cast and tested. Based on the experimental results, observations and analysis the following conclusions were drawn:

5.1.1 Mass Loss Measurements

- For a 5% measured mass loss, the corrosion was almost uniform along the steel bar. As the corrosion increased to 9% there was increasing presence of corrosion pits.

- For beams subjected to 50 days of corrosion (at a current density of 150 $\mu A/cm^2$), Faraday's law was able to predict the corrosion level reasonably well (5% mass loss). However, it overestimated the corrosion levels for exposure times of 100 and 150 days.

- Beams that were corroded for 50 days, wrapped with CFRP sheets in the anchorage zone and then subjected to an additional 100 days of corrosion had the same measured mass loss as the beams that were subjected to a continuous 150 days of exposure. Therefore, it is recommended based on previous studies, that if FRP sheets are to be used to control the corrosion activity, then the sheets should cover the entire beam, rather than just part of it.

5.1.2 Static Beam Test

- Both wrapped and unwrapped beams failed by bond, characterized by concrete splitting. The failure of the CFRP sheets was by rupture of the sheets at the level of the steel bar.

- The presence of CFRP sheets increased the load carrying capacity of the specimen by 39% and the bond strength by 47%. It also increased the bond stiffness by 25% and the load at which the free slip initiated by 36%. Post-failure performance was also improved since the CFRP sheets made the wrapped beam more ductile.

5.1.3 Repeated Loading Results

- In unwrapped beams, longitudinal cracks initiated at the level of the steel bar in the anchorage zone and increased in width and number as the cycling continued until failure. For the unwrapped corroded beams, these cracks were in addition to the pre-existing corrosion-induced cracks. The propagation rate for the longitudinal cracks was divided into three parts: the propagation rate decreased from an initially high value during the first 20% of the specimens' fatigue life, and then the propagation rate ceased or slowed down in the middle 60-70% of the beams' fatigue life. In the last part, the propagation rate increased during the last 10-20% of the beams' fatigue life.

- All unwrapped beams (corroded and uncorroded) failed by concrete splitting. It was noted that the bottom cover was pushed away during cycling, preserving the concrete keys intact for uncorroded beams. A similar observation was made for the corroded beams, except that the height of the concrete keys was reduced by the corrosion.

- The wrapped beams tested in fatigue failed in bond, except for few that failed in flexural fatigue (by a steel fracture). The number and width of the longitudinal cracks in the wrapped beams that failed by bond were less than in the unwrapped beams.

- For wrapped beams failing in bond, it was noted that the concrete in front of the steel bar lugs was crushed and that the rest of the concrete bottom cover was cracked. Also, the CFRP sheets ruptured along the steel bar in the anchorage zone.

- The fatigue strength (measured as the load range applied) of the unwrapped beams corroded to a 5% and a 9% mass loss decreased on average by 12% and 23% respectively at all fatigue lives compared to the fatigue strength of the unwrapped uncorroded beams. In the CFRP wrapped beams, the percentage decrease of the fatigue strength due to the 5% and 9% corrosion levels was on average 16% and 21% respectively compared to the fatigue strength of the wrapped uncorroded beams.

- The addition of CFRP sheets increased the fatigue strength (as measured by the load range applied) compared to that of the unwrapped beams at all corrosion levels and all fatigue lives. The average fatigue strength increased by 32%, 26% and 35% compared to the fatigue strength of unwrapped beams for corrosion levels of 0%, 5% and 9% respectively.

- The strain in the CFRP sheets increased sharply for the first 4 to 8% of a beam's fatigue life. After that, the strain reading levelled off until close to failure. This behaviour was the same for all the wrapped beams irrespective of the corrosion level.

- The damage to the concrete cover due to repeated loading forced a redistribution of the bond stress. The bond stress peak moved along the bonded length from the loaded end at the beginning of the cycling until it reached the free end just before failure.

- For unwrapped beams, the slip behaviour was divided into two stages. In stage one, the slip increased at a slow rate, which increased as the corrosion level increased. In stage two, the slip increased exponentially. It was noted that the transition from stage one to stage two is dependent on the load level for uncorroded beams, but was constant at about 90% of the beams' life for corroded beams.

- For the wrapped beams, the slip followed almost the same behaviour as the CFRP strain. The slip increased at a decreasing rate in the first 4 to 8% of the beams' life, then continued to increase at a slow rate. In the last 10% of the beams' life, the slip increased exponentially.

- The loaded end slip was higher than the free end slip. However, when the slip started to increase exponentially (for both wrapped and unwrapped beams) it was the same at the loaded and free ends.

- The initial slip increased as the maximum load applied increased and the failure slip increased as the corrosion level increased.

- A hypothesis of the mechanics of bond under repeated loading is presented based on the experimental results, test observations and analysis.

- A fatigue slip-growth analysis, similar to the fracture mechanics' crack growth approach, was used to calculate the life of a specimen failing in fatigue of bond. The proposed method was in reasonable agreement with the experimental results. The constants in the proposed model depend on whether the specimen was wrapped with CFRP sheets or not, the level of corrosion, the maximum load applied, and the initial and final slip.

5.2 Future Work

Based on the results of this study the following changes in the variables are recommended as a possible extension of this work. Performing experiments with the below variables will increase the database and knowledge in the bond-fatigue-corrosion problem.

- Use of a higher corrosion level (more than 10% actual mass loss).

- Use of different bonded lengths and bar sizes.

- Vary the concrete strength and concrete cover.

Appendix A

Steel Mass Loss Measurements

Table A.1 Steel mass loss results

Group	Beam notation	Corrosion time (Days)	Steel mass loss (%)*				Average of group
			Ave.	Max.	Min.	Std dev	
UW5	F37-N-T5	50	4.7	5.0	4.5	0.2	5.0
	F40-N-T5		4.4	5.2	3.5	1.0	
	F45-N-T5		5.2	5.3	5.1	0.1	
	F50-N-T5		6.0	6.5	5.5	0.7	
	F55-N-T5		4.8	5.2	4.2	0.4	
W5	F48/52a-W5-T5		6.4	8.0	5.4	1.3	6.1
	F50-W5-T5		6.5	7.9	5.2	1.2	
	F52-W5-T5b		6.5	8.0	5.5	1.2	
	F55-W5-T5		5.5	6.6	4.8	0.8	
	F65-W5-T5		5.6	6.0	5.3	0.4	
Average of beams subjected to 50 days of corrosion							5.6
UW9	F30-N-T9a	100	9.2	10.0	7.6	1.1	8.3
	F35-N-T9a		8.6	10.1	7.4	1.4	
	F37-N-T9a		7.9	9.1	7.2	0.8	
	F40-N-T9a		7.4	7.9	7.0	0.4	
	F45-N-T9a		8.6	9.9	7.3	1.3	
W9	F45-W9-T9		7.8	8.3	7.0	0.6	8.2
	F48-W9-T9		7.7	8.1	7.1	0.5	
	F50-W9-T9a		7.9	8.3	7.4	0.5	
	F52-W9-T9a		9.0	9.5	8.7	0.3	
	F55-W9-T9a		8.5	9.7	7.5	0.9	
Average of beams subjected to 100 days of corrosion							8.3
UW9	F30/40-N-T9b	150	9.8	10.1	9.6	0.2	9.2
	F35-N-T9b		9.6	10.0	9.1	0.5	
	F37-N-T9b		8.4	9.6	7.2	1.0	
	F42-N-T9		8.3	8.8	7.6	0.6	
	F45-N-T9b		9.8	11.1	8.9	1.0	
W9	F47-W9-T9		10.4	11.7	9.3	1.1	10.1
	F50-W9-T9b		11.5	12.3	10.7	0.7	
	F50-W9-T9c		9.0	9.8	7.9	0.8	
	F52-W9-T9b		9.4	10.6	8.5	0.9	
	F55-W9-T9b		10.1	11.4	9.4	0.9	
Average of beams subjected to 150 days of corrosion							9.6
PR	F50-W5-T9	150	10.3	12.6	8.9	1.6	10.3
	F55-W5-T9		9.9	13.3	7.5	2.7	
	F58-W5-T9a		11.0	11.5	10.3	0.5	
	F58-W5-T9b		10.1	11.4	9.2	0.9	
	F60-W5-T9		10.1	11.5	9.6	1.0	

Appendix B

Load-Life Results

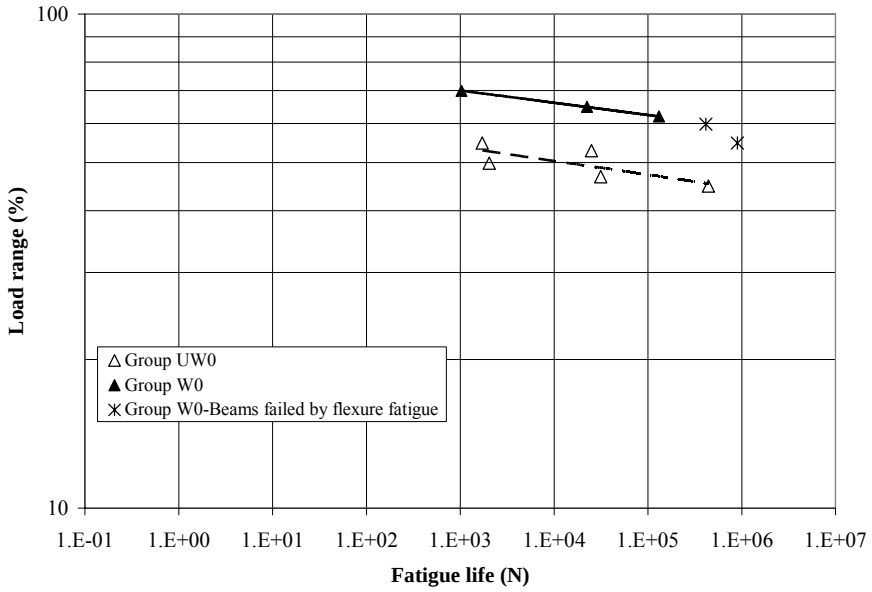

Figure B.1 Load range- life variation for Groups UW0 and W0 (uncorroded)

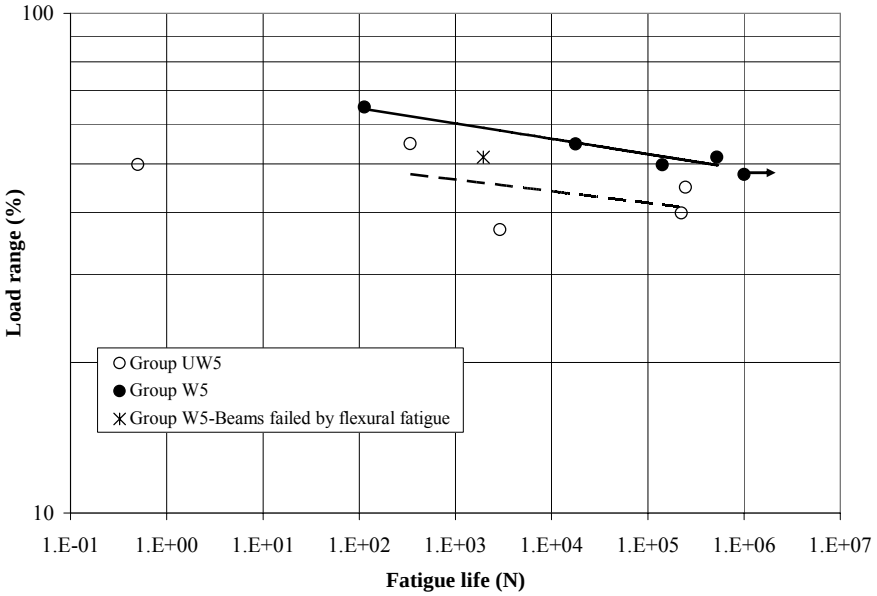

Figure B.2 Load range- life variation for Groups UW5 and W5 (corroded to 5% mass loss)

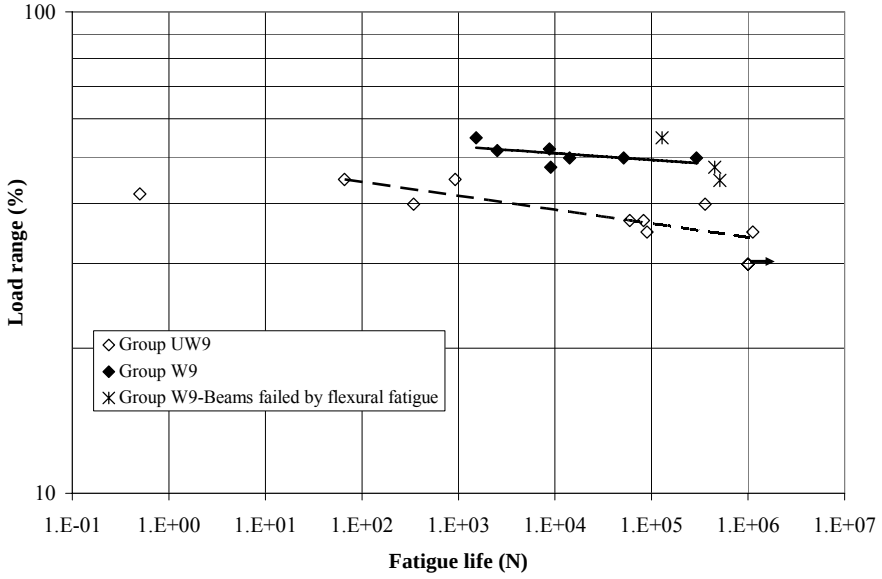

Figure B.3 Load range- life variation for Groups UW9 and W9 (corroded to 9% mass loss)

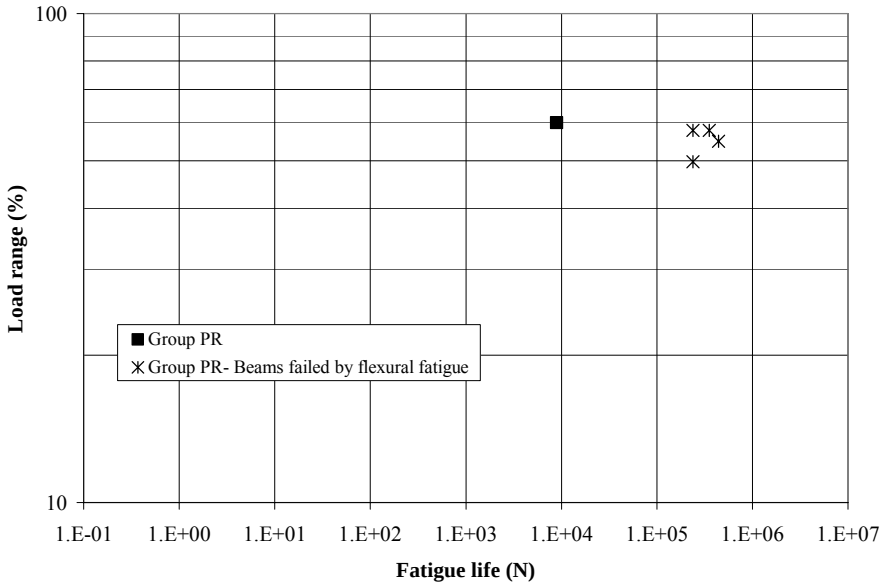

Figure B.4 Load range- life variation for Group PR (post repair)

Appendix C

CFRP Strain-Life Data

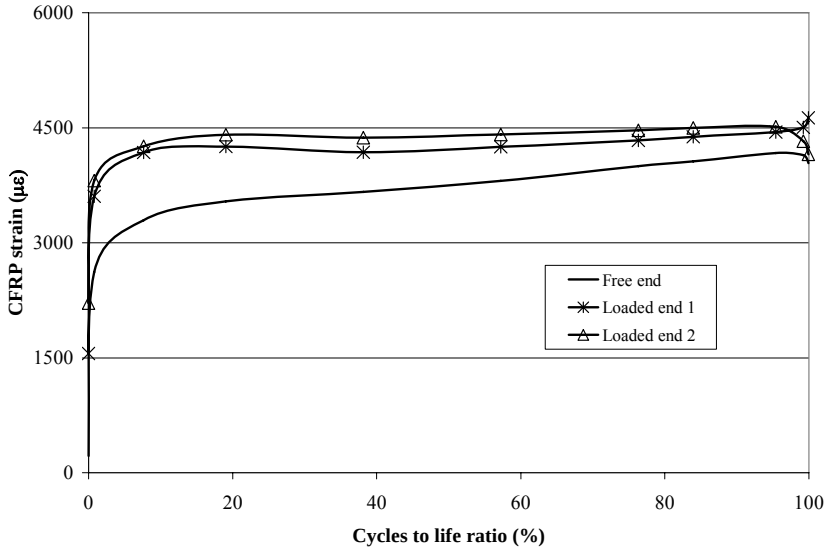

Figure C.1 CFRP strain-life variation for Beam F62-W0-T0

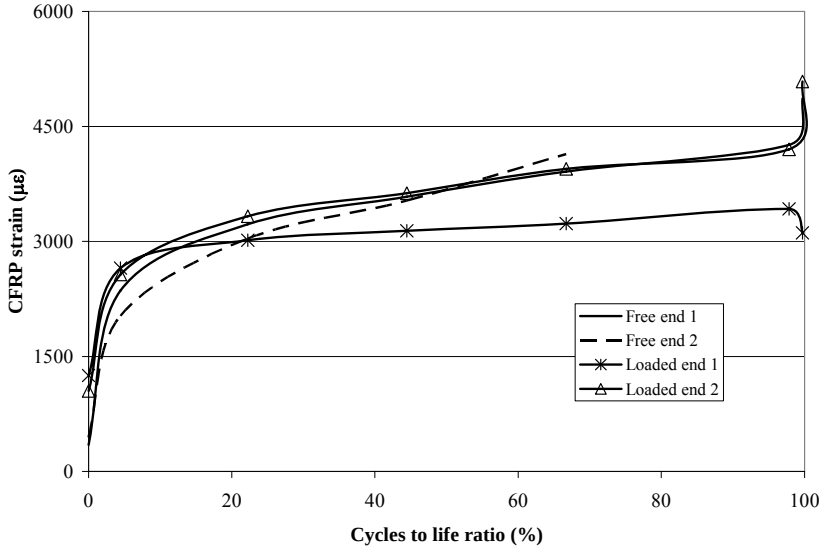

Figure C.2 CFRP strain-life variation for Beam F65-W0-T0

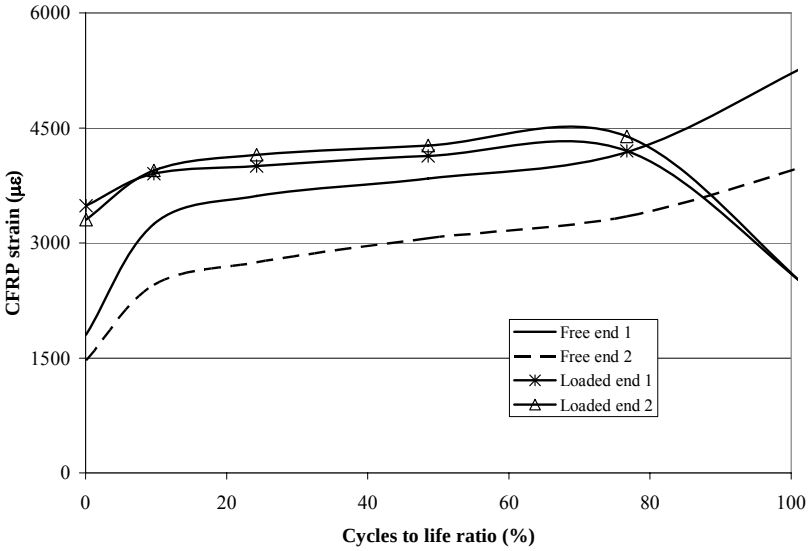

Figure C.3 CFRP strain-life variation for Beam F70-W0-T0

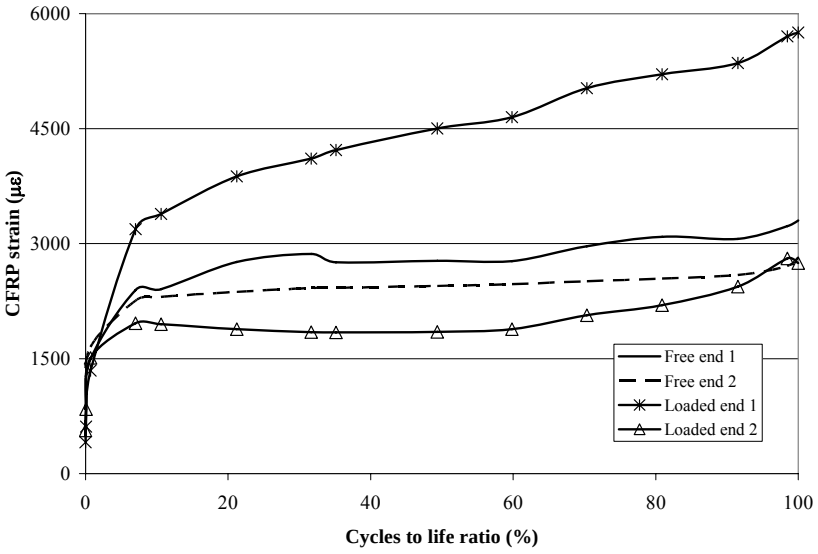

Figure C.4 CFRP strain-life variation for Beam F50-W5-T5

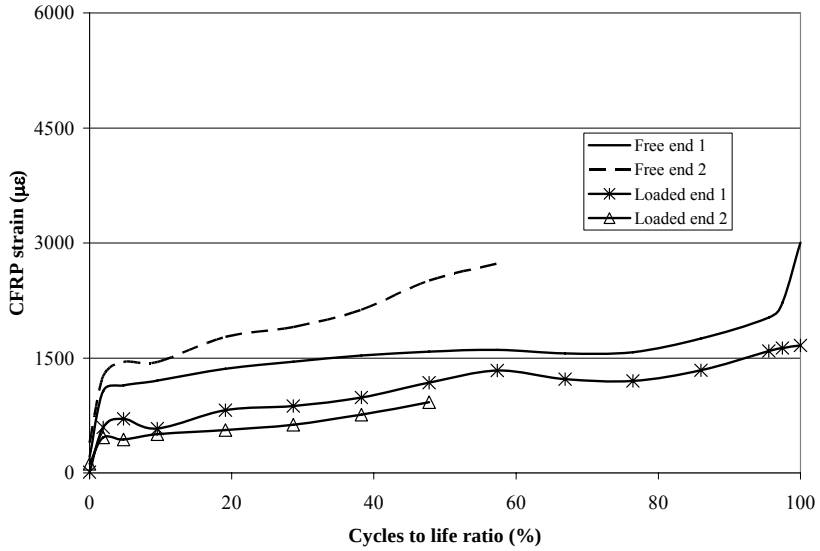

Figure C.5 CFRP strain-life variation for Beam F52-W5-T5a

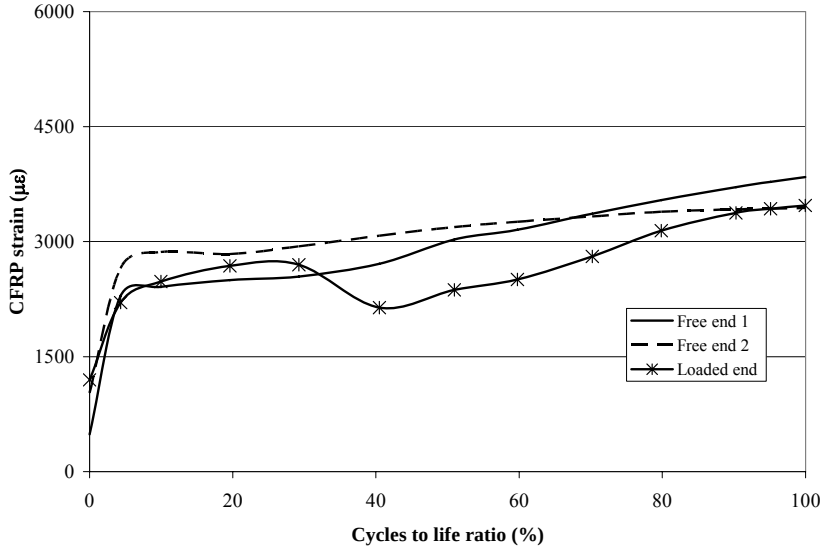

Figure C.6 CFRP strain-life variation for Beam F55-W5-T5

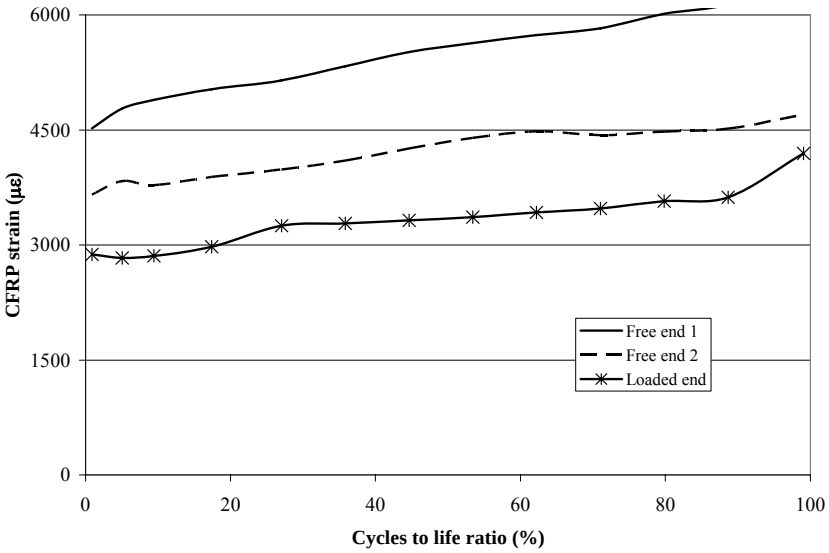

Figure C.7 CFRP strain-life variation for Beam F65-W5-T5

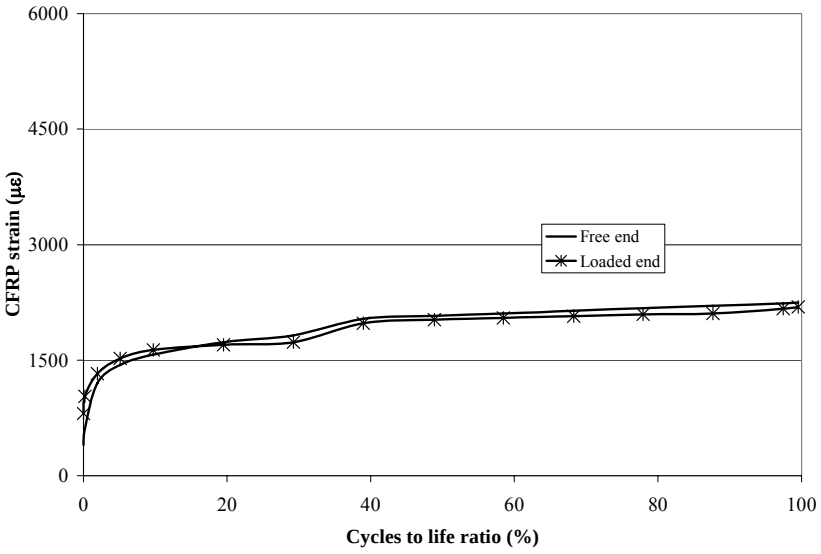

Figure C.8 CFRP strain-life variation for Beam F50-W9-T9a

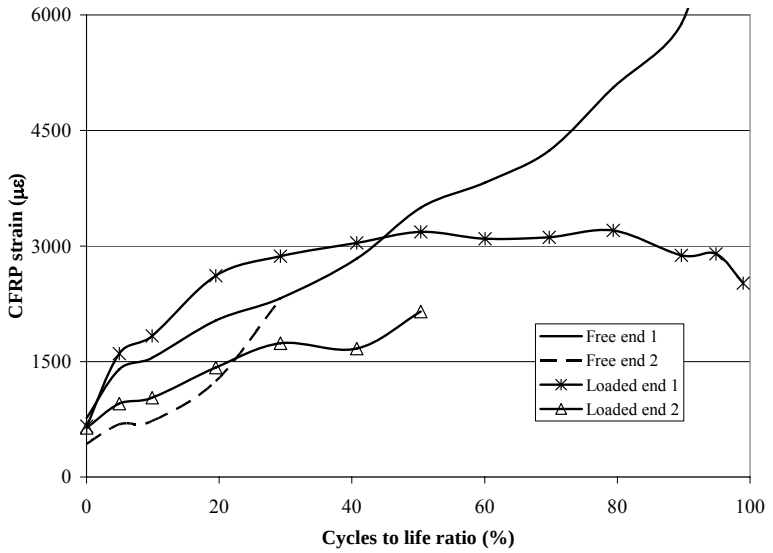

Figure C.9 CFRP strain-life variation for Beam F52-W9-T9a

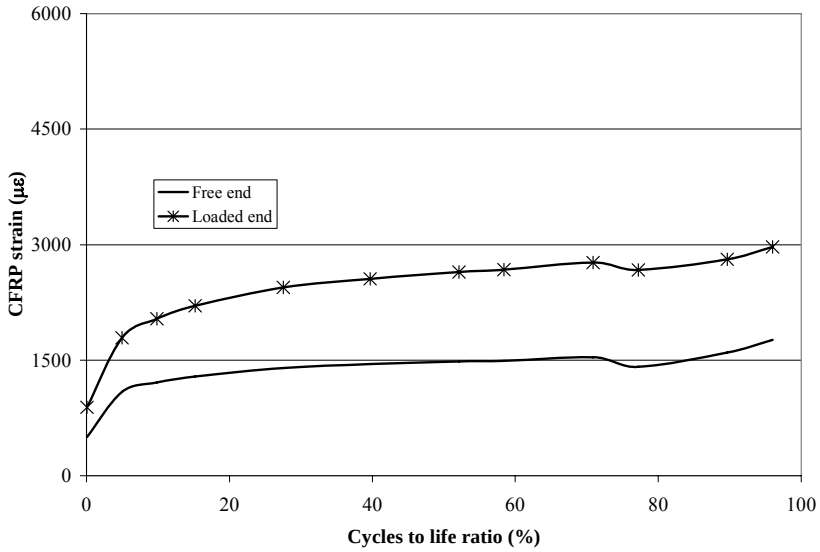

Figure C.10 CFRP strain-life variation for Beam F55-W9-T9a

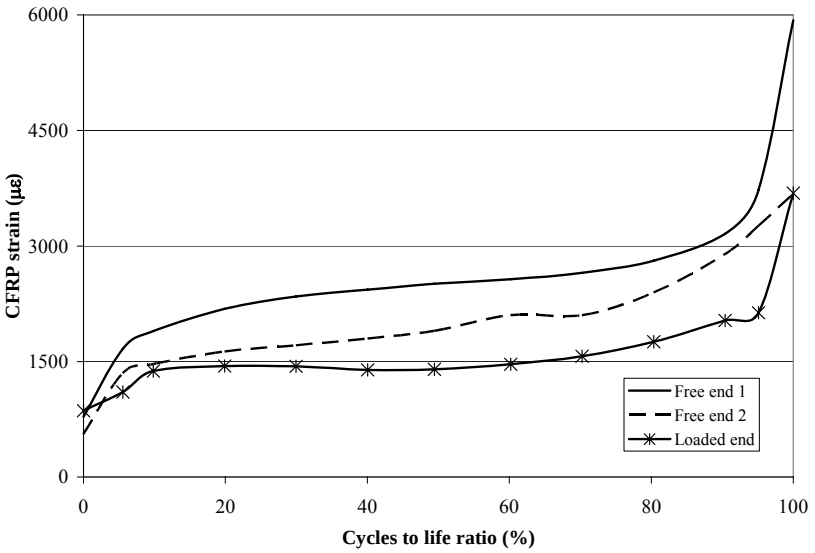

Figure C.11 CFRP strain-life variation for Beam F50-W9-T9b

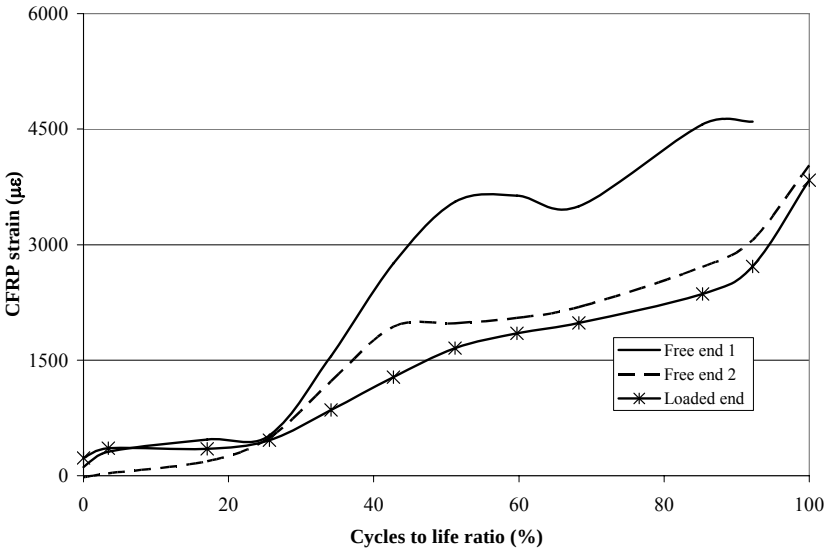

Figure C.12 CFRP strain-life variation for Beam F50-W9-T9c

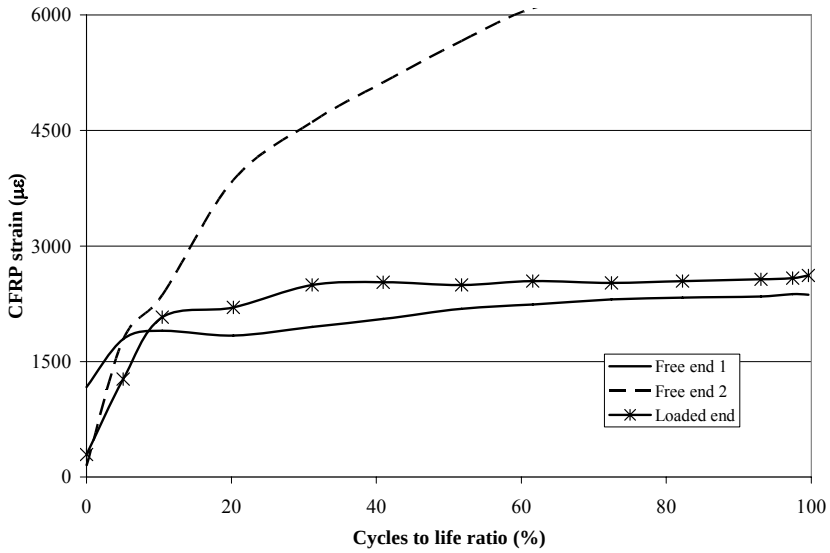

Figure C.13 CFRP strain-life variation for Beam F52-W9-T9b

Appendix D

Steel Strain Variation

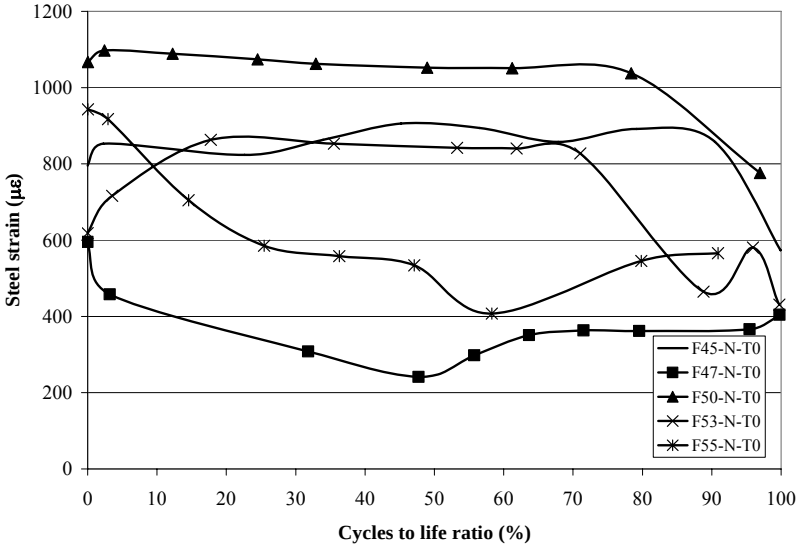

Figure D.1 Steel strain variation for Group UW0

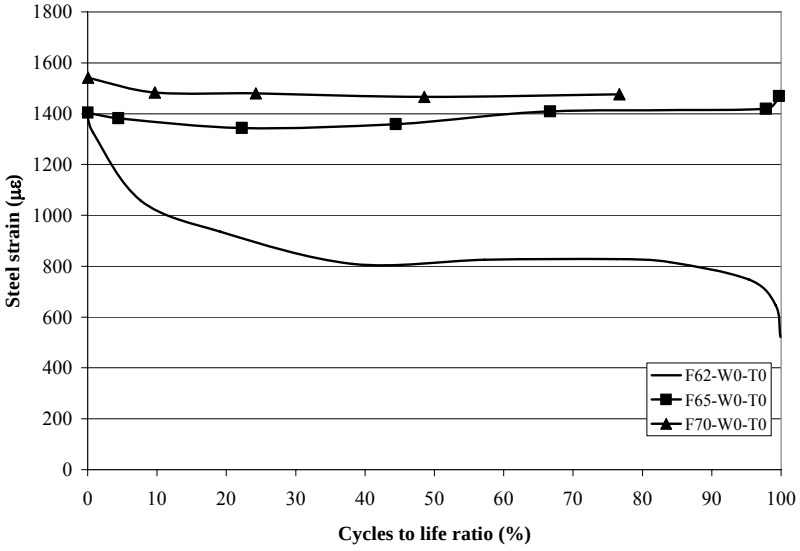

Figure D.2 Steel strain variation for Group W0

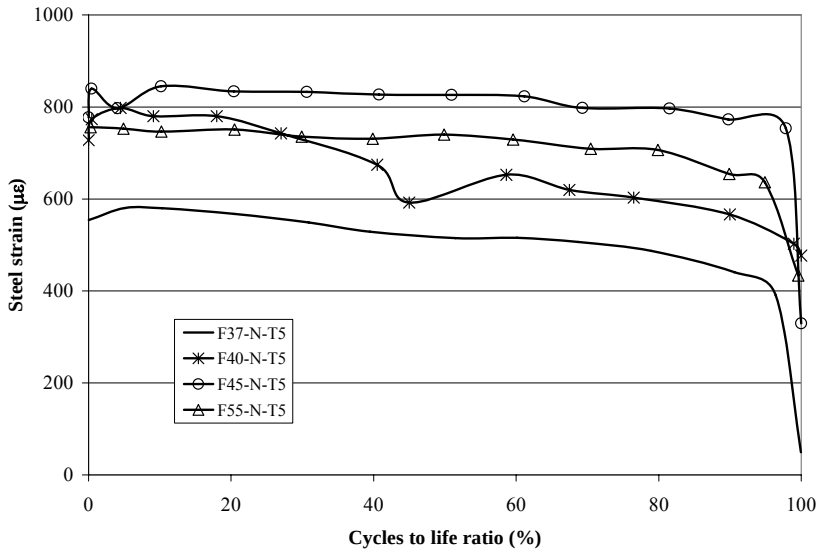

Figure D.3 Steel strain variation for Group UW5

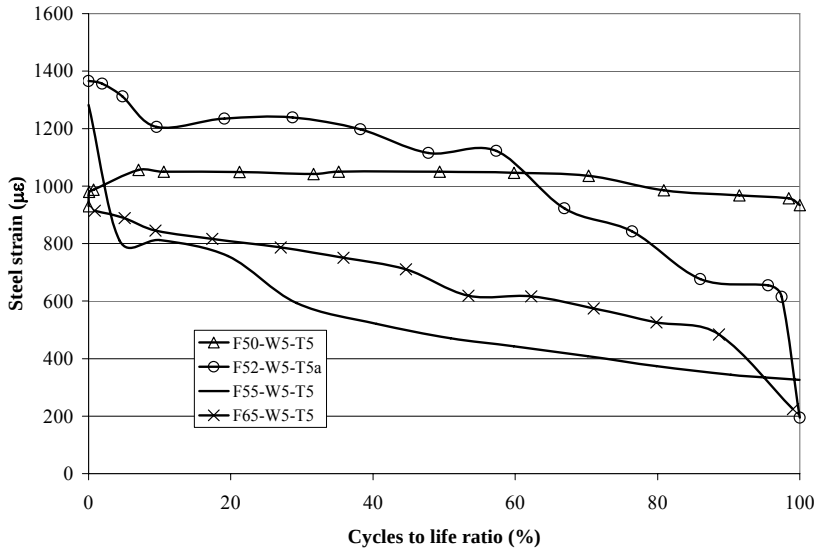

Figure D.4 Steel strain variation for Group W5

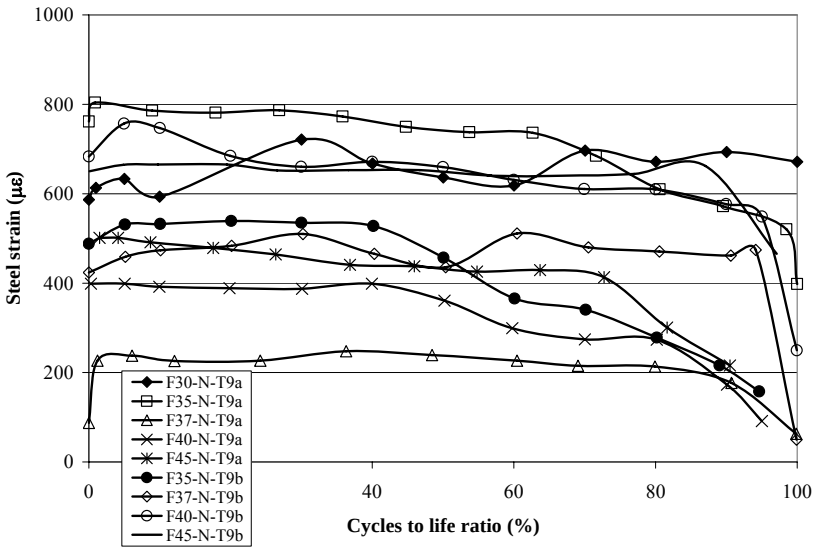

Figure D.5 Steel strain variation for Group UW9

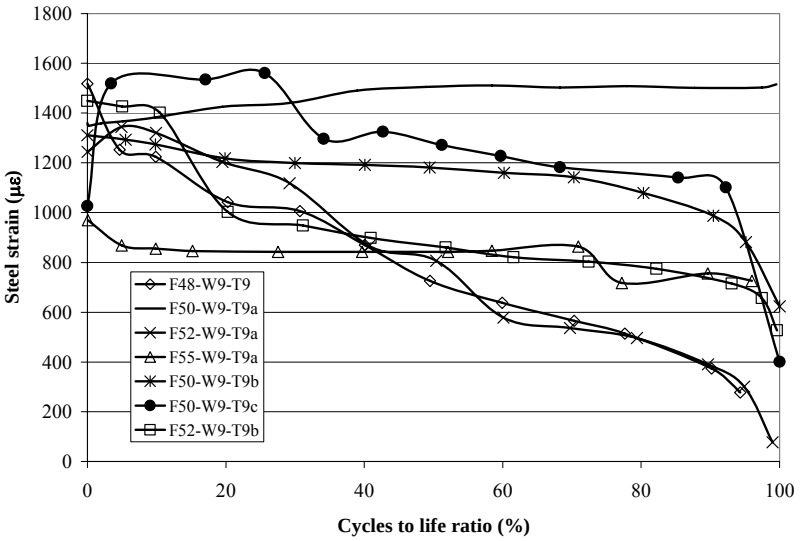

Figure D.6 Steel strain variation for Group W9

Appendix E

Slip-Life Curves

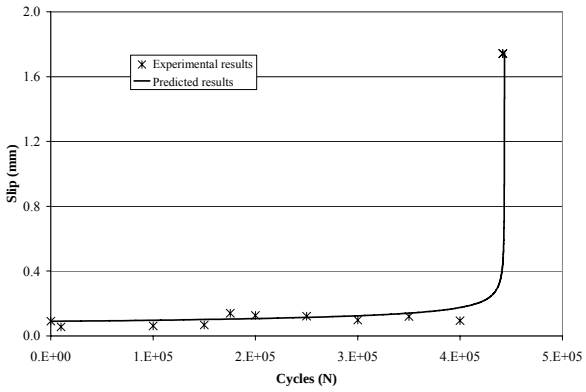

a) Beam F45-N-T0

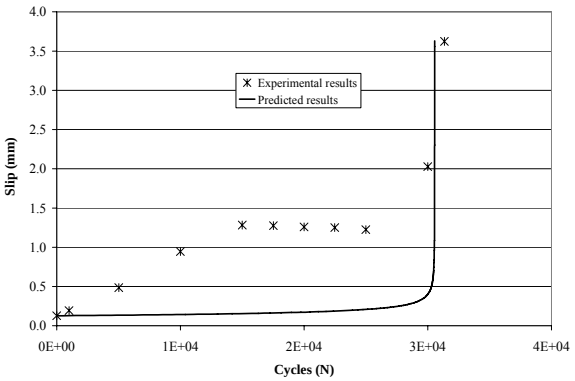

b) Beam F47-N-T0

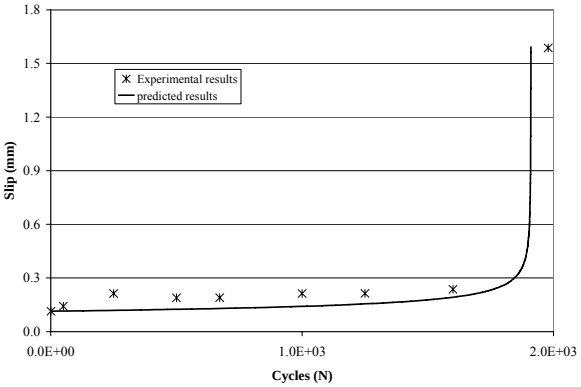

c) Beam F50-N-T0

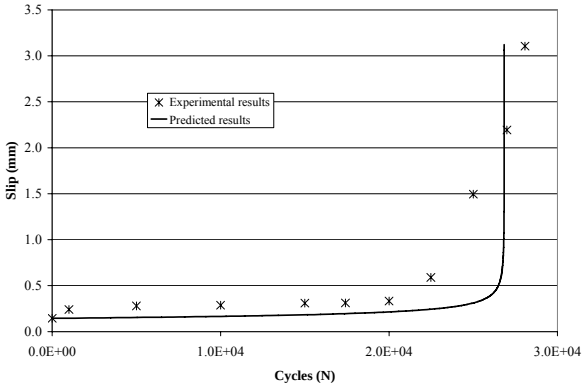

d) Beam F53-N-T0

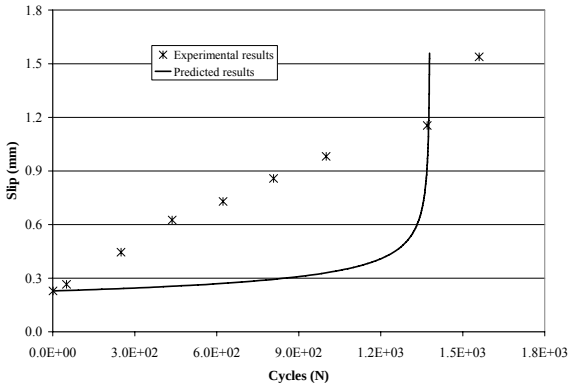

e) Beam F55-N-T0

Figure E.1 Experimental and predicted slip-life data for Group UW0

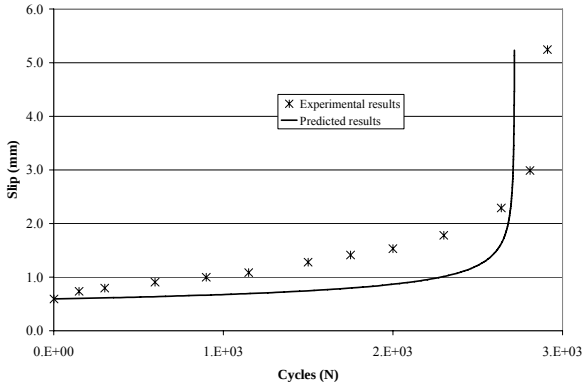

a) Beam F37-N-T5

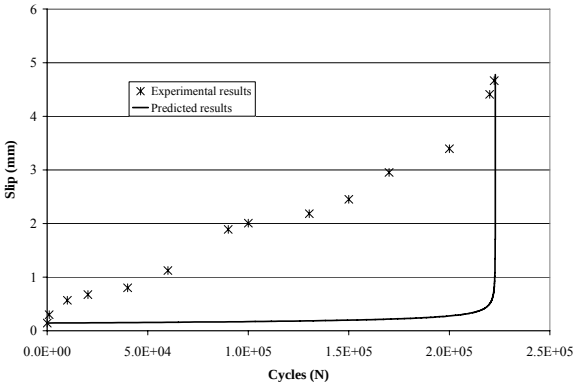

b) Beam F40-N-T5

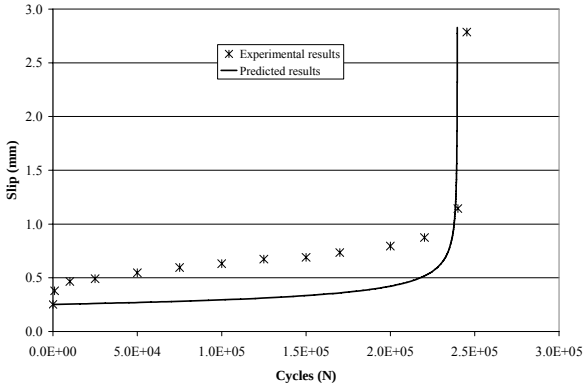

c) Beam F45-N-T5

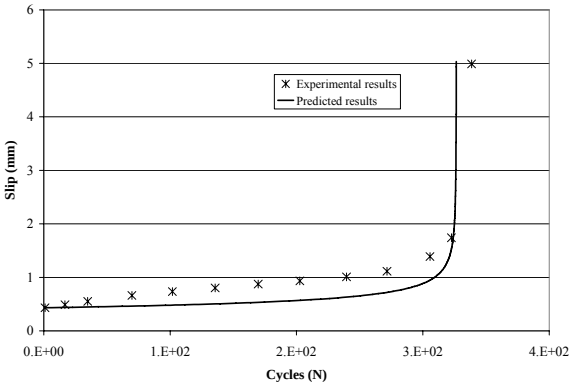

d) Beam F55-N-T5

Figure E.2 Experimental and predicted slip-life data for Group UW5

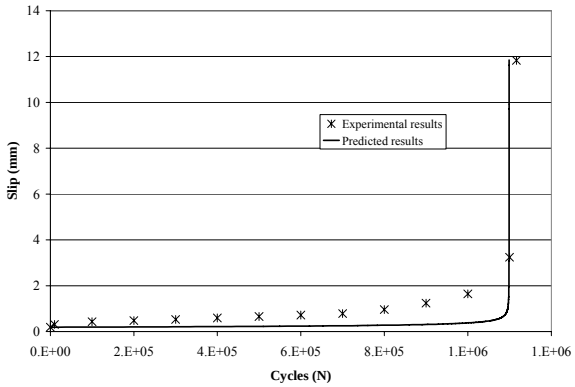

a) Beam F35-N-T9a

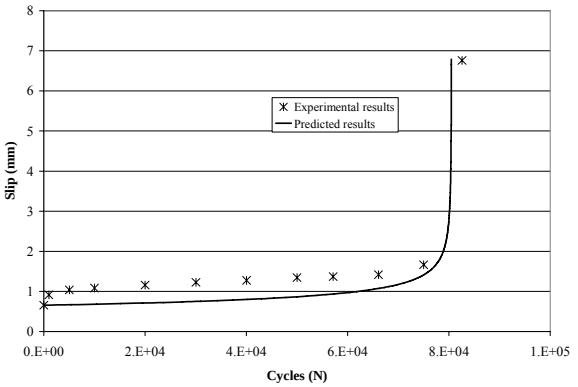

b) Beam F37-N-T9a

Figure E.3 Experimental and predicted slip-life data for Group UW9

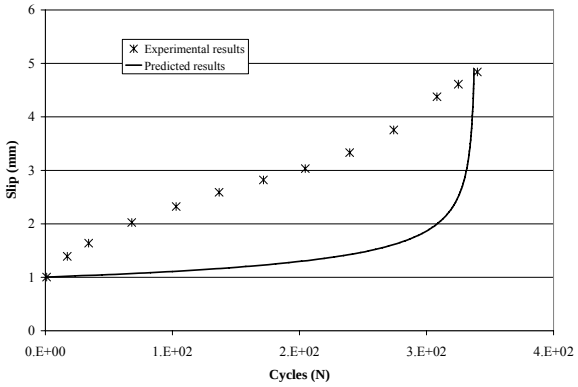

c) Beam F40-N-T9a

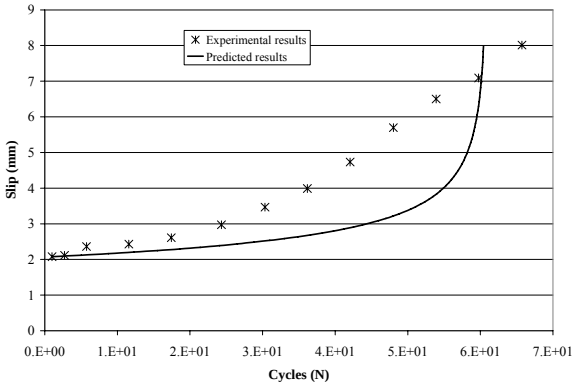

d) Beam F45-N-T9a

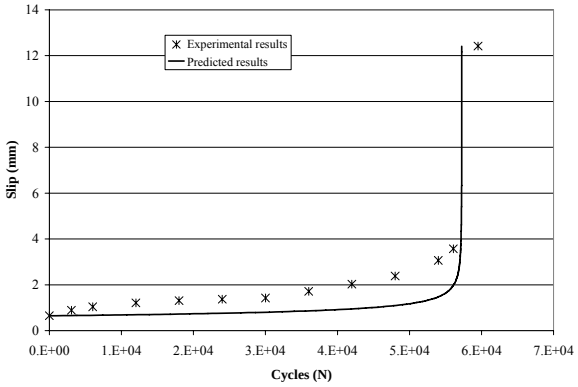

e) Beam F37-N-T9b

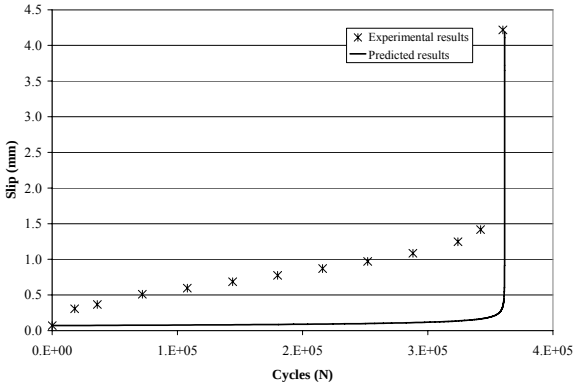

f) Beam F40-N-T9b

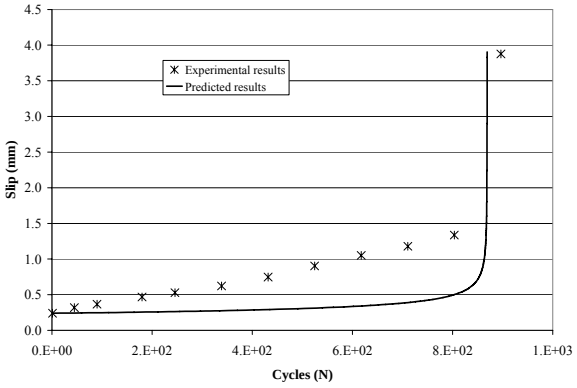

g) Beam F45-N-T9b

Figure E.4 Experimental and predicted slip-life data for Group UW9 (Cont'd)

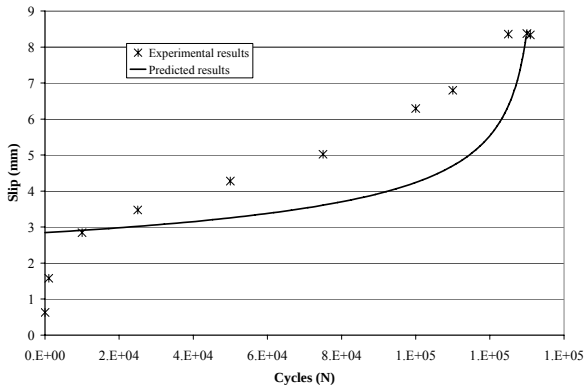

a) Beam F62-W0-T0

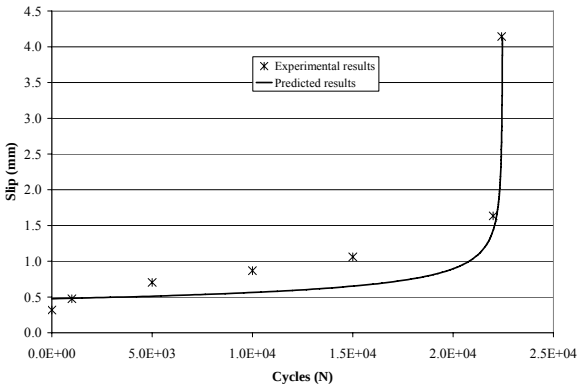

b) Beam F65-W0-T0

Figure E.5 Experimental and predicted slip-life data for Group W0

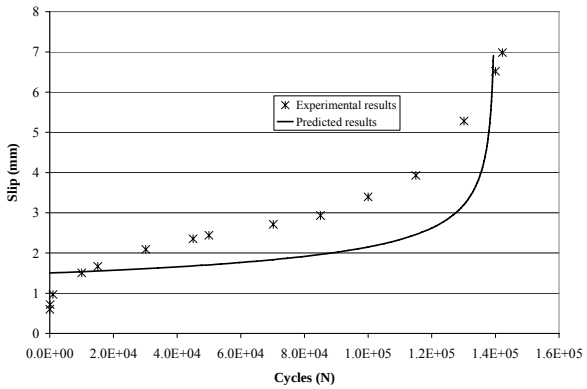

a) Beam F50-W5-T5

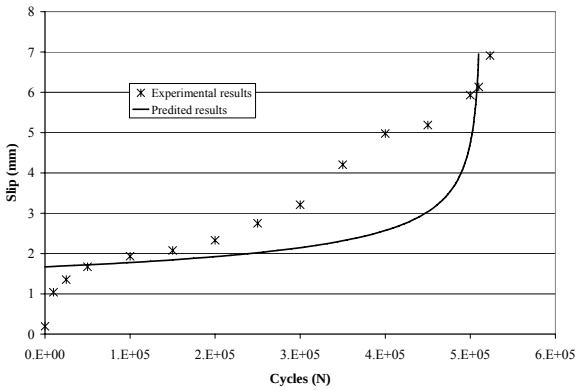

b) Beam F52-W5-T5

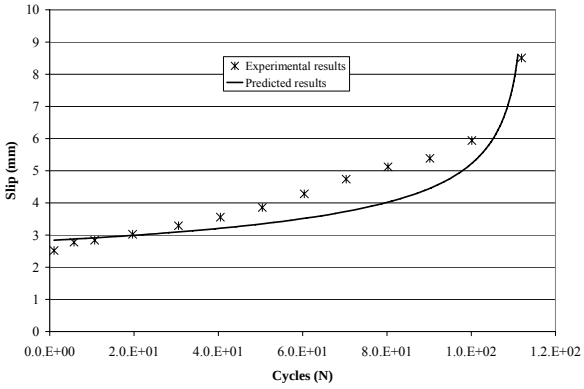

c) Beam F55-W5-T5

Figure E.6 Experimental and predicted slip-life data for Group W5

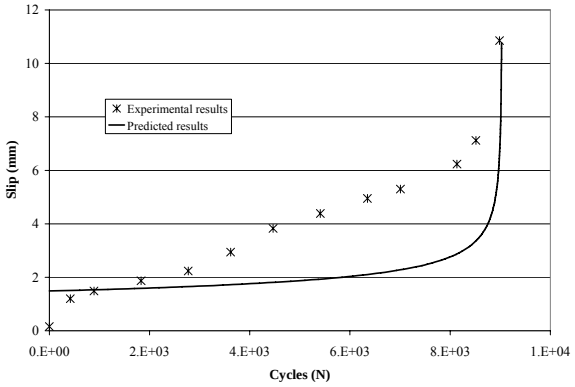

a) Beam F48-W9-T9

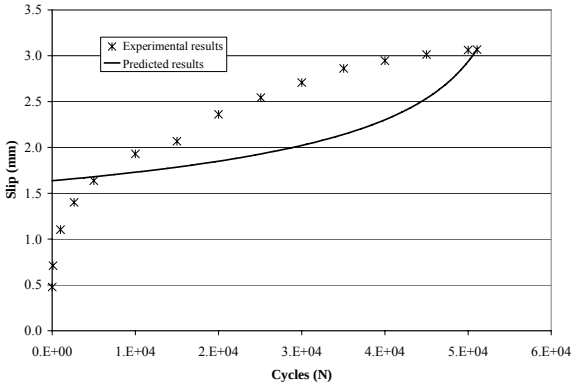

b) Beam F50-W9-T9a

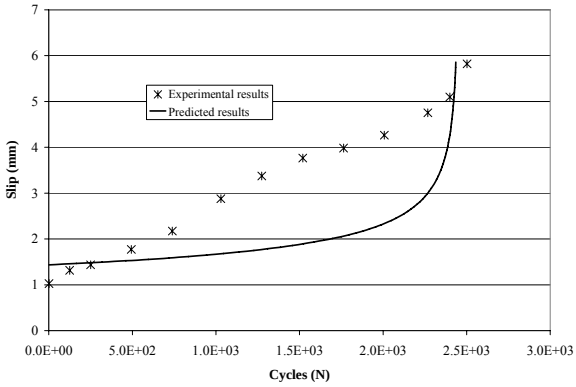

c) Beam F52-W9-T9a

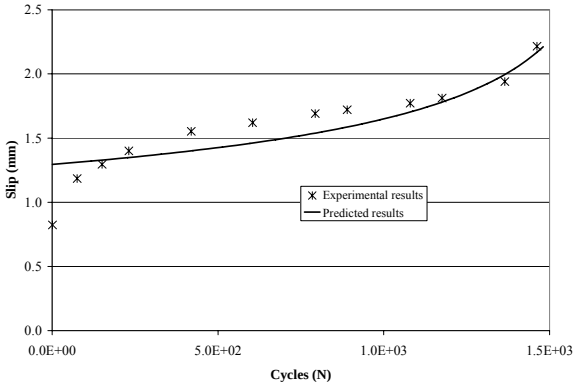

d) Beam F55-W9-T9a

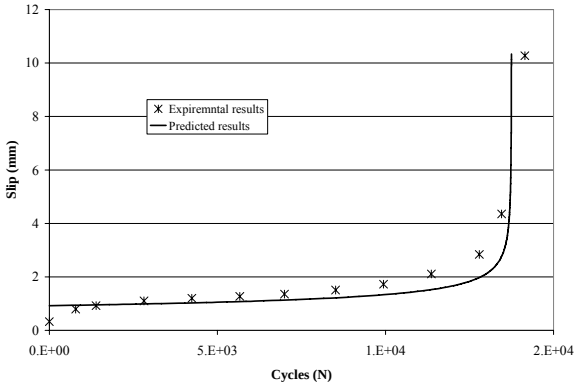

e) Beam F50-W9-T9b

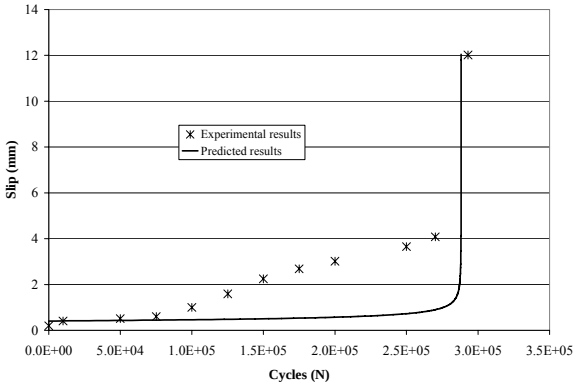

f) Beam F50-W9-T9c

Figure E.7 Experimental and predicted slip-life data for Group W9

Appendix F

Slip Growth rate

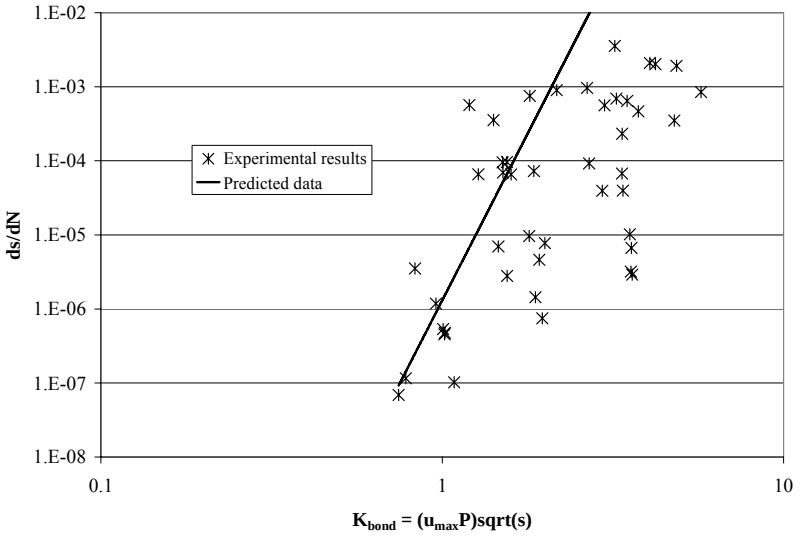

Figure F.1 Experimental and Predicted slip growth rate for group UW0

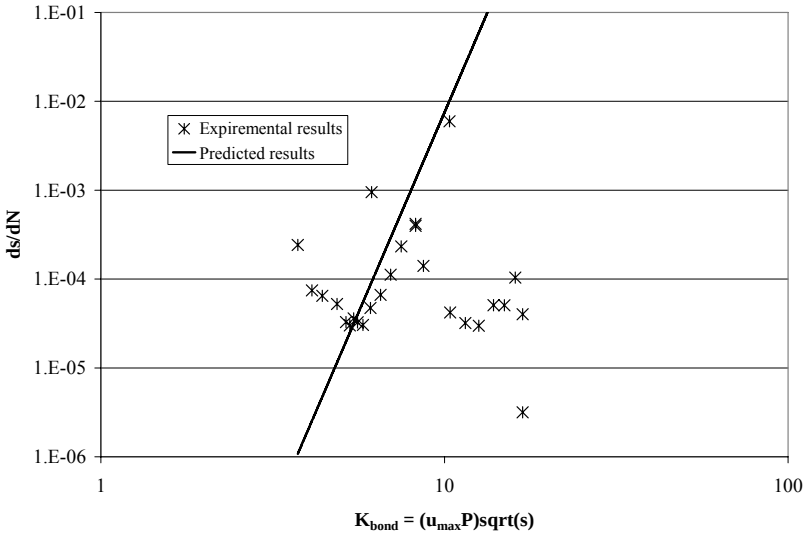

Figure F.2 Experimental and Predicted slip growth rate for group W0

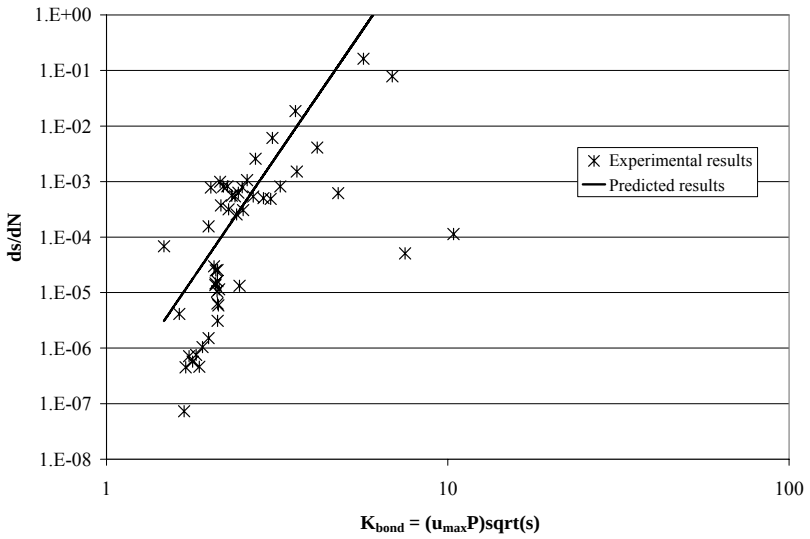

Figure F.3 Experimental and Predicted slip growth rate for group UW5

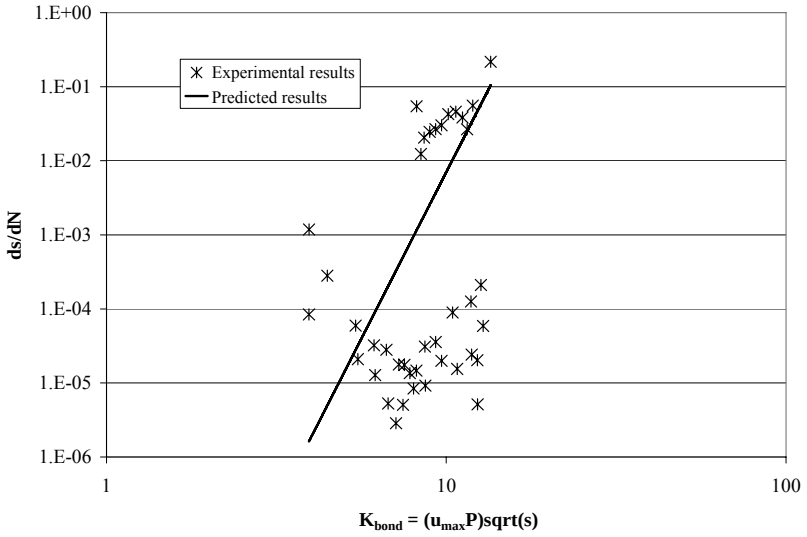

Figure F.4 Experimental and Predicted slip growth rate for group W5

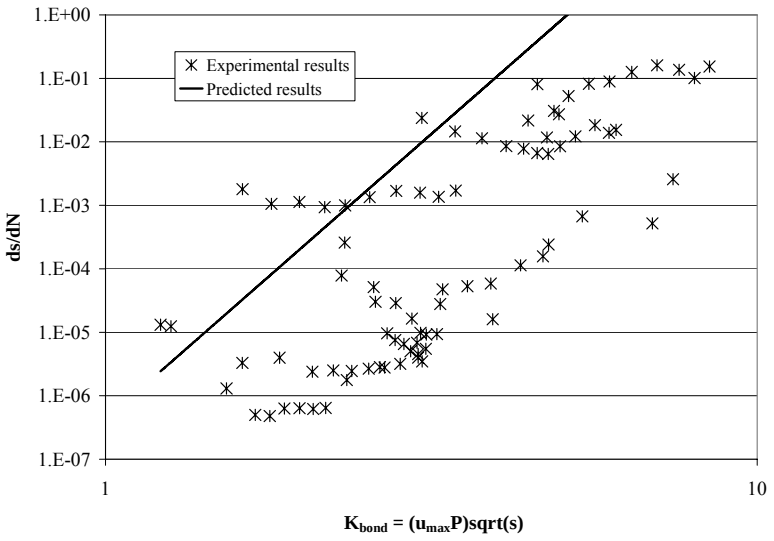

Figure F.5 Experimental and Predicted slip growth rate for group UW9

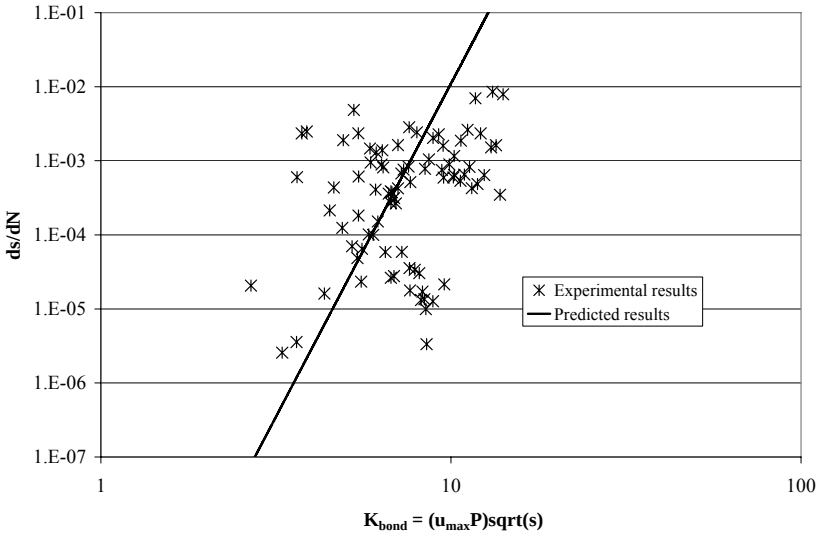

Figure F.6 Experimental and Predicted slip growth rate for group W9

Appendix G

Predicted Load-Life Data

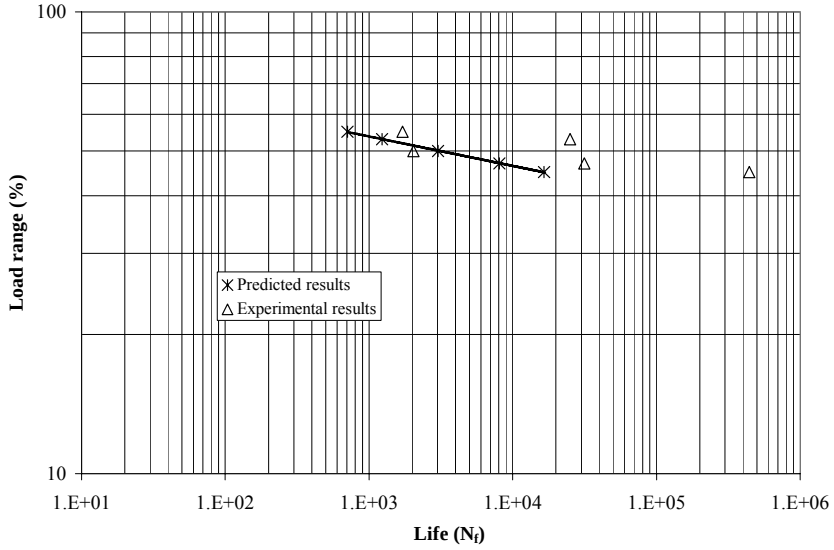

Figure G.1 Experimental and predicted load range-life data for Group UW0

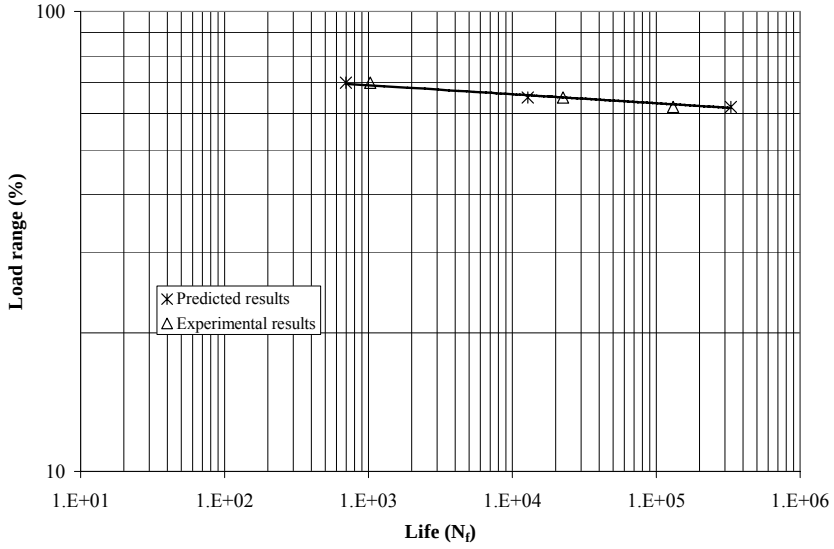

Figure G.2 Experimental and predicted load range-life data for Group W0

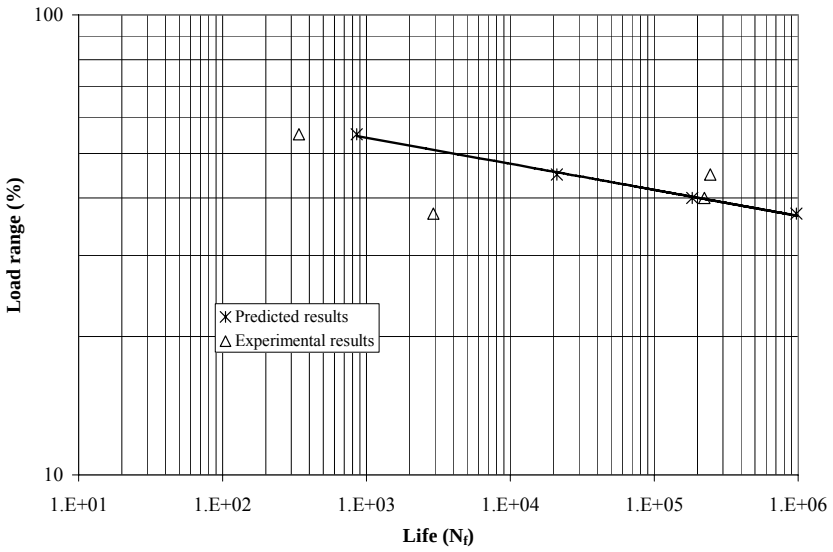

Figure G.3 Experimental and predicted load range-life data for Group UW5

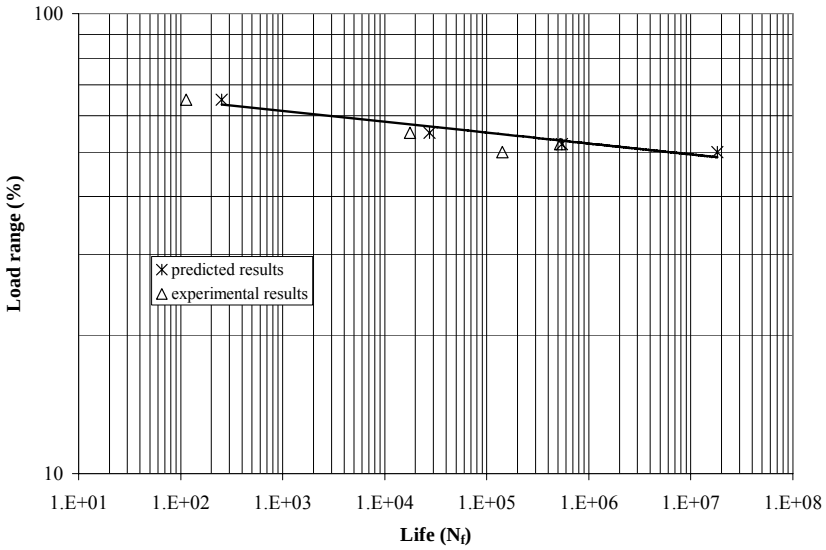

Figure G.4 Experimental and predicted load range-life data for Group W5

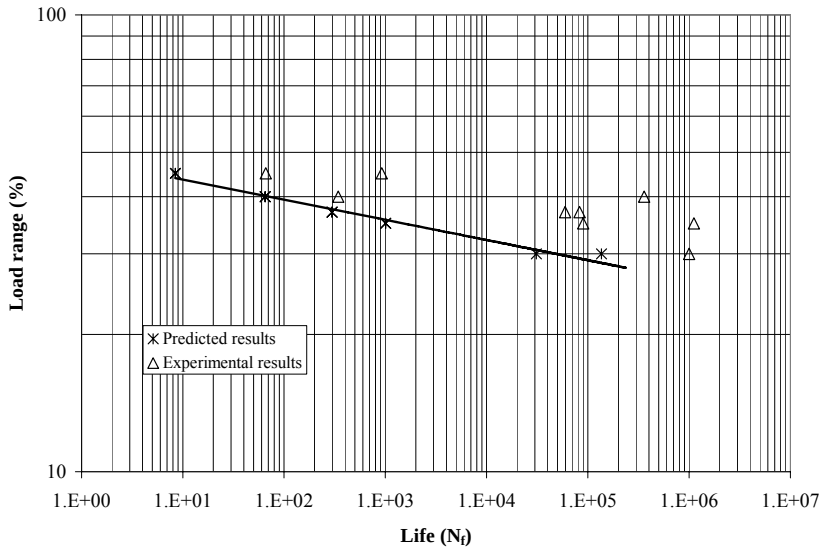

Figure G.5 Experimental and predicted load range-life data for Group UW9

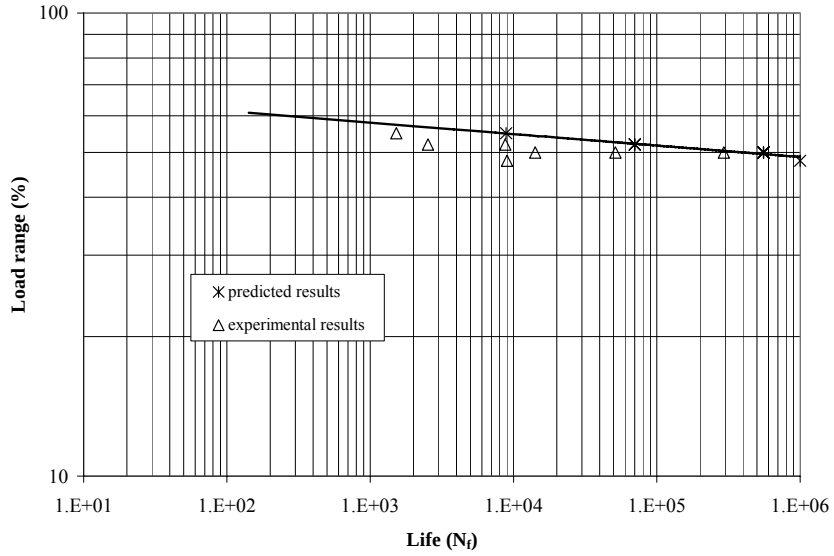

Figure G.6 Experimental and predicted load range-life data for Group W9

Bibliography

ACI Committee 215, 1974. Considerations for Design of Concrete Structures Subjected to Fatigue Loading (ACI 215-74, Reapproved 1999). American Concrete Institute, Farmington Hills, MI, 24p.

ACI Committee 222, 2001. Protection of Metals in Concrete against Corrosion (ACI 222-01). American Concrete Institute, Farmington Hills, MI, 41 p.

ACI Committee 408, 1992. State of the Art Report on Bond under Cyclic Loads (ACI 408.2-92, Reapproved 2005). American Concrete Institute, Farmington Hills, MI, 32 p.

ACI Committee 408, 2003. Bond and Development of Straight Reinforcing Bars in Tension (ACI 408-03). American Concrete Institute, Farmington Hills, MI, 49 p.

ACI Committee 440, 1996. State of the Art Report on Fiber Reinforced Plastic (FRP) Reinforcement for Concrete Structures (ACI 440-96, Reapproved 2002). American Concrete Institute, Farmington Hills, MI, 68 p.

ACI Committee 440, 2002. Bond and Development of Straight Reinforcing Bars in Tension (ACI 440.2-02). American Concrete Institute, Farmington Hills, MI, 49 p.

Aidoo, J.; Harries, K. and Petrou, M., 2004. "Fatigue Behavior of Carbon Fiber Reinforced Polymer-Strengthened Reinforced Concrete Bridge Girders," ASCE Journal of Composites for Construction, V. 8, #6, December, pp. 501-509.

Al-Hammoud, R.; Soudki, K. and Topper, T., 2007. "Fatigue Flexural Behaviour of Corroded Reinforced Concrete Beams Repaired with CFRP Sheets," ACI Structural Journal, submitted for review and possible publication, 20 p.

Almusallam, A.; Al-Gahtani, A.; Aziz, A. and Rasheeduzzafar, 1996a. "Effect of Reinforcement Corrosion on Bond Strength," Construction and Building Materials, V. 10, # 2, pp. 123-129.

Almusallam, A.; Al-Gahtani, A.S.; Aziz, A.R.; Dakhil, F. and Rasheeduzzafar, 1996b. "Effect of Reinforcement Corrosion on Flexural Behavior of Concrete Slabs," ASCE Journal of Materials in Civil Engineering, V. 8, # 3, pp. 123-127.

Al-Sulaimani, G.J; Kaleemullah, M.; Basunbul, I.A. and Rasheeduzzafar, 1990. "Influence of Corrosion and Cracking on Bond Behavior and Strength of Reinforced Concrete Members," ACI Structural Journal, V. 87, # 2, March, pp. 220-231.

ASTM G1, 2003. "Standard Practice for Preparing, Cleaning, and Evaluating Corrosion Test Specimens," American Standards for Test and Materials, Annual Book for ASTM Standards.

Auyeung, Y.; Chung, L. and Balaguru, P., 2000. "Bond Behavior of Corroded Reinforcement bars," ACI Materials Journals, V. 97, #2, March, pp.214-220.

Badawi, M. and Soudki, K., 2005. "Control of Corrosion-Induced Damage in Reinforced Concrete Beams using Carbon Fiber-Reinforced Polymer Laminates," ASCE Journal of Composites for Construction, V. 9, #2, March, pp.195-201.

Balazs, G. and Koch, R., 1992. "Influence of Load History on Bond Behaviour," Proceedings: Bond in Concrete- From Research to Practice, Riga, Latvia, October pp.7.1-7.10.

Balazs, G., 1991. "Fatigue of Bond," ACI Materials Journal, V. 88, #6, November, pp.620-629.

Balazs, G., 1998. "Bond Under Repeated Loading," Proceedings: Bond and Development of Reinforcement-A Tribute to Peter Gergely, Leon, R. Ed., ACI SP-180, pp. 125-143.

Barnes, R.A. and Mays, G.C., 1999. "Fatigue Performance of Concrete Beams Strengthened with CFRP Plates," ASCE Journal of Composites for Construction, V. 3, # 2, May, pp. 63-72.

Bresler, B. and Bertero, V., 1968. "Behavior of Reinforced Concrete under Repeated Loading," ASCE Journal of Structural Division, V. 94, St 6, June, pp. 1567-1589.

Broomfield, J.P., 1997. Corrosion of Steel in Concrete: Understanding, Investigation and Repair, E&FN Spon, London.

Cabrera, J.G. and Ghodoussi, P., 1992. "The Effect of Reinforcement Corrosion on the Strength of the Steel/Concrete Bond," Proceedings: Bond in Concrete- From Research to Practice, Riga, Latvia, October pp.10.11-10.24.

Clark, L.A. and Saifullah, M., 1993. "Effect of Corrosion on Reinforcement Bond Strength," Proceedings: Structural Faults and Repair, 5th International Conference, pp. 113-119.

Craig, B.C. and Soudki, K.A., 2005. "Post-Repair Performance of Corroded Bond Critical RC Beams Repaired with CFRP," Proceedings: FRP Reinforcement for Concrete Structures (FRPRCS-7), 7th International Symposium, Sheild, C. et al. Eds., ACI SP-230, pp. 563-578.

Debaiky, A.; Green, M. and Hope, B., 2002. "Carbon Fiber-Reinforced Polymer Wraps for Corrosion Control and Rehabilitation of Reinforced Concrete Columns," ACI Materials Journal, V. 99, # 2, March, pp. 129-137.

Dowling, N., 1999. Mechanical Behaviour of Materials, Prentice Hall.

El Maaddawy, T. and Soudki, K., 2003. "Effectiveness of Impressed Current Technique to Simulate Corrosion of Steel Reinforcement in Concrete," ASCE Material Journal, V. 15, # 1, pp. 41-47.

El Maaddawy, T. and Soudki, K., 2005a. "Carbon-Fiber-Reinforced Polymer Repair to Extend the Service Life of Corroded Reinforced Concrete Beams." ASCE Journal of Composites in Construction, V. 9, #2, pp. 187-194.

El Maaddawy, T.; Chahrour, A. and Soudki, K., 2006. "Effect of Fiber-Reinforced- Polymer Wraps on Corrosion Activity and Concrete Cracking in Chloride-Contaminated Concrete Cylinders," ASCE Journal of Composites for Construction, V. 10, #2, pp. 139-147.

El Maaddawy, T.; Soudki, K. and Topper, T., 2005b. "Computer-Based Mathematical Model for Performance Prediction of Corroded Beams Repaired with Fiber Reinforced Polymers," ASCE Journal of Composites for Construction, V. 9, #3, June, pp.227-235.

Fang, C.; Lundgren, K.; Chen, L and Zhu, C., 2004. "Corrosion Influence on Bond in Reinforced Concrete," Cement and Concrete Research, V. 34, pp.2159-2167.

FIB Bulletin 10, 2000. Bond of Reinforcement in Concrete (FIB 10). Fédération Internationale du Béton, Lausanne, Switzerland.

Gussenhoven, R. and Brena, S.F., 2005. "Fatigue Behavior of Reinforced Concrete Beams Strengthened with Different FRP Laminate Configurations," Proceedings: FRP Reinforcement for Concrete Structures (FRPRCS-7), 7th International Symposium, Shield, C. et al. Eds, ACI SP-230, pp. 613-630.

Hamad, B.S.; Rteil, A.A. and Soudki, K.A., 2004a. "Bond Strength of Tension Lap Splices in High-Strength Concrete Beams Strengthened with Glass Fiber Reinforced Polymer Wraps," ASCE Journal of Composites for Construction, V. 8, No. 1, February, pp. 14-21.

Hamad, B.S.; Rteil, A.A.; Selwan, B. and Soudki, K.A., 2004b. "Behavior of Bond-Critical Regions Wrapped with Fiber-Reinforced Polymer Sheets in Normal and High-Strength Concrete," ASCE Journal of Composites for Construction, V. 8, # 3, May, pp. 248-257.

Hamad, B.S.; Soudki, K.A.; Rteil, A.A. and Harajli, M.H., 2004c. "Experimental and Analytical Evaluation of the Bond Strength of Reinforcement in Fiber Reinforced Polymer-Wrapped High-Strength Concrete Beams," ACI Structural Journal, V. 101, #6, November, pp 747-754.

Harajli, M.H. and Rteil, A.A., 2004. "Effect of Confinement Using Fiber-Reinforced Polymer or Fiber-Reinforced Concrete on Seismic Performance of Gravity Load-Designed Columns," ACI Structural Journal, V. 101, #1, January, pp 47-56.

Harajli, M.H., 2006. "Effect of Confinement Using Steel, FRC, or FRP on the Bond Stress-Slip Response of Steel Bars under Cyclic Loading," Materials and Structures, V. 39, pp. 621-634.

Harajli, M.H.; Hamad, B.S. and Rteil, A.A., 2004. "Effect of Confinement on Bond Strength between Steel Bars and Concrete," ACI Structural Journal, V 101, #5, September, pp. 595-603.

Harries, K.A.; Ricles, J.R.; Pessiki, S. and Suase, R., 2006. "Seismic Retrofit of Lap Splices in Nonductile Square Columns using Carbon Fiber-Reinforced Jackets," ACI Structural Journal, V. 103, # 6, November, pp. 874-884.

Heffernan, P.J. and Erki, M.A., 2004. "Fatigue Behavior of Reinforced Concrete Beams Strengthened with Carbon Fiber Reinforced Plastic Laminates," ASCE Journal of Composites of Construction, V. 8, #2, April, pp.132-140.

Kawamura, A.; Maruyama, K.; Yoshida, S. and Masuda, T., 1995. "Residual Capacity of Concrete Beams Damaged by Salt Attack," Proceedings: Concrete under Severe Conditions- Environment and Loading, Sakai, K. et al. Eds, E. Spon, London, UK, pp. 1448-1457.

Koch, R. and Balazs, G., 1992. "Influence of Preloading on Bond Strength and Related Slip," Proceedings: Bond in Concrete- From Research to Practice, Riga, Latvia, October pp.7.11-7.21.

Kono, S.; Inazumi, M. and Kaku, T, 1998. "Evaluation of Confining Effects of CFRP sheets on Reinforced Concrete Members," Proceedings: Composites in Infrastructure, 2nd International Conference, Saadatmanesh, H. and Ehsani, M. R., Eds, Tucson, AZ, USA, Vol. I, pp. 343-355.

Kono, S.; Matsuno, K. and Kaku, T., 1999. "Experimental Study on Bond-Slip Behavior of Longitudinal Bars in Reinforced Concrete Beams Confined with Fiber Reinforced Polymer

Sheets," Proceedings: FRP Reinforcement for Reinforced Concrete Structures (FRPRCS-4), 4th International Symposium, Dolan, C.; et al. Eds, ACI SP-188, pp. 333-346.

Kwak, H.G. and Kim, J.K., 2006. "Implementation of Bond-Slip Effect in Analyses of RC Frames Under Cyclic Loads Using Layered Section Method," Engineering Structures, V.28, pp. 1715-1727.

Lee, C.; Bonacci, J.; Thomas, M.; Maalej, M.; Khajehpour, S.; Hearn, N.; Pantazopouou, S. and Sheikh, S., 2000. "Accelerated Corrosion and Repair of Reinforced Concrete Columns using Fibre Reinforced Polymer Sheets," Canadian Journal of Civil Engineering, V. 27, # 5, pp. 941-948.

Lutz, L.A. and Gergely, P., 1967. "Mechanics of Bond and Slip of Deformed Bars in Concrete," ACI Journal, V. 64, # 11, November, pp. 711-721.

Mangat, P.S. and Elgarf, M.S., 1999a. "Bond Characteristics of Corroded Reinforcement in Concrete Beams," Materials and Structures, V. 32, March, pp. 89-97.

Mangat, P.S. and Elgarf, M.S., 1999b. "Flexural Strength of Concrete Beams with Corroding Reinforcement," ACI Structural Journal, V. 96, # 1, January, pp. 149-158.

Masoud, S.; Soudki, K. and Topper, T., 2001. "CFRP Strengthened and Corroded RC Beams under Monotonic and Fatigue Loads," ASCE Journal of Composites for Construction, V. 5, # 4, November, pp. 228-236.

Masoud, S.; Soudki,K. and Topper, T., 2005. "Post-Repair Fatigue Performance of FRP-Repaired Corroded RC Beams: Experimental and Analytical Investigation," ASCE Journal of Composites in Construction, V. 9, # 5, September, pp. 441-449.

Mor, A.; Gerwick, B.C. and Hester, W.T., 1992. "Fatigue of High-Strength Reinforced Concrete," ACI Materials Journal, V. 89, # 2, March, pp. 197-207.

Oh, B.H. and Kim, S.H., 2007. "Realistic Models for Local Bond Stress-Slip of Reinforced Concrete under Repeated Loading," ASCE Journal of Structural Engineering, V. 133, #2, pp. 216-224.

Okada, K.; Kobayashi, K. and Miyagawa, T., 1988. "Influence of Longitudinal Cracking due to Reinforcement Corrosion on Characteristics of Reinforced Concrete Members," ACI Structural Journal, V. 85, # 2, March, pp. 134-140.

Papakonstantinou, C.G.; Petrou, M.F. and Harries, K.A., 2001. "Fatigue Behaviour of RC Beams Strengthened with GFRP Sheets," ASCE Journal of Composites for Construction, V. 5, # 4, November, pp. 246-253.

Perry, E. and Jundi, N., 1969. "Pullout Bond Stress Distribution under Static and Dynamic Repeated Loading," ACI Journal, V. 66, # 5, May, pp. 377-380.

Plizzari, G.; Lundgren, K. and Balazs, G., 2002. "Bond and Splitting in Fibre Reinforced Concrete under Repeated Loading," Proceedings: Bond in Concrete-From Research to Standards, Budapest, Hungary, pp. 221-229.

Rehm, G. and Eligehausen, R., 1979. "Bond of Ribbed Bars under High Cycle Repeated Loads," ACI Journal, V. 76, # 2, February, pp. 297-309.

Rodriguez, J.; Ortega, L. and Casal, J., 1994. "Corrosion of Reinforcement Bars and Service Life of Reinforced Concrete Structures: Corrosion and Bond," Proceedings: Concrete Across Borders, Odense, Denmark, V. 2, pp. 315-326.

Rodriguez, J.; Ortega, L.M. and Casal, J., 1997. "Load Carrying Capacity of Concrete Structures with Corroded Reinforcement," Construction and Building Materials, V. 11, # 4, June, pp. 239-248.

Sika, 2007. www.sika.ca, accessed April 28, 2007.

Soudki, K. and Masoud, S., 2006. "Evaluation of Corrosion Activity in FRP Repaired RC Beams," Cement and Concrete Composites, V. 28, #10, November, pp. 969-977.

Soudki, K.A. and Sherwood, T., 2003. "Bond Behavior of Corroded Steel Reinforcement in Concrete Wrapped with Carbon Fiber Reinforced Polymer Sheets," ASCE Journal of Materials in Civil Engineering, V. 15, # 4, August, pp. 358-370.

Soudki, K.A. and Sherwood, T.G., 2000. "Behaviour of Reinforced Concrete Beams Strengthened with Carbon Fibre Reinforced Polymer Laminates Subjected to Corrosion Damage," Canadian Journal of Civil Engineering, V. 27, # 5, October, pp. 1005-1010.

Suh, K.; Mullins, G; Sen, R. and Winters, D, 2007. "Effectiveness of Fiber-Reinforced Polymer in Reducing Corrosion in Marine Environment," ACI Structural Journal, V. 104, #1, pp. 76-83.

Tachibana, Y.; Maeda, K. I. and Kajikawa, M., 1990. "Mechanical Behavior of RC Beams Damaged by Corrosion of Reinforcement," Proceedings Corrosion of Reinforcement in Concrete Construction, 3rd International Symposium, UK, pp. 178-187.

Tilly, G.P., 1979. “Fatigue of Steel Reinforcement Bars in Concrete: A Review,” Fatigue of Materials and Structures, V. 2, # 3, pp. 251-268.

Toutanji, H.; Zhao, L.; Deng, Y.; Zhang, Y. and Balaguru, P., 2006. “Cyclic Behavior of RC Beams Strengthened with Carbon Fiber Sheets Bonded by Inorganic Matrix,” ASCE Journal of Materials in Civil Engineering, V. 18, #1, February, pp. 28-35.

Uomoto. T.; Tsuji, K. and Kakizawa, T., 1984. “Deterioration Mechanism of Concrete Structures caused by Corrosion of Reinforcing Bars,” Transactions of Japan Concrete Institute, V. 6, pp. 163-170.

Verna, J.R. and Stelson, T.E., 1962. “Failure of Small Reinforced Concrete Beams under Repeated Loading,” ACI Journal, V. 59, #10, October, pp. 1489-1503.

Whitmore, D.W. and Ball, J.C., 2004. “Corrosion Management,” ACI Concrete International, V. 26, #12, December, pp. 82-85.